Developing Novel Carriers to Deliver Targeted Immunotoxins for the Treatment of Primary and Metastatic Non-Small Cell Lung Cancer

Author

Zhang, Kai

Published

2017

Thesis Type

Thesis (PhD Doctorate)

School

School of Medical Science

DOI

10.25904/1912/2927

Developing novel carriers to deliver targeted immunotoxins for the treatment of primary and metastatic non-small cell lung cancer

Kai ZHANG

Bachelor of Science – Bioinformatics

Master of Science – Molecular Biology

School of Medical Science

Menzies Health Institute Queensland

Griffith Health

Griffith University

Submitted in fulfilment of the requirements for the degree of

Doctor of Philosophy

April 2017

STATEMENT OF ORIGINALITY

This work has not previously been submitted for a degree or diploma in any university. To the best of my knowledge and belief, the thesis contains no material previously published or written by another person except where due reference is made in the thesis itself.

(Signed)_____

Kai Zhang

DEDICATION

I would like to dedicate this thesis to special people in my life:

Hui Zhang and Yanming Zhang, my amazing parents for their wonderful love, patience, sacrifice and supports during this journey.

Xin Zhang, my wonderful cousin for his wisdom and encourage, always helped me get back on the track when I was down.

Ming Q, Wei, a dedicated researcher for not only being my principle supervisor but also a true friend in life.

Mohsen Sohrabi, my great friend and my amazing colleague for his advice and suggestions during the whole time.

Caroline Atkinson, an amazing researcher with full of wisdom and a great friend in life.

ACKNOWLEDGEMENT

I would like to thank all my supervisors for their support, encouragement and motivation. This work would not have been possible without their sincere support. I wish to express the deepest appreciation to Professor Ming Q, Wei in trusting and giving me the opportunity to work in his lab at Griffith University. His motivation, enthusiasm, and patience have been critical in completing my research. I would like to acknowledge the continuing support of Associate Professor Jenny Wilson who made my research possible, shaped my experiments, contributed to my knowledge and academic behavior. Her lessons have critically affected me on how I think, plan and live. My sincere thanks to Associate Professor Zhiping (Gordon) Xu for sharing his valuable knowledge and experiences with research modeling.

I would also like to thank Dr Yi'an Zhu for her precious experience and insightful advice. My sincere thanks to Dr Min Chen who led me to the field of science at the University of Queensland

I would like to thank all my colleagues, who kindly helped me during my candidature. The learning experience and the time I spent together with all of you will always be cherished in my memory.

Finally, I acknowledge the support of Griffith University for providing me GUIPRS, GUIPRS, CAPRS, Conference Travel Scholarships and other financial support to finish my PhD program at Griffith University.

Acknowledgement of Published and Unpublished Papers Included in this Thesis

Section 9.1 of the Griffith University Code for the Responsible Conduct of Research ("Criteria for Authorship"), in accordance with Section 5 of the Australian Code for the Responsible Conduct of Research, states:

To be named as an author, a researcher must have made a substantial scholarly contribution to the creative or scholarly work that constitutes the research output, and be able to take public responsibility for at least that part of the work they contributed. Attribution of authorship depends to some extent on the discipline and publisher policies, but in all cases, authorship must be based on substantial contributions in a combination of one or more of:

- conception and design of the research project
- analysis and interpretation of research data
- drafting or making significant parts of the creative or scholarly work or critically revising it so as to contribute significantly to the final output.

Section 9.3 of the Griffith University Code ("Responsibilities of Researchers"), in accordance with Section 5 of the Australian Code, states:

Researchers are expected to:

- Offer authorship to all people, including research trainees, who meet the criteria for authorship listed above, but only those people.
- accept or decline offers of authorship promptly in writing.
- Include in the list of authors only those who have accepted authorship
- Appoint one author to be the executive author to record authorship and manage correspondence about the work with the publisher and other interested parties.
- Acknowledge all those who have contributed to the research, facilities or materials but who do not qualify as authors, such as research assistants, technical staff, and advisors on cultural or community knowledge. Obtain written consent to name individuals.

Included in this thesis are papers in Chapters 2 and 5 which are co-authored with other researchers. My contribution to each co-authored paper is outlined at the front of the relevant chapter. The bibliographic details/status for these papers including all authors are:

Chapter 2:

Kai Zhang; Zhiping Xu; Ji Lu; Zhiyong Tang; Huijun Zhao; David A, Good; Ming Q, Wei. 2014. The potential for Layered Double Hydroxides-Based, Innovative Drug Delivery Systems. 2014. International Journal of Molecular Science; Open Access: Volume 15, Page 7409-7428.

http://www.mdpi.com/1422-0067/15/5/7409

Kai Zhang; Caroline Akinson; Ming Q, Wei. 2016. Recombination Immunotoxin Therapy for Cancer Treatment. Toxin; Open Access (submitted)

Chapter 3, 4 and 5

Kai Zhang; Ji Lu; Weiyu Chen; Ming Q, Wei. 2016.

EGFR-targeted plasmid-Layered double hydroxide complexes show enhanced anti-tumor activity. Toxin; Open Access (submitted)

(Signed)_____(Date) 5/04/2017

Kai Zhang

(Countersigned)_____ (Date) 5/04/2017

Supervisor: Prof. Ming Q, Wei

LIST OF CONFERENCE PRESENTATIONS

Zhang K, Lu J, Wei, M. Q Developing Plasmid-Layered double hydroxide complexes for the treatment of primary and metastatic non-small cells lung cancer Paper presented at International Student Research Form, Beijing, China. 2016 (12 June to 15 June 2016).

Zhang K, Lu J, Tang, Z. Y, Zhao, H. J, and Wei, M. Q. Developing novel carriers to deliver targeted immunotoxins for the treatment of primary and metastatic non-small cells lung cancer. Poster presented at Gold Coast Health and Medical Research Conference, Gold Coast, Australia 2015 (December 2015).

Zhang K, Lu J, Zhao, H. J, and Wei, M. Q. Developing potential gene therapy of EGF-PE38 immunotoxin by employing the Layered Double Hydroxides drug delivery system. Poster presented at Gold Coast Health and Medical Research Conference, Gold Coast, Australia 2014 (December 2014)

Zhang K, Wei, M. Q. Adoptive immunotherapy CAR-T cell. Paper presented at Cancer Research Centre Annual Conference 2015, Gold Coast, Australia (24 November 2015)

TABLE OF CONTENTS

LIST OF TABLES

LIST OF FIGURES

ABBREVIATIONS

5-Fu	5-fluorouracil
6-FAM	6-Carboxyfluorescein
A_{230}	absorbency at 230
A_{260}	absorbency at 260
A_{280}	absorbency at 280
Al	Aluminium
A549	Homo Sapiens Lung Carcinoma cell line
ALL	Acute lymphoblastic leukemia
AML	Acute myeloid leukemia
ATCC	American Type Culture Collection
AMML	Acute Myelomonocytic Leukemia
ATP	Adenosine triphosphate
ATLL	Adult T-cell leukemia/lymphoma
ADP	Adenosine diphosphate
ALP	alkaline phosphatase activity
AIBN	Australian Institute for Bioengineering & Nanotechnology
bp	base pair
BCL	B-cell lymphoma
°C	Celsius
cm	centimetre
CO_2	Carbon dioxide
CR	complete remission
CCC	covalently closed circular
CCR4	C-C chemokine receptor type 4
CD7	Cluster of Differentiation 7
CD19	Cluster of Differentiation 19
CD22	Cluster of Differentiation 22
CD25	Cluster of Differentiation 25
CD64	Cluster of Differentiation 64
CD89	Cluster of Differentiation 89
CD317	Cluster of Differentiation 317
CPE	*Clostridium perfringens enterotoxin*
CMML	Chronic myelomonocytic leukaemia
CHO	Chinese hamster ovary
CPT	Camptothecin
CsA	cyclosporine
CTCL	Cutaneous T cell lymphoma
CD-siRNA	Cell Death siRNA

dsFv	disulfide-stabilized Fv
DT	Diphtheria toxin
DS water	Distill water
DLT	Dose Limiting Toxicity
DNA	deoxyribonucleic acid
DNase	deoxyribonuclease
DCC	Colorectal Cancer
DSC	disuccinimidyl carbonate
DMF	double hydroxide-fluorouracil
DMEM	Dulbecco's modified Eagle's Medium
DMSO	Dimethyl sulfoxide
EF-2	elongation factor 2
EE-F	EGF-ETA-Forward
EE-R	EGF-ETA-Reverse
EC_{50}	Half maximal effective concentration
EEO	electroendosmosis
EDTA	ethylenediaminetetraacetic acid
ERK2	AKA MAPK1, Mitogen-activated protein kinase 1
EGFR	epidermal growth factor receptor
ETA	Exotoxin A
Fe	Iron
Fv	Fragment variable
Fab	Fragment Antigen-Binding
FBS	Phosphate Buffer Saline
FITC	Fluorescein isothiocyanate
FTIR	Fourier transform infrared spectroscopy
FBF	Fenbufen
FDA	Food and Drug Administration
g	gram
Ga	Gallium
GFP	green fluorescent protein
HTI	hydrotalcite-like
HTt	hydrotalcite-type
HCl	Hydrochloric acid
HL-60	*Human promyelocytic leukemia cells-60*
HER2	Receptor tyrosine-protein kinase
HEK293	Human embryonic kidney cells 293
hDPSCs	human dental pulp stem cells
hCG	Human chorionic gonadotropin
IC_{50}	half maximal inhibitory concentration
kPa	kilopascal
L	liter
LB	Luria-Bertani

Li	Lithium
Lipo 2000	Lipofectamine 2000
LDHs	Layered Double Hydroxides
LDH@$mSiO_2$	LDH/silica core-shell nanostructures
µL	microliter
µM	micromolar
mg	milligram
Mg	Magnesium
MG-63	osteosarcoma cells
mL	milliliter
mol	molar
mmol	millimolar
mm	millimeter
mM	millimolar
mRNA	Messenger RNA
mAb	monoclonal antibody
MTX	Methotrexate
MDR	multidrug resistance
MCF-7	Homo Sapiens Breast Adenocarcinoma cell line
MOLT-4	T-lymphoblastic leukemia
MNNG/HOS	osteosarcoma cells
ng	nanogram
nm	nanometer
N_2	Nitrogen gas
Np	Naproxen
NB	neuroblastoma
NEB	New England Biolabs
NAD	nicotinamide adenine dinucleotide
NCI	National Cancer Institution
NTP	nucleoside triphosphate
NFkB	Nuclear Factor Kappa B
NSCLC	Non-small cell lung cancer
NIH3T3	3-day transfer, inoculum 3 x 10^5 cells
NaOH	Sodium hydroxide
NAD	Nicotinamide adenine dinucleotide
NSAIDs	Non-Steroidal Anti-Inflammatory Drugs
OD_{600}	optical density at 600 nanometer
OC	open-circular
ORF	Open Reading Frame
pH	potential of hydrogen
PE	*Pseudomonas exotoxin*
PR	partial remissions
PBS	phosphate-buffered saline

PCR	polymerase chain reaction
PEG	polyethylene glycol
psi	pound per square inch
PPT	Podophyllotoxin
PTCL	Peripheral T-Cell Lymphoma
PBMCs	peripheral blood mononucleated cells
REs	Restriction Enzymes
RIP	ribosome-inactivating proteins
SDS	Sodium dodecyl sulfate
scFv	single-chain variable fragment
siRNA	Small interfering RNA
Sao-2	Sarcoma osteogenic
SCLC	small cells lung cancer
TG	Thermogravimetry
TAE	tris/acetate/ethylenediamine tetra -acetic acid (buffer)
Tyr	tyrosine
TEM	Transmission electron microscopy
Tris-Cl	Tris-buffered saline with HCl
UQ	University of Queensland
v/v	volume per volume
Vero3	African monkey kidney cells
VLS	vascular leak syndrome
w/v	weight per volume
XRD	X-ray crystallography
YOYO-1	Oxazole Yellow
Zn	Zinc

Chapter 1: Introduction

1.1 Title

Developing novel carriers to deliver targeted immunotoxins for the treatment of primary and metastatic non-small cell lung cancer

1.2 Lay Title

Test whether CMV-EGF-ETA plasmids could be delivered by the Layered Double Hydroxides (LDHs) nanoparticles into cancer cells and induce cells death.

1.3 Background

Non-small cell lung cancer (NSCLC) accounts for 85% of lung cancer which is a leading cause of cancer death. Most patients (>80%) present with advanced NSCLC when curative surgery is no longer an option. Other conventional therapies, such as chemotherapy, radiotherapy and existing molecular targeted therapy have neither significantly extended the life span of most patients, nor improved their quality of life. This is not only because of the large tumor load in the advanced stage of NSCLC but its metastasis. This project devises a novel approach to shield the “magic bullet” and help it locate and kill targeted cancer cells.

NSCLC is an epithelial cancer. Elevated levels of cell surface molecules, such as the epidermal growth factor receptor (EGFR), a growth-factor-receptor tyrosine kinase, and the Claudin family of molecules forms gap junction and

barriers for drug delivery. Our lab has developed two specifically targeted immunotoxins. One is the variable domain of a single chain antibody fragment (425scFv) specific for EGFR, fused with an apoptosis-inducing domain of a protein, derived from a fragment of Exotoxin A (ETA) of *Pseudomonas aeruginosa*, the other is a hybrid molecule that utilizes the high-affinity of receptor-binding fragment of *Clostridium perfringens enterotoxin* (CPE) which naturally binds to CLDN-4 through its C-terminal 30 amino acid. Preliminary results *in vitro* have shown these recombinants molecules were significantly and selectively toxic to cancer cells *in vitro*. 50% of NSCLC proliferation was inhibited at a concentration (IC_{50}) of 7.5 ng/mL, as well as 90% of A549 cells at IC_{50} of 6 ng/mL.

However, delivery of these *in vivo*, especially repeated use of such proteins for long term therapy of solid epithelial cancers such as NSCLC elicit an immune response, limiting their use. My Master's degree research has focused on Layered double hydroxide (LDH), an inorganic nanoparticle which has been employed for developing a drug delivery system. Recently, LDHs have been widely employed in medical research as drug carriers. Many bio-molecules have been either attached to the surface of or intercalated into LDHs through co-precipitation or anion-exchange reaction, including amino acid and peptides, ATPs, vitamins, even polysaccharides. Taken advantage of the unique properties of LDH materials, LDH nanoparticles successfully achieved delivering drugs into targeted cells *in vitro* and in some case *in vivo* without side-effects. Compared with old-fashioned drug delivery methods which are suffering from problems such as drug degradation, poor bioavailability, low circulation stability, the LDH, as a new drug carrier, is much simpler to synthesize in the laboratory

with high transferring efficiency, high drug loading density, and low toxicity to target cells or organs. In addition, the LDHs nanoparticles could also achieve: 1) the Improvement of loaded drug “survival” ability; it has been discovered that the drug-loaded LDH could remarkably enhance the drug solubility in either aquatic environment or in the gastric fluid environment. The thermo-gravimetric analysis also showed that drugs appeared to be more stable after the intercalation with LDH nanoparticles. The presence of LDH nanoparticles could not only prevent loaded drugs from unexpected degradation, most importantly, lead to an enhancement of gastric mucus permeation and protection of gastrointestinal mucus from the ulcer-genic activity. 2) Sustained release of drugs; controlled drug release could be achieved in both gastric environment (pH 1~2) and intracellular environment (~pH 7.5). As discussed above, the appropriate modification is required for drug release to appear in a liner manner at pH value of 1~2. However, at pH value of 7.5, the different mechanism, ion exchange, was the most responsible for the sustained drug release. The LDHs based drug delivery systems are therefore well positioned to overcome some hurdles that usually impede successfully drug delivery.

Therefore, the question is raised, could LDHs drug delivery systems be employed for efficient gene delivery to targeted cancer cells, in this case, the CMV-EGF-ETA plasmid? In details, could the system achieve high drug loadings? Could the system provide perfect shelters to the plasmids from unexpected degradation *in vitro* for drug accumulation at targeting points? Could the system achieve controlled release inside tumor environment for sustain and long term treatment?

In summary, this research will investigate whether the LDHs drug delivery systems could encapsulate immunotoxins CMV-EGF-ETA and facilitate the immunotoxin to reach the targeted immunotoxins *in vitro*, which will be for the first time that the newly developed drug delivery systems are employed for the establishment of a novel therapy for NSCLC.

1.4 Hypothesis, Objective and Aims

1.4.1 Hypothesis

Nano-based structures could encapsulate immunotoxins CMV-EGF-ETA and reduce these proteins' immunogenicity, enabling long term repeated delivery of these tumor-selective and toxic agents *in vivo*, facilitating the establishment of a novel therapy for NSCLC.

1.4.2 Objective

To develop a novel, nano-based carrier to deliver targeted immunotoxin for the treatment of primary and metastatic non-small cell lung cancer.

1.4.3 Aims

To test the hypothesis, I specifically aim:

1. To establish the Mg-Al hydroxide LDH nanoparticle drug delivery system in the lab and optimize the synthesis of the LDH to ensure efficient drug loading. (Chapter 3)
2. To design and synthesize the new immunotoxin CMV-EGF-ETA based on two plasmids existed in Prof. Ming Q, Wei's lab 425 (scFv)-ETA and pEGFP-C1 through gene reconstruction and gene cloning. (Chapter 4)

3. To examine the interaction between the plasmids (immunotoxin CMV-EGF-ETA) and the nanoparticle Mg-Al LDH nanoparticles. (Chapter 5, Section 5.4.1)
4. To examine the release and therapeutically anticancer efficacy of LDH nanoparticle- immunotoxin (in plasmid form) complex *in vitro*. (Chapter 5, Section 5.4.2)

Chapter 2: Literature review

Potential for Layered Double Hydroxides-Based, Innovative Drug Delivery Systems

This section includes a co-authored published paper. The bibliographic details of co-authored paper, including all authors, is:

Kai Zhang, Zhi Ping Xu, Ji Lu, Zhi Yong Tang, Hui Jun Zhao, David A. Good and Ming Qian Wei

International Journal of Molecular Biology; Open Access: Volume 15, Page 7409-7428

http://www.mdpi.com/1422-0067/15/5/7409

First author contribution to the paper involved: Literature review and drafting the manuscript.

Other authors contribution to the paper involved: Critical review and revisions were conducted by ZPX, JL, ZYT, HJZ, DG and MQW

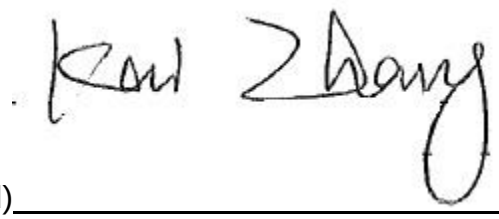

(Signed)_____(Date) 5/04/2017

Kai Zhang

(Countersigned) 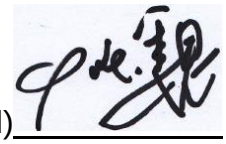 (Date) 5/04/2017

Supervisor: Prof. Ming Q, Wei

(Countersigned) 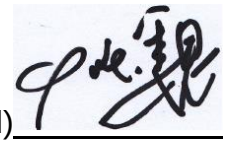 (Date) 5/04/2017

Supervisor: Prof. Ming Q, Wei

2.1 Potential for Layered Double Hydroxides-Based, Innovative Drug Delivery Systems

Kai Zhang [1*], Zhi Ping Xu [2], Ji Lu [2], Zhi Yong Tang [3,4], Hui Jun Zhao [4], David A. Good [1,5] and Ming Qian Wei [1*]

[1] School of Medical Science & Griffith Health Institute, Gold Coast Campus, Griffith University, Southport, QLD 4222, Australia; E-Mail: kai.zhang4@griffithuni.edu.au

[2] Australian Institutes for Bioengineering & Nanotechnology, University of Queensland, St Lucia, QLD 4072, Australia; E-Mails: gordonxu@uq.edu.au (Z.P.X.); ji.lu@uqconnect.edu.au (J.L.)

[3] National Centre for Nanoscience and Technology, Chinese Academy of Sciences, Beijing 100190, China; E-Mail: zytang@nanoctr.cn

[4] Griffith Schools of Environment, Gold Coast Campus, Griffith University, Southport, QLD 4222, Australia; E-Mail: h.zhao@griffith.edu.au

[5] School of Physiotherapy, Faculty of Health Science, Australian Catholic

University, Brisbane, QLD 4014, Australia

***Corresponding author:**

E-Mails: kai.zhang4@griffithuni.edu.au (K.Z.); m.wei@griffithuni.edu.au

(M.Q.W.);

Tel.: +61-7-5678-0745 (K.Z. & M.Q.W.); Fax: +61-7-5552-8908 (K.Z. & M.Q.W.).

Keywords: layered double hydroxides (LDHs); drug delivery; gene therapy; chemotherapy

2.1.1. Layered Double Hydroxides in Gene Delivery

2.1.1.1 Gene delivery overview

Given that the anions locating at the LDH interlayer can be replaced by other organic or inorganic, simple or complex anions, it is possible that the negatively charged oligonucleotides can be intercalated into the LDH inner space *via* ion-exchange mechanism (Figure 2.1). Moreover, it has also been shown that the more guanine and cytosine the small DNA/siRNA possessed, the higher intercalation efficiency achieved [1]. Once the oligonucleotide was intercalated into the LDHs nanoparticles, the host could protect the loaded nucleotide from the attack of DNase. On the other hand, there has been an ongoing debate regarding the manner of the association between large nucleotides and the LDH host. In several studies, it was believed that the DNA plasmids were intercalated into LDH layers [2-5]. However, we found that lager DNA fragments (1000 base pair or more) or plasmid DNA vectors adapted a secondary structure in an aquatic environment forming a supercoiled structure, which was not completely accessible to intercalation in the interlayer galleries by means of anion exchange [6,7]. Given that observed plasmid/LDH aggregation and lower-than-theoretically possible DNA: LDH ratio, DNA molecules might be more adsorbed to the surface of LDH carriers *via* ionic bond rather than intercalated into LDH layers. Therefore, the hypothesis of employing LDHs for cellular delivery of large DNA and protection from unexpected degradation might need to be further confirmed.

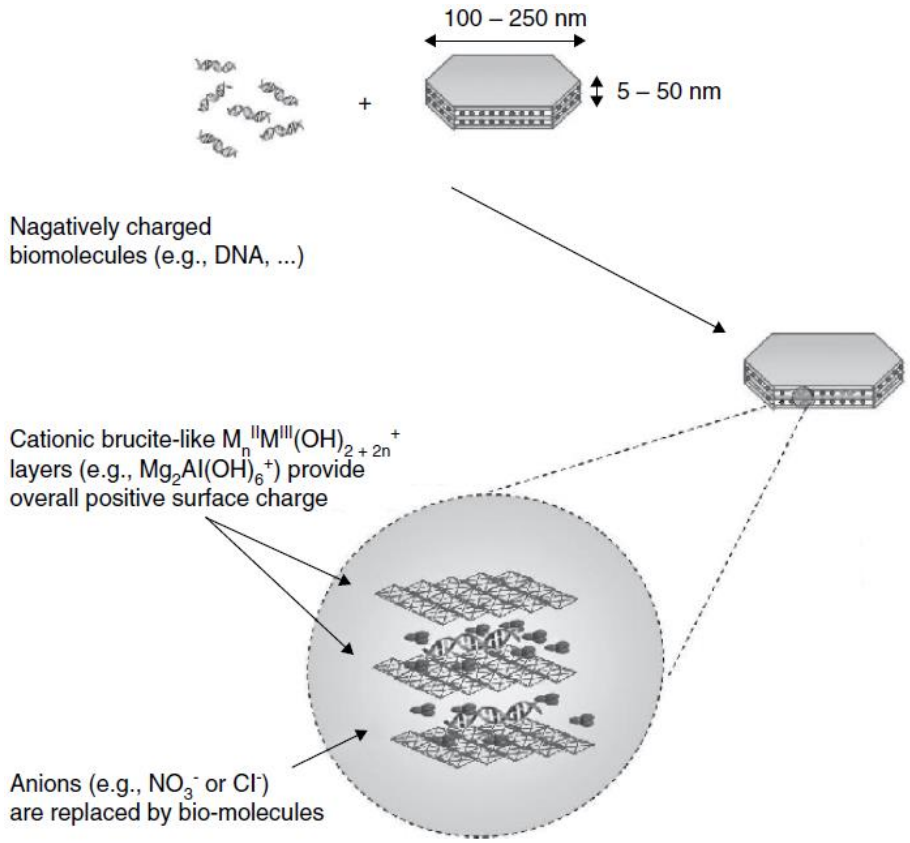

Figure 2.1. The intercalation mechanism of oligonucleotides with LDH nanoparticles [6].

Naked gene delivery has been confronted with hurdles, such as DNA/siRNA instability resulting in unexpected degradation, low cell membrane penetration efficiency, and inability to reach the nuclear zone for gene expression. It is believed that the LDH-mediated cell transfection not only can protect the DNA/siRNA from immature degradation but also can effectively penetrate the cell membrane and readily release the nucleotides into cytoplasm near the nucleus, leading to high transfection efficiency and prolonged gene expression. Choy *et al*. firstly revealed the cellular uptake mechanism of the LDH nanoparticles (~150 nm), they were shown to primarily internalize into cells *via* an energy-dependent endocytic pathway, clathrin-mediated endocytosis [8]. Interestingly, given that the clathrin-mediated endocytosis is the most common

internalization pathway in all mammalian cells, the LDH nanoparticle might be able to pass through all type of cells membrane, suggesting its high cell penetration capability as drug delivery system. It is possible that the LDH is transported to endosomes and subsequently to the Golgi apparatus and/or lysosomes after internalization, following the typical clathrin-mediated trafficking pathway, which was illustrated in Figure 2.2 [9]. It has been proved that the gene expression or specific gene silencing occurred six to eight hours after the LDH-mediated cell transfection, suggesting that the LDH host could efficiently release the DNA/siRNA into the cytoplasm [4,10]. The rapid gene expression/silencing could be explained by several steps: (1) The DNA/siRNA loaded LDHs hybrids (50~250 nm), which provided overall positive charge, could be attracted by the negatively charged cell membrane and rapidly adhered to the surface of the membrane; (2) After the adsorption, the LDH host could efficiently penetrate the cell membrane *via* clathrin endocytosis pathway and quickly enter the cytoplasm; (3) Eventually, the DNA/siRNA could be released near the nucleus when the LDH host dissolves, therefore the plasmids could easily to enter the nuclear zone resulting in expression or targeting specific mRNA for gene silencing [9]. The cellular uptake of LDHs increased in a concentration-dependent manner up to the dose of 200 μg/mL. This could be explained by the receptor-mediated endocytosis employed by the LDHs internalization mechanism. Moreover, the cellular uptake amount of LDHs was highly particle size-dependent, the clathrin-mediated endocytosis would select the LDH nanoparticles ranged from 50 to 200 nm for penetrating cells and could achieve high uptake and long retention in cells, whereas the LDHs over 200 nm did not select specific cellular entry [8].

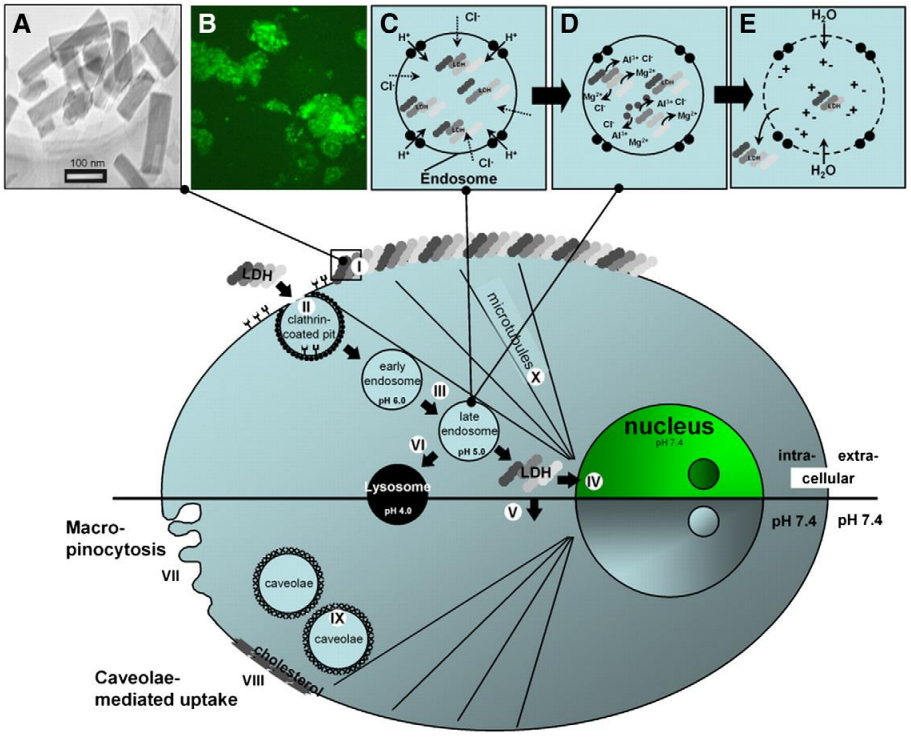

Figure 2.2. Schematic illustration of LDH-FITC nanoparticle intracellular fate. (A) TEM image of LDH-FITC nanoparticles; (B) CHO cells transfected with LDH-FITC nanoparticles; (C) Pumping protons into the endosome to facilitate acidification for subsequent proteolysis of nutrients, followed by an influx of chloride ions; (D) Acid-driven dissolution of LDH-FITC nanoparticles in the late endosome to buffer acidification and ions were released; (E) Entrance of water molecules to the endosome due to an increase in ionic strength, leading to osmotic swelling and endosome burst, which releases LDH-FITC nanoparticles into the cytoplasm. Step I. Adhesion of LDH-FITC nanoparticles to the cell membrane; II. Clathrin-mediated endocytosis; III.Endosomal changes; IV. Nuclear localization of LDH-FITC; V. Cytoplasmic distribution of LDH-FITC; VI.Lysosomal pathway; VII.Unspecific uptake through macropinocytosis. VIII–IX. Caveolae-mediated endocytosis; X. Microtubule directing the freed LDH-FITC nanoparticles to the nucleus [9].

2.1.1.2. Small Nucleotide Intercalation with LDH Nanoparticles

In 2000, Choy *et al*. firstly intercalated c-myc (a gene overexpressed in cancer cells) antisense oligonucleotide into the inner layers of Mg-Al LDH nanoparticles simply *via* ion-exchange reaction [18]. LDHs nanoparticle was prepared *via* co-

precipitation of mixing Mg/Al ions with NaOH (pH=10). After the ion-exchange reaction, an extended basal spacing was obtained indicating that the oligonucleotide was successfully intercalated into LDH layers. Cellular internalization experiments were then performed by employing FITC as a reporter molecule; a significant uptake of cellular DNA/LDH hybrid was observed (Figure 2.3A). Moreover, the longer the time of cell exposure to LDH hybrids, the greater the cellular uptake rate (Figure 2.3B). These experiments went on to prove that, not only could the c-myc/LDH hybrids be internalized by cells, but also the antisense oligonucleotides were involved in cell metabolism. They exposed HL-60 cells to the AS-myc-LDH hybrids at a concentration of 20 μM for four days. A strong suppression of cancer cells growth (65%) was detected, showing that the LDH nanoparticles can deliver small nucleic acid into target cells. They also found that such inhibition of cell growth was time and dose-dependent [9].

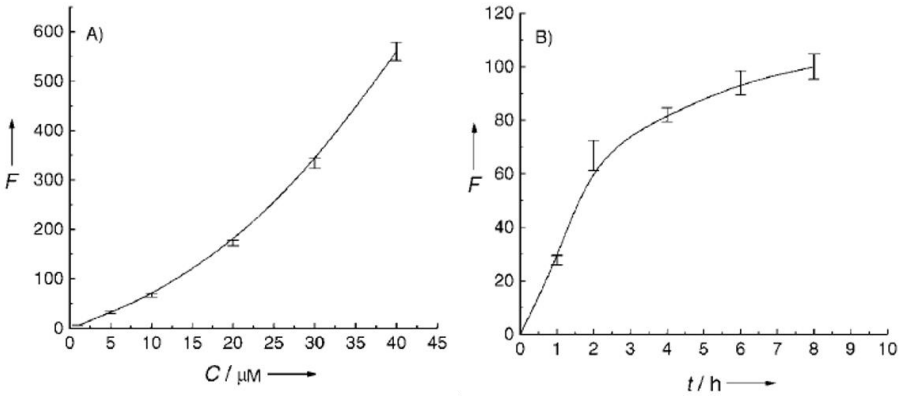

Figure 2.3. Kinetic profiles of FITC-LDH internalizing into cells at A) increasing concentration of hybrids and at B) different exposure times [2].

Small interfering RNAs (siRNAs) have emerged in medical research for diseases caused by single gene mutation because of its ability to silence a specific gene, yet its application was limited due to their instability both *in vitro*

and *in vivo* [11]. In 2010, Ladewig *et al*. employed the Mg/Al-LDH nanoparticles as siRNA carrier to penetrate mammalian cells membrane for specific gene silencing [12]. The anti-MAPK1 (ERK2) siRNA/LDH complexes were synthesized following Xu *et al*.'s protocol published in 2006 [13]. HEK293Tcells were transfected with anti-MAPK1 siRNAs using both Lipofectamine and LDH nanoparticles and harvested after 8–48 hours incubation. Western blotting showed that a significant ERK2 gene knockdown occurred after eight hours' siRNA/LDH exposure and lasted at least another eight hours (Figure 2.4). After 24 hours' incubation, the knockdown of target gene expression was still able to be detected in cells transfected with siRNA/Lipofectamine; whereas relatively weak gene suppression was observed in cells exposed to the siRNA/LDH nanoparticles. These results showed that the siRNA/LDH could achieve a faster and more effective target gene knockdown with less functioning time, suggesting that the LDH drug delivery system possessed higher membrane-penetrating and drug controlled-releasing efficiency *in vitro.*

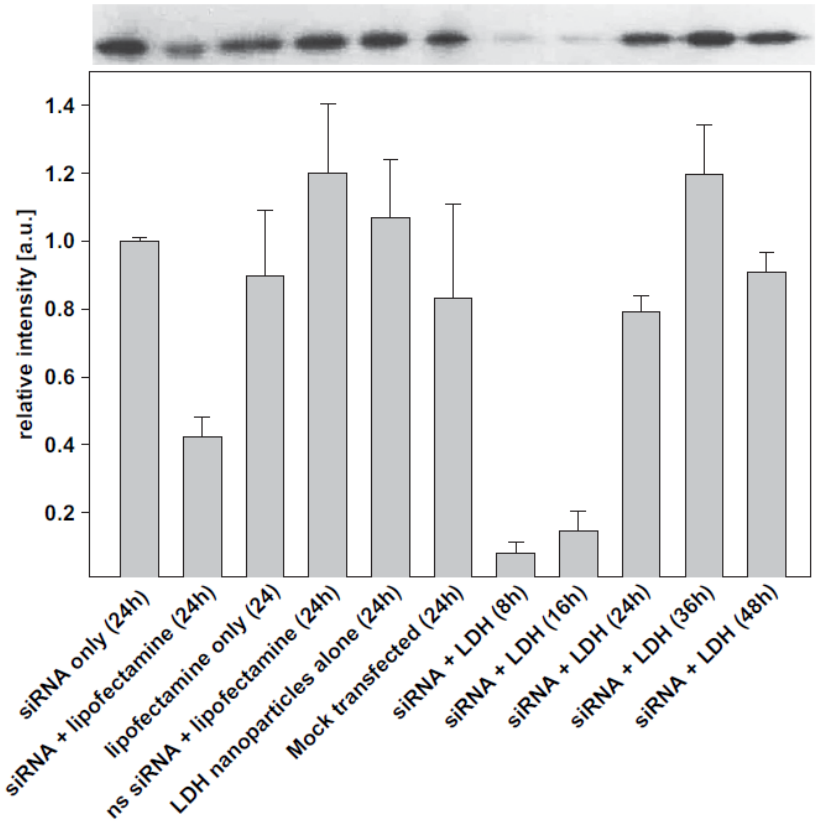

Figure 2.4. The knockdown profile of ERK2 by LDH delivered anti-MAPK1 (ERK2) siRNA to HEK293 cells [12].

The LDH system was employed to deliver siRNA into cortical neurons to develop gene therapies targeting neurological diseases caused by single gene mutation such as Huntington's disease [10]. The siRNA sequence was covalently coupled to the 6-FAM fluorophore at the 5' end. Then the siRNA/LDH hybrids were synthesized at 37°C in an aquatic environment and the drug loading was achieved at a mass ratio of 1:1 (siRNA: LDH). Cortical neurons were then exposed to 1.0 µg/mL of siRNA/LDH for 4 and 24 hours. They found that over 80% of neurons were transfected with 6FAM-siRNA/LDH complexes in four hours but no significant increase was observed after 24-hour incubation (Figure 2.5). Furthermore, the Deleted in Colorectal Cancer (DCC) gene knockdown was carried out on cortical neurons. When cells were transfected

with siRNA/LDH hybrids for further 48 hours, an average knockdown efficiency of 49% on cortical neurons was obtained, leading to a conclusion that efficient, targeted gene silencing in neurons can be achieved by LDH mediated siRNA delivery (Figure 2.6).

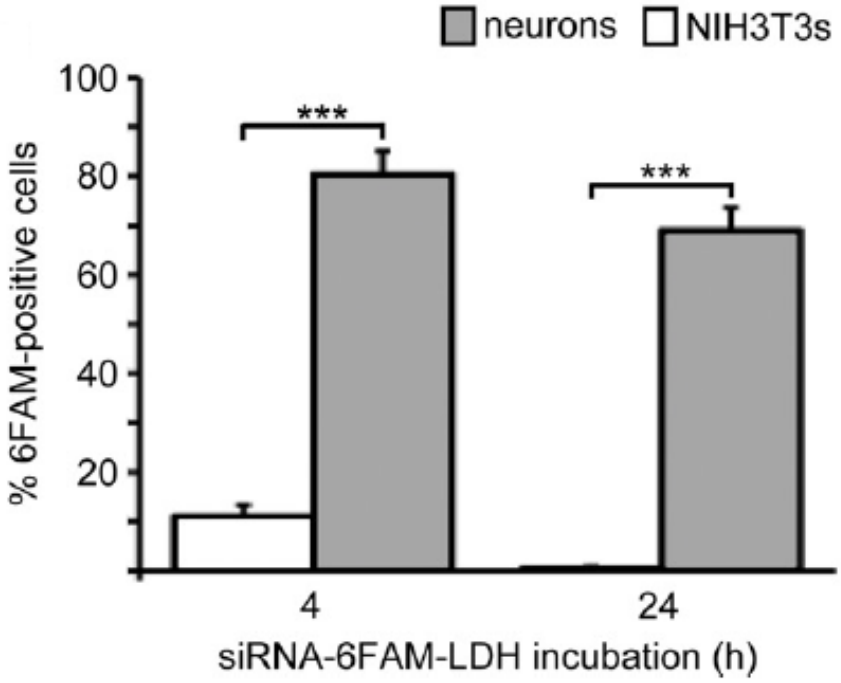

Figure 2.5. The 6FAM labeled complexes uptake efficiency of neurons and NIH3T3 cells after 4 and 24-hour incubation [10].

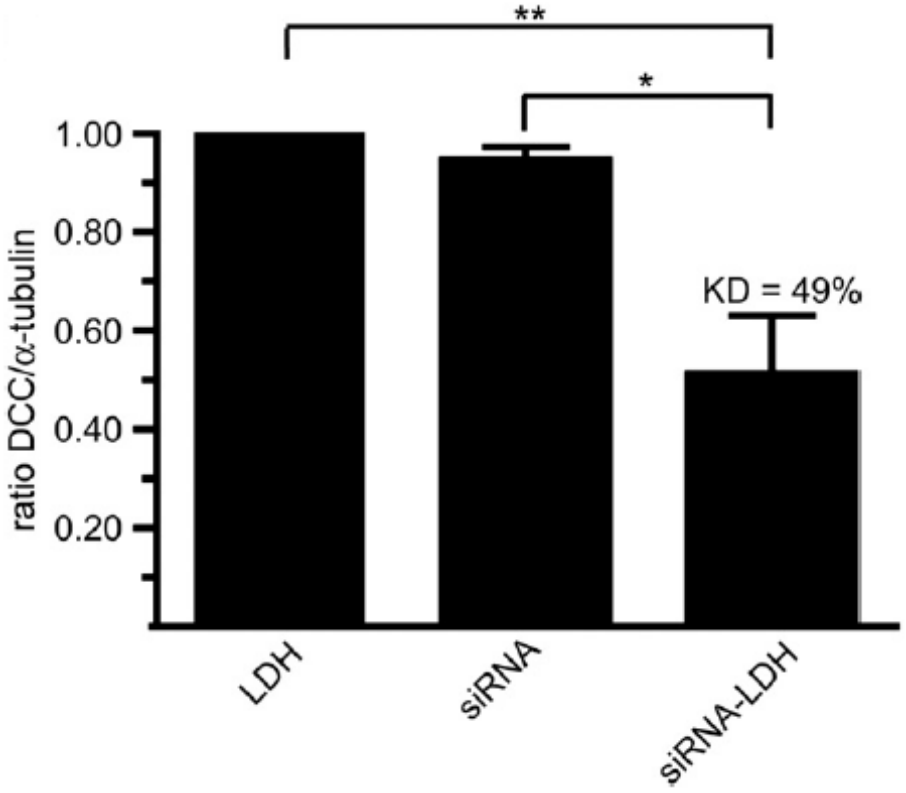

Figure 2.6. The knockdown profile of DCC by LDH mediated delivery of siRNA to neurons [10].

2.1.1.3. Large Nucleotides Intercalation with LDH Nanoparticles

It was also demonstrated that even relatively larger DNA fragments (100–500bp) could be associated with LDH nanoparticles. Desigaux *et al*. investigated the interaction of DNA fragments with Mg/Al, Mg/Fe and Mg/Ga nanoparticles separately [3]. DNA/LDH hybrids were synthesized as described [2]. LDH/DNA hybrids were recovered after 48 h of aging by ultracentrifugation at 13,000 rpm, extended interlayer distances were detected in all three LDH systems, from ~0.77 nm of all nitrate parent LDHs to ~2.11 nm (Mg/Al), ~1.80 nm (Mg/Fe), and ~1.96 nm (Mg/Ga), respectively. They further explored the Mg/Ga LDH's ability to deliver DNA fragments into carcinoma HeLa cells. DNA fragments including short fragments, long fragments and DNA plasmid were modified with fluorescent signal YOYO-1 and intercalated into Mg/Ga LDH nanoparticles.

Carcinoma HeLa cells were exposed to the fluorescent DNA/LDH complexes for two hours and examined under a microscope. As we can see in Figure 2.7, most of the fluorescent signals could be clearly observed in the cell cytoplasm and the cell nucleus as well as around the cell membrane. These data directly proved that the relatively larger nucleotides or even DNA plasmids could be efficiently accumulated within cells by employing LDH mediated delivery.

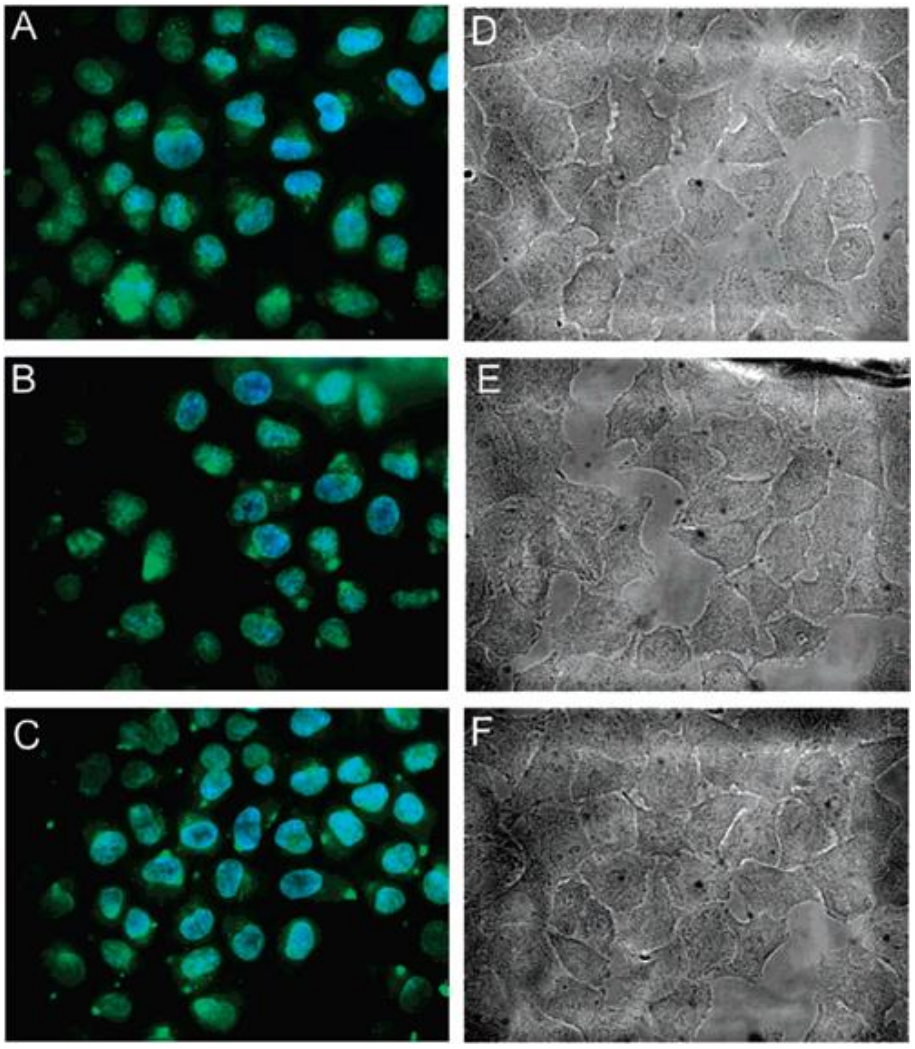

Figure 2.7. The image of hybrids cellular uptake by HeLa cells. Cells were incubated with LDH/DNA including short DNA fragment (A, D), long DNA fragment (B, E) and DNA plasmid (C, F). D-F corresponds to the transmission images of the same cells [3].

The interaction of DNA plasmids in various size with $Mg_2Al(OH)_6NO_3$ LDH nanoparticles under different experimental conditions was investigated by Ladewig *et al*. [14]. With the increasing size of plasmid, fewer plasmids loading efficiency was evident (Figure 2.8). Moreover, the variation of an experimental condition such as increasing the temperature during the reaction can increase the LDH loading ability, yet an expected enhanced LDH loading capacity (DNA: LDH ratio) was not observed. This could be accounted for by the incompletion of anion change between NO^{3-} with DNA even through in some case the amount of DNA is far more than required, which is much different from the case of small DNA fragments [15-18].

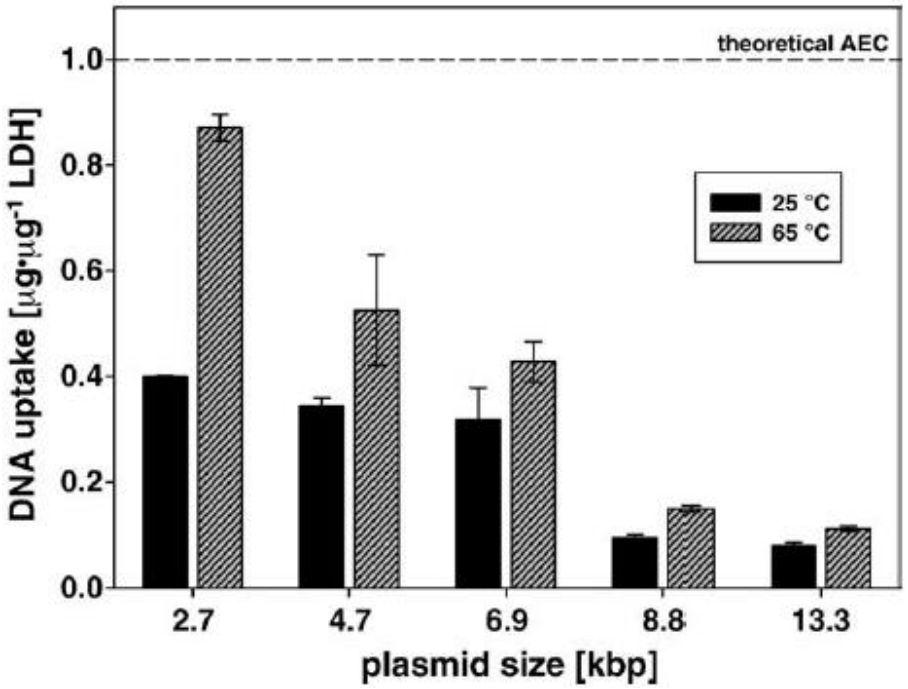

Figure 2.8. The LDH loading efficiency of LDH with plasmids in various sizes under different experimental conditions [14].

Masarudin *et al*. have successfully transfected Vero3 (African monkey kidney) cells with the plasmid pEGFP-N2, which contains the GFP gene employing Mg/Al-LDH nanoparticles [4]. The cells were exposed to the plasmid-LDH

hybrids (0.1 mg/mL) for 24 hours at 37°C and a clear fluorescence was observed under microscope (Figure 2.9), indicating that not only was the pEGFP-N2 plasmid safely delivered into targeted cells by the LDH carriers, but also could be successfully expressed and involved in cell metabolism. Furthermore, the delivery efficiency of LDH was compared to another commercial transfection reagent, Lipofectamine™ 2000. The Vero3 cells were treated with plasmid-LDH hybrids and a Lipofectamine-plasmid mixture containing the same amount of plasmid for 48 hours. Fluorescence was observed at 6–8 h post-treatment on LDH group, whereas it took 10 hours to detect the signal from Lipofectamine group (Figure 2.10). Even though the transfection efficiency between both vectors was comparably similar, the authors pointed out that, from the cost-operative point of view, their system still benefited. It is indeed a large advantage that the LDH system can be synthesized with low cost reagent and loading drug could be easily achieved *via* the anion exchange mechanism.

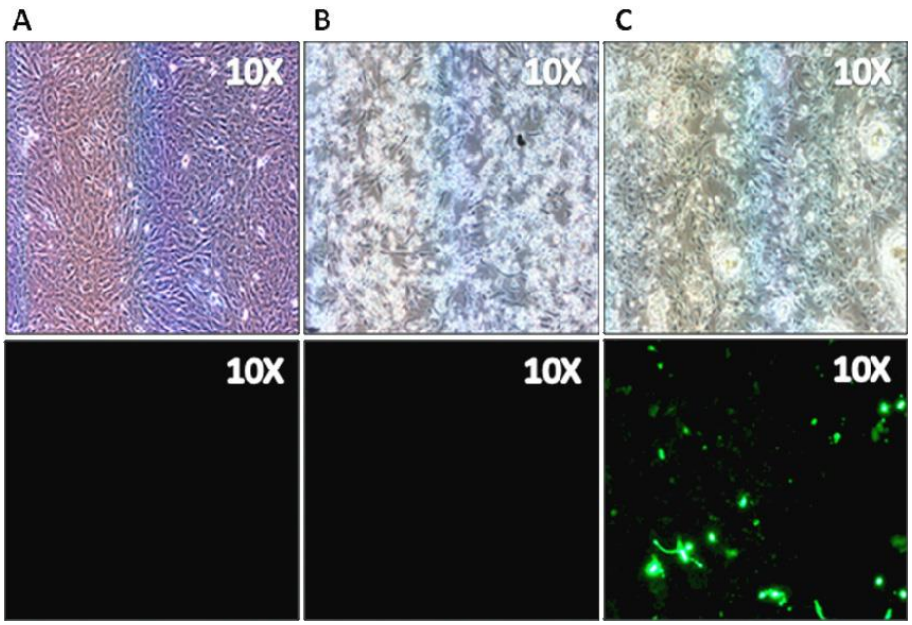

Figure 2.9. 24 hours' exposure of Ver3 cells to A) pEGFP-N2 alone; B) Mg/Al-LDH alone; C) Plasmid-LDH hybrids. Fluorescence was observed in group C after 6 hours but was not detected on group A and B [4].

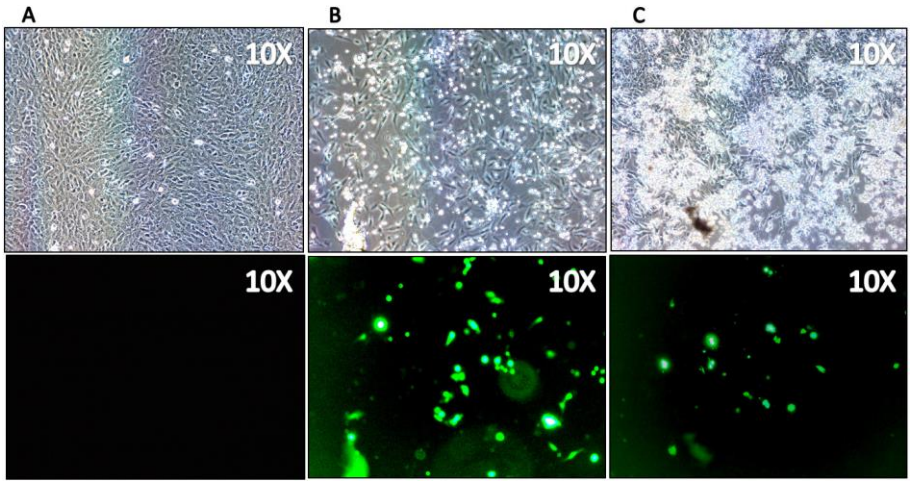

Figure 2.10. 24 hours' exposure of Ver3 cells to A) no treatment; B) plasmid-LDH hybrids; C) Lipofectamine-plasmid mixture [4].

2.1.2. The Delivery of Non-Steroidal Anti-Inflammatory Drugs (NSAIDs)

Non-steroidal anti-inflammatory drugs are aromatic organic compounds associating with carboxylic groups that can be easily ionized; therefore, it is possible that these drugs can be intercalated into LDH layers simply *via* ion-exchange [19]. It is believed that the synthesis of the NSAIDs/LDH hybrids could improve drug solubility in an aquatic environment and enhance drug absorption by living organisms [20].

2.1.2.1. The LDH Application with Fenbufen

Fenbufen (FBF) is normally used in relieving cancer pains as well as in the treatment of rheumatoid arthritis and osteoarthritis [21]. However, their negative effect on both the gastrointestinal tract and the central nervous system limit its

application. The synthesis of the FBF/LDH complexes with the controlled release is expected to alleviate these side effects [22].

In 2004, Li *et al*. first intercalated FBF into the inner layer of the LDH nanoparticles by co-precipitation in a nitrogen environment [23]. Given that the original gallery height is 0.39 nm and the thickness of brucite-like layer itself is 0.48 nm [2,24], XRD analysis showed that the spacing between LDH layers expanded to 1.87 nm after intercalation with FBF, which was consistent with previous study [25]. A significant impact on the FBF-LDH intercalation was observed regarding under differing pH value (Figure 2.11). Space increased from 1.87 nm to 3.00 nm while the pH value increased from 8 to 13, suggesting a possible change of interlayer FBF from a monolayer to a bilayer structure. They also investigated the effect of varying the chemical composition of the host layers to the intercalation efficiency of FBF. The same interlayer spacing of 2.35 nm was obtained regardless of different chemicals used to synthesize LDH (Figure 2.12).

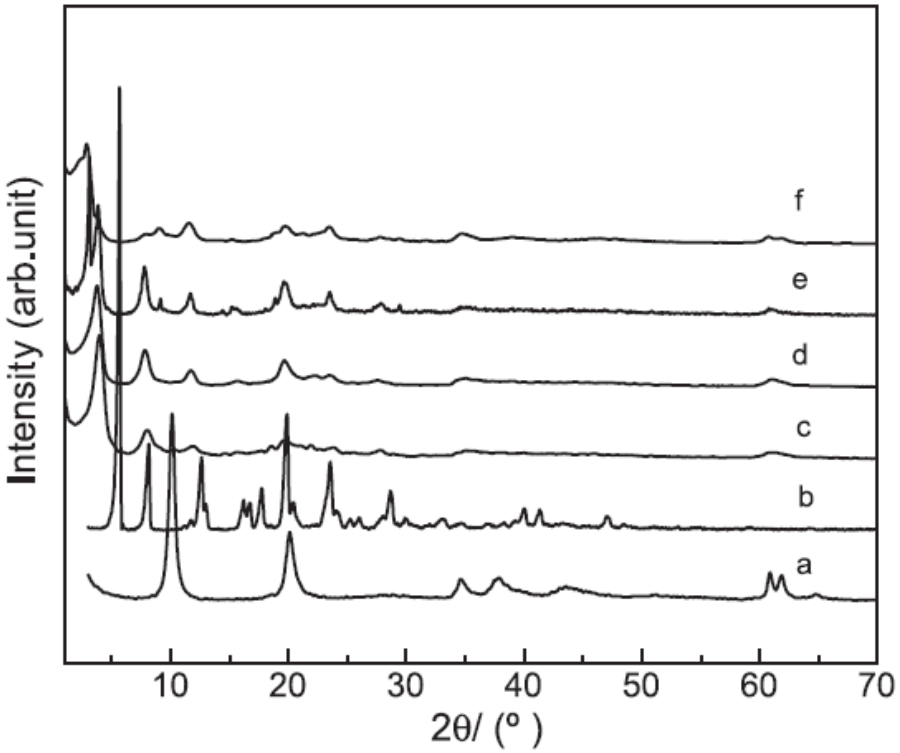

Figure 2.11. XRD patterns of Mg/Al-LDH-FBF synthesized under different pH conditions. (a) LDH; (b) FBF; (c) pH 8; (d) pH 10; (e) pH 12; (f) pH 13 [23].

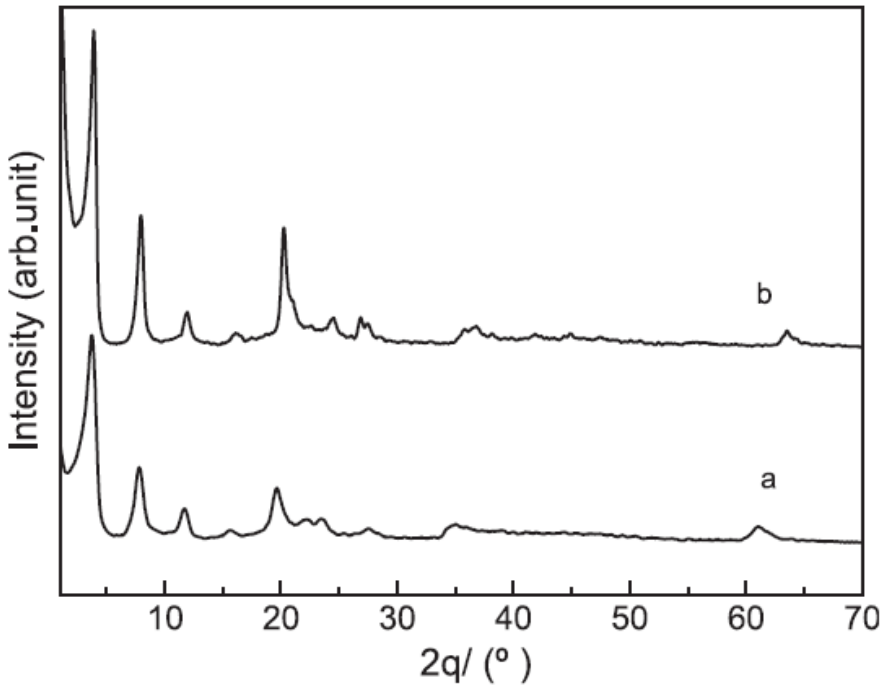

Figure 2.12. XRD patterns of FBF-LDH with different chemical composition. (a) Mg/Al-FBF-LDH; (b) Li/Al-FBF-LDH [23].

The FBF intercalations with Mg, Al-LDH and Mg, Al, Fe-LDH have been explored by Del Arco *et al*. following three different preparation methods, namely co-precipitation, ion-exchange, and reconstruction, as well as the solubility of the drug/LDH complex in a water environment [26]. Despite a failed synthesis of FBF/Mg-Al-Fe LDH using reconstruction method (the present of Fe inhibited the intercalation of the drug into LDH); other routes achieved a drug loading range of 31%–44%. In addition, the presence of the LDH was proven to significantly enhance the solubility of FBF in an aquatic environment, irrespective of the LDH acting as an additive or hosting matrix.

The controlled release study of FBF/LDH hybrids was also performed by Li *et al*. [27]. Both Mg/Al-LDH and Li/Al-LDH were employed to intercalate with FBF and were re-suspended in phosphate buffer at pH 7.8. They observed that both hybrids triggered fast drug release in the first 10 minutes and reached the maximum amount of 40% (Li/AL-LDH) and 59% (Mg/Al-LDH) over 120 minutes, indicating that the Mg/AL-LDH hybrids release system were more efficient. What is more, the slower linear increase after the rapid release of FBF from the Mg/Al-LDH inferred that the Mg/Al-LDH was a more sustained system for drug release, which suggests that Mg/Al-LDH materials are more suitable for a controlled-release host. However, the application of LDH can be limited in the stomach (pH 1.2). Taking this into account, Evans *et al*. coated the Mg/Al-LDH with enteric polymers and explored the controlled release of the new complexes [27]. The pure FBF/LDH hybrids and the coated complex were separately re-suspended in an aqueous medium with an initial pH at 1.2 for 2 hours followed by 6.8 for another 2 hours, and eventually at 7.4 for additional 5 hours. They found that pure FBF/LDH hybrids achieved a complete FBF release within a

very short time, which proved that pure LDH was not capable of delivering drugs in certain realistic conditions; whereas the modified complexes survived at pH 1.2 and gradually released FBF while the pH increased. However, only the FBF-LDH coated with Eudragit S 100 managed to appear in a liner manner and finally peaked at 70% release efficiency over 9 hours, suggesting a sustained but slow drug release occurred (Figure 2.13). It can be concluded that unmodified LDH nanoparticles are not versatile carriers in the application, and some materials used for LDH modification somehow reduced the LDH drug release capability. Therefore, finding appropriate LDH modification methods for specific conditions is crucial for their further application.

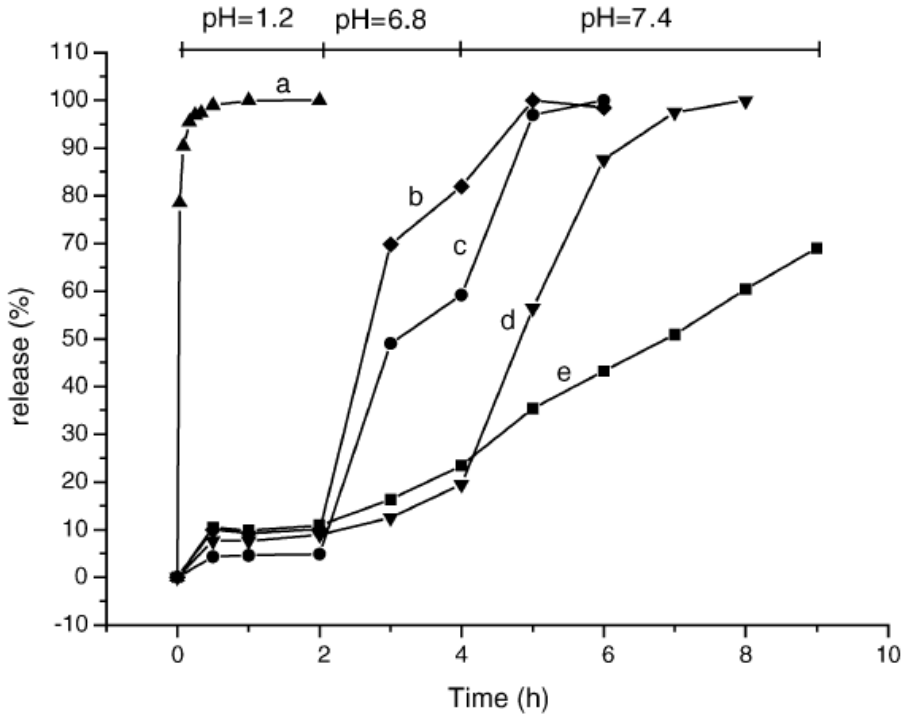

Figure 2.13. FBF release profile of (a) FBF-LDH (complexes); (b) FBF coated with Eudragit L 100; (c) complexes coated with Eudragit L 100; (d) FBF coated with Eudragit S 100; (e) complexes coated with Eudragit S 100 [27].

2.1.2.2. The LDH Application with Naproxen

Given that Naproxen (Np) can exhibit analgesic and anti-inflammatory effects, it is commonly used for the treatments of osteoarthritis and musculoskeletal disorders [28,29]. However, Naproxen has been characterized by its poor solubility in water and readily cell-absorbing, which might cause gastric and duodenal ulcers formation in application [30-32]. It is hoped that the LDH mediated drug delivery system could help Naproxen to reduce adverse second effects and produce a controlled-release formulation.

Wei *et al* have firstly obtained the Np-LDH complex and studied its stability under different temperature condition [33]. Mg/Al–NO_3 LDH was synthesized by following the protocol previously published by Meyn *et al* [34]. Naproxen was intercalated into LDH nanoparticles simply *via* ion exchange mechanism in a water solution with final pH of 8.0 and the mixture was incubated at 70˚C under nitrogen environment for more than 39 hours. Since the original interlayer spacing of Mg/Al LDH precursor they observed was 0.854 nm and the thickness of LDH basal layer was 0.480 nm [14], XRD detected an extended interlayer distance of 2.347 nm of Np-LDH complex, giving an interlayer increase of 1.867 nm. The XRD pattern proved that the Naproxen was successfully associated with Mg/Al LDH nanoparticles. Thermal decomposition experiments were conducted in a temperature range from 0˚C to 700˚C and monitored by situ FT-IR, situ HT-XRD and TG respectively. They found out that pure naproxen started to decay at 170˚C and achieved complete decomposition at about 250˚C. However, the naproxen in Np-LDH maintained stable at 170˚C and the decomposition did not occur until the temperature reached 250˚C. The thermo-gravimetric analyses demonstrated that the presence of the LDH nanoparticle

significantly enhanced the thermal stability of intercalated naproxen, suggesting that the inorganic layered material could have prospective application as the basis of a novel drug delivery system.

Hou and Jin have studied the effects of pH value on the absorption of naproxen on LDHs as well as the release of naproxen from the Np-LDH hybrids [42]. A similar LDH preparation method [35] was utilized to synthesize the Zn-Al LDH nanoparticles. A series of $ZnCl_2 \cdot 6H_2O/AlCl_3 \cdot 6H_2O$ mixed solutions at different molar ratio but containing same total metal ion concentration of ~0.5 mol/L were prepared and co-precipitated by adding diluted ammonia water to form Zn/Al LDH. A given amount of naproxen (15 mmol/L) was exposed to Zn/Al LDH individually at pH 8.5 to examine the naproxen absorption efficiency. According to these authors, the maximum naproxen uptake amount, or as the authors referred equilibrium values (Aeq value), was observed after 160 minutes' incubation irrespective of the LDHs types (Figure 2.14). They also demonstrated that these absorption isotherms could adapt the Langmuir model. The study of pH effect on the uptake of naproxen was carried out in the range of pH value 6-11. They found out that the Aeq values decreased in all four LDHs systems while the pH values of environment increased. This could be simply explained: the increasing environmental pH value could effectively reduce the LDHs nanoparticles positive charge density resulting in less electrostatic attraction between naproxen and LDHs basal layers and the Aeq values decreased.

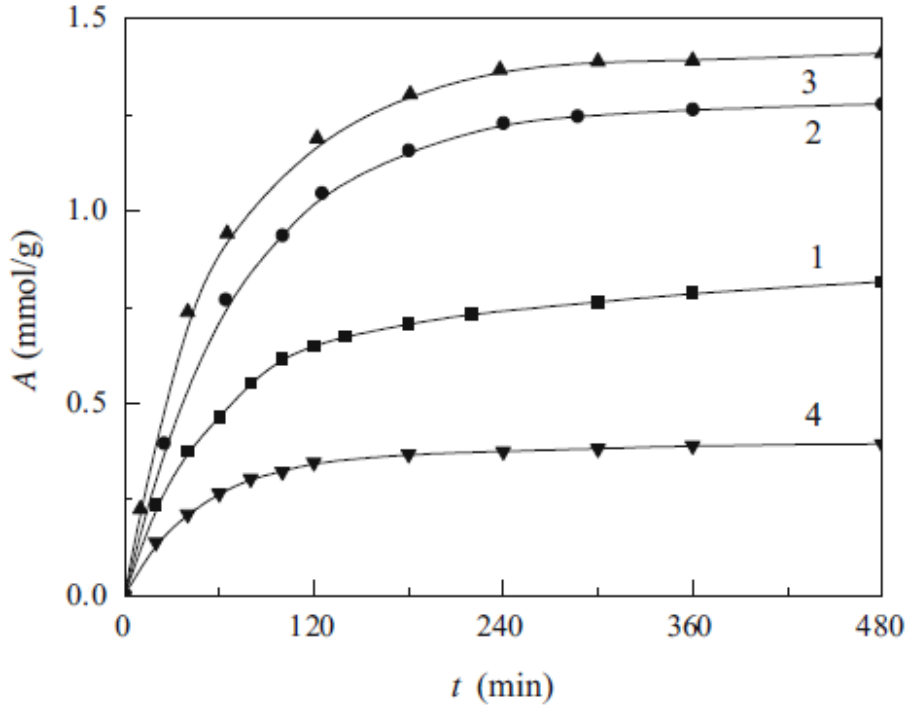

Figure 2.14. The time course of naproxen adsorption on different LDHs Samples. 1) $Zn_{0.48}Al_{0.52}$-Cl LDH; 2) $Zn_{0.59}Al_{0.41}$-Cl LDH; 3) $Zn_{0.63}Al_{0.37}$-Cl LDH; 4) $Zn_{0.68}Al_{0.32}$-CO_3 LDH [35].

The profile of LDH nanoparticles loaded with other NSAID, such as Flurbiprofen, Ibuprofen, Diclofenac, Indomethacin, were widely investigated as well [35-39]. In a combination of discussion about Fenbufen and Naproxen, there is three possible conclusions: (1) NSAID-LDH synthesis; Two different methods were employed for LDH synthesis, co-precipitation and reconstruction. It is believed that co-precipitation showed more advantages over reconstruction. The co-precipitation leads to a perfect single layered structure whereas the reconstructed LDH could be “contaminated” by other unwanted anions (a layered MgAl-CO_3 phase existed in MgAl-OH). Moreover, the co-precipitation LDHs possessed a larger gallery than the reconstructed LDHs, indicating a relatively higher drug loading efficiency; (2) Improvement of loaded drug “survival” ability; it has been discovered that the drug-loaded LDH could

remarkably enhance the drug solubility in either the aquatic environment or in the gastric fluid environment. The thermo-gravimetric analysis also showed that drugs appeared to be more stable after the intercalation with LDH nanoparticles. The presence of LDH nanoparticles could not only prevent loaded drugs from unexpected degradation but most importantly, lead to an enhancement of gastric mucus permeation and protection of gastrointestinal mucus from ulcer-genic activity; (3) Sustained release of drugs; controlled drug release could be achieved in both gastric environment (pH 1~2) and intracellular environment (~pH 7.5). As discussed above, the appropriate modification is required for drug release to appear in a liner manner at pH value of 1~2. However, at a pH value of 7.5, the different mechanism, ion exchange, was the most responsible for the sustained drug release.

.

2.1.3. The Delivery of Anti-Cancer Drugs

Chemotherapies with cytotoxic drugs have been widely developed and employed for cancer treatment. However, the frequent employment of these drugs often leads to the development of cancer cell resistance to these agents during treatment [40-42]. The complex nature of cancer cells presents a great obstacle in developing ideal cancer chemotherapy with high drug efficacy and low side effects [43]. However, it might be achieved by drug-LDH Nano-hybrids. The application of LDH nanoparticles for cancer therapy with several commonly used anti-cancer drugs is summarized.

2.1.3.1. The Delivery of Methotrexate (MTX)

Methotrexate (MTX) is an anti-metabolite and anti-folate drug, which can lead abnormal cells through programmed cell death by effectively interfering with cell

metabolism. These have been used in treatment for certain human cancers, such as osteosarcoma (bone cancer) and leukemia [44].

Choy *et al*. have explored the intercalation of MTX with LDH nanoparticles in a series of studies [40,45,46]. It has been demonstrated that the cellular uptake of MNNG/HOS (osteosarcoma cells) to LDH-associated MTX was significantly enhanced [47]. As shown in Figure 2.15 A, the concentration of MTX in MTX-LDH treated cells was considerably higher than that in the cells treated with MTX only at all incubation time. Moreover, cytotoxicity test showed that MTX-LDH was more toxic than MTX only to MNNG/HOS cells (Figure 2.15 B) [46], as well as Saos-2 and MG-63 cells (data not shown) [45]. These results indicated that the MTX-LDH Nano-hybrids could penetrate the cell membrane more effectively than MTX only, leading to enhanced drug efficacy. One more thing to be noted here is that the LDH nanoparticles along had no influence to cell viability at levels up to 500 μg/mL.

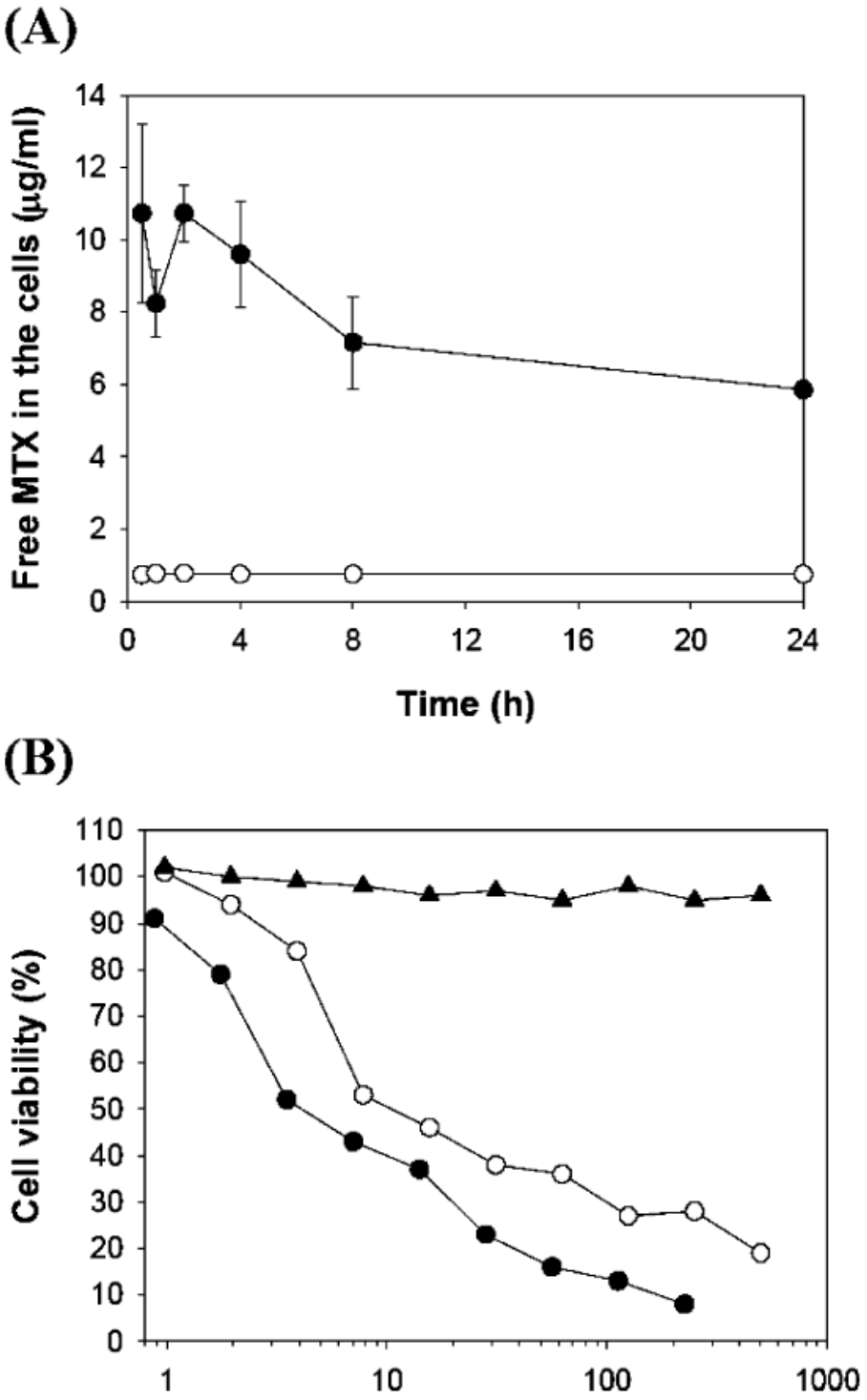

Figure 2.15. A) Cellular uptake profile of MTX in MNNG/HOS cells treated with MTX only (○) or MTX-LDH hybrids (●). B) Cell viability of MNNG/HOS cells treated with LDH (▲), MTX only (○) and MTX-LDH hybrids (●). [46]

Given that the MTX could deactivate the cell's metabolism in the manner of inhibiting DNA synthesis and eventually contribute to anti-proliferation [47],

these authors also investigated the effect of MTX and MTX-LDH on cell cycle distribution to further confirm the MTX-LDH efficacy [46]. Cells were incubated with MTX and MTX-LDH hybrids respectively over 20 hours, resulting in drug accumulation in the G1 phase and certain amount of cell death in the S and G2 phase (Figure 2.16). However, it is worthy to note that the inhibition of DNA synthesis was more successful in cells treated with MTX-LDH hybrids than those with MTX only, giving 75.09% vs. 63.8% at 10 μM/mL, and the gap even increased at higher drug concentrations.

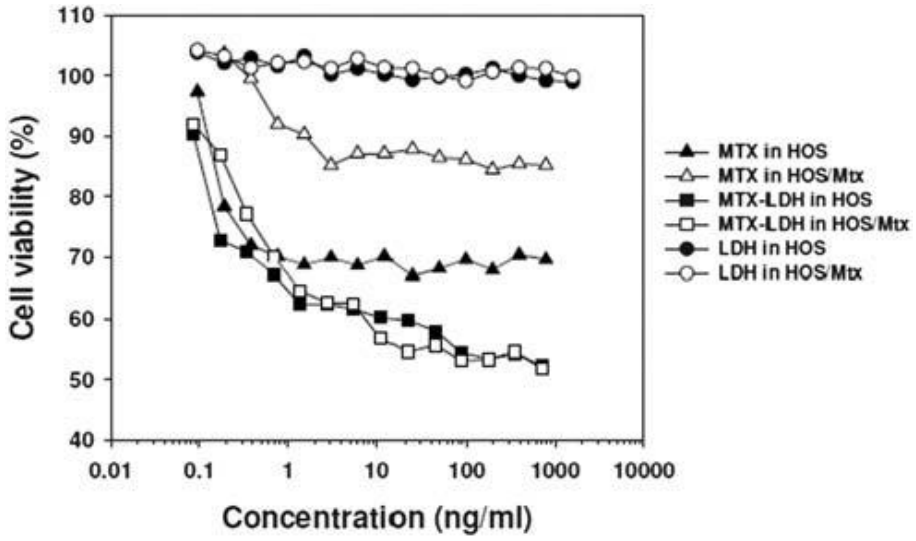

Figure 2.16. Cell growth inhibition profile of LDH, MTX only and MTX-LDH hybrids in wild-type HOS and HOS/Met cells [46].

Subsequent study revealed that the MTX-LDH hybrids effective penetration through the cell membrane and its high cytotoxicity to cancer cells could be accounted for by not only the cellular retention of the MTX-LDH hybrids in cancer cells but also the clathrin-mediated endocytosis pathway employed by the hybrids, which is completely different from the cellular uptake mechanism for MTX only. Amazingly, they also found out that the MTX-LDH hybrids could overcome drug resistance [40]. The inhibition of cell proliferation of the MTX

resistance cells (HOS/Mtx) treated with free MTX was significant decreased compared to wild-type HOS cells, indicating that drug efficacy was dramatically compromised due to the MTX resistance. On the other hand, both HOS cells and HOS/Mtx cells were remarkably inhibited to a similar degree. These results could also be explained by the uptake mechanism that MTX-LDH hybrids employed. In addition, 5-fluorouracil (5-Fu) was also encapsulated into LDH *via* co-precipitation to further evaluate the potential of drug-LDH complexes as cancer chemotherapy agents [47]. It was showed that both 5-Fu and MTX were intercalated in LDH nanoparticles, achieving higher efficiency of inhibiting cancer cell proliferation in a manner of concentration dependence.

2.1.3.2. The Delivery of Camptothecin and Podophyllotoxin

Camptothecin (CPT) and Podophyllotoxin (PPT), inhibitors of topoisomerase I and II during DNA synthesis and eventually leading to cell death, have been studied as potential cancer therapeutics [48-53]. Like NADIS, the application of these drugs has been significantly hindered by several deficiencies such as poor water solubility, fast metabolic inactivation, drug resistance and poor bioavailability [53]. However, improvement could be achieved by employing LDH nanoparticles.

Tyner *et al*. have proved that the association with LDH nanoparticles could remarkably enhance the CPT solubility in an aquatic environment [54]. They observed an approximately threefold increase in solubility of CPT-LDH hybrids compared to the naked drug, which was further confirmed by Dong *et al*. [55] and Liu *et al*. [56]. Controlled release experiment obtained similar results to NSAIDs associating with LDH, which could be summarized: when drug-LDH

complexes expose to a pH 4.2 environment, rapid drug release is obtained due to dissolving of the LDH host; however, sustained drug release could be achieved in a pH 7.2 environment, where the ion exchange was the most responsible for releasing the drugs [54]. Xue *et al*. firstly modified the procedure of PPT-LDHs synthesis to achieve higher PPT loading efficiency [57]. They co-precipitated tyrosine (Tyr) with LDH resulting in Tyr incorporation into the interlayer space. Therefore, the interlayer space was pre-opened and an environment of inviting drugs was created. Eventually, a drug loading efficiency of 34% w/w of drug/material was achieved. Preliminary anticancer experiments *in vitro* revealed that tumor cells growth was significantly inhibited by PPT-LDH hybrids, representing higher tumor suppression effects. This theory was further demonstrated by Qin *et al*. [58]. They found out that the PPT-LDH hybrids not only showed higher efficacy to inhibit cancer cells growth compared to naked PPT but also showed a long-term suppression effect and were more readily internalized into tumor cells *in vitro*. *In vivo* experiments for evaluating PPT-LDH anti-tumor efficacy were conducted on nude mice bearing HeLa tumor. PPT-LDH hybrids and naked PPT were intraperitoneally injected into mice at a PPT dose of 5 mg/kg body weight. They discovered that remarkable therapeutic tumor suppression 46.39% inhibition rate was achieved by PPT-LDH complexes (Figure 2.17). In addition, given that high dose of PPT has a life-threatening toxicity to mice [59], it was revealed that the presence of LDH could remarkably reduce the toxicity of PPT, representing the reduction of side effects seen with PPT.

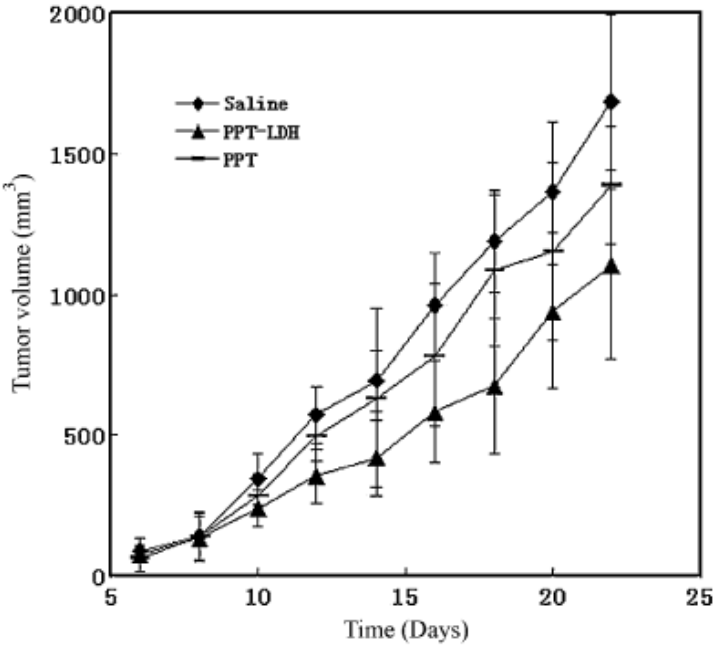

Figure 2.17. Tumor suppression effect by naked PPT and PPT-LDH injected into mice at a dose of 5 mg PPT/kg measured by solid tumor growth. [58]

2.1.4. Recent Applications of LDHs in Medicine

Researchers have used LDHs nanoparticles to impart functionality to a variety of devices in medicine. For example, Li *et al*. have utilized the LDHs as DNA vaccine delivery vector to enhance anti-melanoma immune response [60]. Pristine LDHs were prepared by co-precipitation method and were mixed and shaken with pcDNA3-OVA plasmid for four hours under 37°C for DNA/LDH complexes synthesis. Two selected types of mice B16-OVA and C57Bl/6 were separately immunized by the DNA/LDH complex. Seven days after the last immunization, these mice were challenged with B16-OVA melanoma cells. They found out that, after the delivery of the DNA/LDH complexes by the intradermal immunization in two types of mice, the presence of the LDHs could assist the plasmid DNA to induce an enhanced serum antibody response significantly greater than naked DNA vaccine. Over 60% tumor-free and inhibition of melanoma growth were observed in mice that treated with DNA/LDH complexes,

whereas no tumor-free mice were found in the control group. They further evaluated this vaccination strategy in a model, which was more analogous to the clinical setting. The therapeutic effect of DNA/LDH complexes immunizations was challenged in mice with the pre-established tumor. After a six-day treatment with DNA/LDH complexes in C57BL/6 mice, they observed a significant delay in tumor growth and potent prolongation of mean survival time (from 35 days to 50 days). These results suggested that the LDHs mediated cellular transportation could significantly enhance the therapeutic efficacy of DNA immunization, as well as protective immunity against the tumor.

Chronic otitis media is a common disease often accompanied by recurrent bacterial infection, resulting in the destruction of the middle ear bones. D. Hesse *et al*. employed LDHs as an efficient delivery system for ciprofloxacin in the middle ear *in vivo* [61]. The middle ear implants were individually coated with Mg/Al LDHs loaded with ciprofloxacin. Two groups of Male New Zealand White rabbits (12 each) were infected with Pseudomonas aeruginosa, right after the surgery for group 1 and 1 week later after the implantation for group 2. Clinical examination showed that only two rabbits, one of each group, appeared behavioral syndromes and lost 11% of their initial body weight after four days. The clinical neurological examination showed that only one rabbit developed mild imbalance and mild to severe head tilt throughout the whole examination period after infection, whereas three animals showed vestibular signs in group 2 after the infection. Microbiological examination revealed that more animals in group 2 than that in group 1 (yet only 5 vs.1) were detected germs on blood as well as on Gassner agar. Histopathological examination reported that all the 24 animals were accompanied with pulmonary oedema, yet one in group 2

developed severe meningoencephalitis; the remaining rabbits of both groups showed no inflammation of the brain. All these evidences demonstrated that the LDH nanoparticles impregnated with a medical drug can be used as an effective antibiotic delivery system for the challenge of a forced infection *in vivo*. Moreover, it seems that animals underwent concomitant infection during the prostheses implantation developed a better outcome than subjects that were infected with P. aeruginosaone week after the implantation, suggesting a fast the LDHs drug release and efficiency.

L. Tammaro *et al*. used LDHs nanoparticles to develop a fluoride-releasing dental material, which could constantly release fluoride over time without any initial toxic burst effect [62]. LDHs loaded with fluoride (LDH-F) were incorporated into commercial light-activated restorative material Bis-GMA/TEGDMA dental resin, Fluoride release study showed that an initial rapid release was observed and followed by a release linearly depending on the time (days). Interestingly, the fluoride release inversely depended on concentration, which could reflect the strong influence of the LDHs lamellar clays morphology. Amazingly, these authors also pointed out that the extrapolated release could last up to one year, with a concentration released every day, which is far from the possible adverse fluoride effect. It has been proposed that the failure of dental restorations depends on the degree of which the human dental pulp stem cells (hDPSCs) can survive as well as the sensitivity of these cells to injury to trigger an appropriate repair response[63,64]. Given that even a low amount of fluoride can benefit the growth and differentiation of the hDPSCs, authors further investigated whether the active fluoride-releasing materials could affect the proliferation of hDPSC. It was demonstrated that the materials with four

different LDH-F concentrations (mass fraction 0.7, 5, 10, and 20%) showed no significant inhibition of proliferation on hDPSC. Moreover, the activity of alkaline phosphatase activity (ALP), an early marker of odontogenic differentiation of pulp cells, gradually increased for 28 days during the growth of cells that had been cultured on fluoride-releasing restorative materials (0.7% and 10%), suggesting that the slow release of small amount of fluoride from active material could positively modulate hDPSCs differentiation.

2.1.5. Conclusion and Future Directions

LDHs have been widely employed in medical research as drug carriers. In addition, many bio-molecules have been either attached to the surface of or intercalated into LDHs through co-precipitation or anion-exchange reaction. Some molecules that have been used include amino acid and peptides, ATPs, vitamins, and even polysaccharides [6]. Taken advantage of the unique properties of LDH materials, LDH nanoparticles successfully achieve drug delivery into targeted cells *in vitro* and in some case *in vivo* without side-effects [65]. The LDHs based drug delivery systems are therefore well positioned to overcome many hurdles that usually impede successfully drug delivery [6].

Nevertheless, despite numerous advantages, LDH have been encountering obstacles caused by its nature, some of these hurdles critically limit their future application in medicine and other aspects [6,66]. Firstly, current studies of drug delivery mediated by LDHs are still focused on intercalating small biomolecules (chemo-drugs, small DNAs and siRNAs and peptides). Only a few successful attempts at large molecules have been reported. This might be due to its restricted inner layer space and limited surface area. Large molecules are

believed to attach to the surface of LDH other than being intercalated into inner layers. Therefore, increasing the surface area of LDH could be crucial for loading and delivering large biomolecules. Efforts have been made to modify the LDH synthesis procedure to create LDH nanoparticles with new 3-D structure, the Nano-sheet, which is reported to possess larger surface area [67]. However, this is still a field where new research is required. Additionally, since the relatively large plasmids are attached to the LDH surface, they may not be protected from unexpected degradation unless the hybrids are coated with other polymer films to preserve the drug and LDH host being degraded, which is one of the drawbacks of the naked LDHs delivery system. Other drawbacks, including quick aggregation in cultured solution or PBS, easily decomposed in a critical environment, rapid drug release after transfection *in vitro*, relatively low targeting transportation, have been greatly limiting the biological applications as well. Even though the surface of the LDH is believed hard to be functionalized due to its simple composition, attempts were made to improve LDHs drug delivery efficiency. Tyner *et al*. coated the LDH with disuccinimidyl carbonate (DSC) for improving LDH transportation activity [54]. It was proved that the surface modified samples showed 30-fold more activity compared to control group. Meanwhile, this enhancement to the delivery scheme caused by LDH surface modification could provide potential site-directing of the Nano-hybrids. Efforts were also made to slow down the rapid drug release *in vitro* to achieve sustained drug liberation and prolong drug efficacy. Alcantara *et al*. encapsulate LDHs by two biopolymers: (i) zein, a highly hydrophobic protein and (ii) alginate, a polysaccharide widely applied for wrapping drugs. Preliminary studies showed that the bio-composite could successfully survive in the stomach-like environment (pH 1~2). The hydrophobic nature of zein could prevent water

molecules entering the complexes which could cause LDH host decomposition from swelling and eventually controlled drug liberation was achieved [68]. E. Valarezo *et al*. employed poly (ε-caprolactone) to coat LDHs *via* the electrospinning technique [69]. The release curves appeared in a liner manner in the second step even though it was companied with an initial rapid drug release, indicating that the presence of the poly (ε-caprolactone) could, to certain extend, compromise the drug release rate. Bao *et al*. synthesized novel LDH/silica core-shell nanostructures (LDH@mSiO_2), which contained MgAl-LDH nanoplate core and ordered mesoporous silica shell *via* surfactant-templating method [70]. Studies showed that released drug amount achieved 80% over 10 hours after the drug-loaded LDH@mSiO_2 multidrug resistance were placed in PBS buffer (pH=7.4), whereas the control group liberate 80% of drugs within one hour. Recently, more biocompatible compounds have been employed to functionalize the surface of the LDHs for its medical applications. For instance, the polysaccharide family was attracting a growing attention for LDHs modification to achieve sustainable development. Given the resemblance of their structure with many body components, most polysaccharides are intrinsically biocompatible [71]. Therefore, the common use of the polysaccharides has been justified as binders, fillers and thickeners in solid and liquid formulations and as components for site-specific oral delivery systems [72]. Wicklein *et al*. developed and evaluated lipid-based LDH carriers of efficacious vaccines against influenza A [73]. LDHs were coated with xanthan gum polysaccharide with additional quality of feasible surface modification with biomimetic lipid membrane. Immunogenicity tests in mice revealed that virus immobilized on the lipid bio-hybrid elicited high titers of serum virus-specific antibodies, indicating that a strong immunoreaction was induced. Moreover,

Huang *et al*. used liposomes to encapsulate the Dextran-magnetic layered double hydroxide-fluorouracil (DMF), a dextran coated LDHs nanoparticles loaded with the anticancer drug fluorouracil, which concerned the entrapment efficiency and slow-released effect [74]; Ribeiro *et al*. also coated LDHs with pectin for controlled release in the treatment of colon diseases [75]. All these attempts have opened alternatives for the delivery of the drug in the desired location.

Another direction for LDH future development could be achieving “drug co-delivery”. This is a new concept that has been proposed recently for biocompatible inorganic material-based Nano-systems in their application of cancer therapies. It is believed that the drug co-delivery method could overcome multidrug resistance (MDR), one of the four severe issues that are encountered during cancer treatment, by concurrently inhibiting the action or reduce the expression of anti-cancer drug efflux transporters and enhancing the activity of the drugs [76]. Both organic and inorganic material-based co-delivery Nano-systems to overcome MDR have been reviewed by several outstanding papers [76-80]. However, few reports have been published about the application of LDH in drug co-delivery due to the related research being still in its infancy. Recently, Li *et al*. firstly developed the co-drug delivery strategy using LDH anion exchange capacity to encapsulate the anti-cancer drug 5-Fu into the inner-layer and load the All-stars Cell Death siRNA (CD-siRNA) onto the surface of LDH nanoparticles [81]. Amazingly, they demonstrated that the combined strategy remarkably enhanced the complexes cytotoxicity to different types of cancer cell lines compared with a single agent. Therefore, the co-delivery of siRNA and anti-cancer drug *via* LDH has shown great potential as an

alternative approach for developing cancer therapy. Furthermore, the development of LDH-mediated drug co-delivery will expand the inorganic drug family and hopefully open a door to achieve an improved organic/inorganic hybrid delivery Nano-system.

2.2 Immunotoxin therapy for cancer treatment

2.2.1 Introduction of Immunotoxins

Triggering host immune response by antibody-based therapy against tumors is a promising approach with positive clinical documents [82,83]. It was proposed that a “magic Bullet” targeting cancer antigens could be developed, killing tumor cells within the human body without harming healthy cells [84]. Protein toxins that naturally derived from bacteria or plant, such as *Pseudomonas* exotoxin (PE), Diphtheria toxin (DT), ricin, saporin, are believed to be the most potent cytotoxic agents which are capable of inhibiting protein synthesis and induce apoptosis efficiently [85]. Since these toxins are therapeutically “blind” harming cells un-discriminatorily, directing these agents to tumors with appropriate ligands is necessary. The emergence of the monoclonal antibody (mAb) reawakened the interest in inventing the “magic bullet” for cancer treatment [86]. Designed mAbs could efficiently interact with the antigens on cancer cells and constructed biomolecules containing toxins could chemically link with mAb of a single defined specificity [87,88]. The combined agents were named immunotoxins since the immune response to specific antigens helps the toxins targeting tumor cells.

Over 3 decades of dedication by researchers all over the world, the development of immunotoxins for cancer treatment agents continues. Several

studies have progressed to clinical trials after displaying promising results in tissue culture systems and animal tumor models. In addition to the clinical trials summarized by Antignani & FitzGerald [89], there are many published reports of new trails showing encouraging results [90-99], with more completed (NCT00006981, NCT00003020 etc.) or currently ongoing (NCT01408160, NCT01362790 etc.). One targeted toxin, DT-IL2, also known as denileukin diftitox or Ontak has been approved by U.S. Food and Drug Administration (FDA) for treating patients with persistent or recurrent cutaneous T-cell lymphoma [100-103]. Given the evidence that other highly expressed markers exist on cancer cells, these studies provide further rationale for targeting these molecules with immunotoxin therapy for cancers[104-106].

As immunotoxin therapy for tumors continues to develop, dose-limiting toxicities causing leaking vascular are still the major obstacles limits its application. Others include lack of specificity, poor stability, and heterogeneous composition [83]. Identification of additional tumor targets with limited off-target toxicity and immunosuppressive regimens to improve immunotoxin tolerance and prevention of anti-therapeutic immune responses could be the future direction for immunotoxin therapy development [107]. In the present review, a brief history of immunotoxin will be summarized. Groundbreaking studies of its clinical application for cancer treatment in the recent year will be highlighted and an outlook of the possible future progress is proposed.

2.2.2 Immunotoxin: toxins armed with targeting molecules

Immunotoxins that have been successfully designed for cancer therapy typically consist of three domains (Figure 2.18). A binding domain for cell recognition,

leading the toxins to targeted cells; a translocation domain, allowing the toxin to pass the through the cell membrane to enter the cytoplasm; an activity domain (the toxin), which interfere with certain cell pathways and induce cell apoptosis [88]. In some cases, the translocation domain could also be replaced by a cleavable linker [108] which can remarkably increase the cytotoxicity of native toxins. Most of the toxin's translocation domain and activity domain is retained, yet the natural binding domain has been replaced by an independently designed moiety, which is more efficient to bind cancer cells. Several possible options for the binding domain have been significantly enhanced the therapeutic efficiency of immunotoxin, such as Fv fragment.

Figure 2.18. The basic structure of designed Immunotoxin based on Diphtheria toxin, Pseudomonas exotoxin, and ricin. Abbreviations: A: activity domain; T: translocation domain; B: binding domain; L: linker. The A-T-B model represents the basic structure of an immunotoxin. Recent studies showed that the translocation domain could be replaced with a linker. A Furin cleavable linker has been used for linking Fv with *Pseudomonas* exotoxin (PE), which could increase the cytotoxicity of PE. Another study also used a linker consists of four glycines and a serine residue (G4S) to link Diphtheria toxin (DT) with scFv (1567) or Bi-svFv (1567) for targeting CCR4+ cell [109]. The A chain of ricin contains both A and T domains, which are not clearly separated [88].

In the last three decades, three generation of immunotoxins has been created. The first generation of immunotoxin was created by chemically coupling native toxins to antibody [88]. A disulfide bond was usually employed as the chemical linker between intact toxin molecules and monoclonal antibodies. However, the

native toxin still possessed its natural binding site, significantly compromising the function of mAb in the immunotoxin. The second generation of immunotoxin was designed to address the issue. Like their predecessors, mAbs were still chemically linked with toxins however, the toxins had been modified. Here, the binding site of toxins was removed, leaving their activity domain. The resulting toxin fragments were coupled with mAb. Even though this method increased the safety level of drug dose usage to experimental animals, the first and second generations of immunotoxins are still flawed. One of the severe and undesirable side effects is vascular leak syndrome (VLS), caused by the lack of specificity of the immunotoxin. The first and second generations of immunotoxins could still weakly bind to normal cells. Given that most of the immunotoxins were intravenously injected, endothelial cells were exposed to high dose of immunotoxin drug and could be seriously damaged by unexpected attacks resulting invascular collapse [110,111].

To address undesired binding, the binding domain of the third-generation immunotoxin was replaced by a growth factor, cytokine or fragment variable domain of an antibody by expressing reconstructed plasmids in a microorganism such as Escherichia coli. Fragment variable domain (Fv) along with a consistent sequence form the light chain or the heavy chain in the Fragment Antigen-Binding (Fab) region located at the Y-arm of an antibody. The Fv region is the most important functional region of antibodies binding antigens, which shapes the paratope at the amino terminal, end of the antibody monomer. By replacing the whole mAb just with its own paratope region the size of recombinant immunotoxin reduced and the binding specificity is significantly increased [111,112]. Another issue needed to be addressed for

the recombinant immunotoxins was their lack of stability. Normally, a single-chain Fvs (scFvs) are fused to toxins for immunotoxin targeting however, single-chain Fvs were not stable in clinical use. In the Fab region of an antibody, the Fvs located in the heavy and light chain are stabilized by a disulfide bond, which is removed during the synthesis of the scFvs. Consequently, the scFvs could bind to each other forming disulfide bonds within heavy and light chains, resulting in aggregation and loss of drug efficacy. The invention of disulfide-stabilized Fv (dsFv) solved this problem. The peptide linker between the heavy and light chains in the scFv was substituted by a disulfide bond that created by genetic modification of the Fv sequence. Either two cysteines were inserted into the Fv sequence or two amino acids (one on each chain) were replaced by cysteines in order to form disulfide bond for Fv sequence stabilization (Figure 2.19).

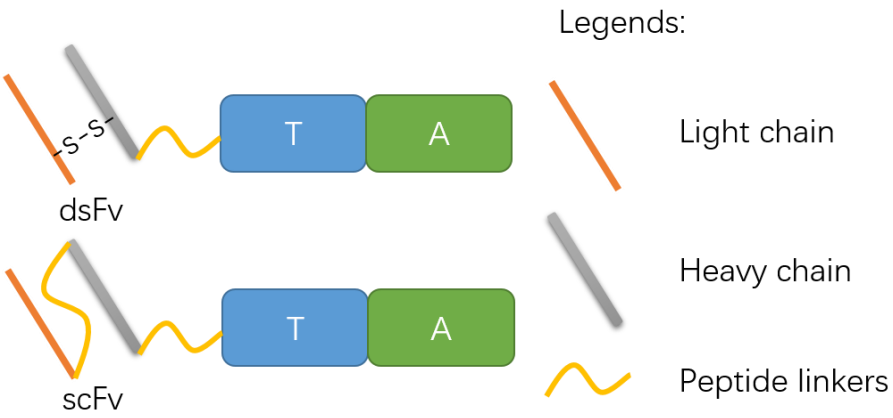

Figure 2.19. The third generation of immunotoxins. Abbreviations: A: activity domain; T: translocation domain. Most of them are produced by a microorganism and the whole mAb is replaced by its own agent-binding portion, the Fv region. The heavy or light chain in the Fv region are either genetically linked (scFv) or held together by a disulfide bond (dsFv)

2.2.3 Mechanism of Toxin-induced cell apoptosis

Microorganisms produce and secrete toxins to protect themselves in hostile environments and to gain advantages when competing for nutrients. Seeds of plants also contain toxins that help them survive in wild. Some toxins act on the cell surface while others must accumulate inside of the cells. Because toxins can kill cell readily, they have been investigated for possible cancer therapy. Though it is believed that bacterial toxins, such as PE and DT, have higher efficacy and fewer side effects to human, immunotoxins containing the plant toxin ricin have also been tested in clinical trials.

PE is a single-chain polypeptide toxin containing 613 amino acids [113]. It possesses three structural domains inhibiting protein synthesis in eukaryotic cells [114]. Structure domain Ia is the cell recognition and binding domain; structure domain II is responsible for facilitating the toxin to pass across the membrane and be accumulated in the cell cytoplasm; structure domain III and part of domain Ib functions as an enzyme that interferes with an essential cellular pathway, causing ADP-ribosylation and inducing cell apoptosis [115].

DT is also a single-chain peptide that produced by toxigenic strains of Corynebacterium diphtheria in a precursor form and is secreted into the environment as 535 amino acids after losing 25 amino acids through protein modification [116-119]. It contains two subunits: A 21.1kDa N-domain (amino acid residues 1-193) has the similar function of PE domain III & Ib, which catalyzes the NAD^+-dependent ADP-ribosylation of elongation factor 2 (EF-2) and cause cell death; a 41.2kDa C-domain (amino acid residues 194-535) carries both translocating and cell recognition domains [120,121]. The two

domains are connected by a stable disulfide bond between Cys186 with Cys201 and 14 amino acid residues in between are exposed and form a loop [122].

Ricin can be found in the bean of the castor oil plant, Ricinis Communis. It is a 66kDa type II ribosome-inactivating proteins (RIP) consist of two polypeptides chains linked by a disulfide bond formed between amino acid 259 of the A-chain and amino acid 4 of the B-chain. B chain is a 32kDa with 262 amino acids containing the cell binding domain which is specific for galactose residues on the cell surface [123]. The 32kDa A chain has rRNA N-glycosylase function which is able to specifically and irreversibly hydrolyses the N-glycosidic bond of the adenine within the 28S rRNA, resulting in adenine depurination and protein synthesis inhibition [124].

PE, DT, and ricin are also referred as AB-toxin because of their structure. Domain A has the enzymatic activity while domain B contains the translocation and cell binding moiety. Most of the AB-toxin are stabilized by a disulfide bond between domain A and B [125]. The bacterial toxins PE and DT catalyze the same substrate andcell mutants that resistant to one are often cross-resistant to the other [126,127]. However, PE (66kDa) and DT (60kDa) do not share significant similarity regarding DNA coding or protein sequences and only a small amount of homology can be observed, which primarily is in the region that encodes activity domains [128]. Even though PE and DT are not genetically similar to each other, their toxic mechanisms of killing cells are alike (Figure 2.20).

The first step is to bind the cells *via* interaction with specific receptor molecules on the surface of the targeted cells. It has been reported that the receptor for PE is the α2-microglobulin receptor [129] and the receptor for DT is the precursor of the heparin-binding EGF-like growth factor [130]. In addition to serving as binding sites for the AB-toxins, they also provide other functions in the intoxication. It has been proven that the integrity of the DT receptor is crucial for DT to cross the biological membrane [131] Replacement of cytoplasmic domain or point mutation on the receptor can significantly compromise the toxin translocation efficiency [132,133]. In many the recombinant immunotoxins used in clinical trials, the natural binding site of the toxin has been replaced with growth factor, cytokine or fragment variable domain of an antibody in order to increase their binding specificity.

Translocating the toxins to cytosol takes place in the second step at the surface of the cells through clathrin-endocytosis pathway. The toxins are wrapped by clathrin-coated pits and transferred into endocytic vesicles [134,135]. Low pH allows both toxins to be fully stretched and expose their hydrophobic domains, which facilitate them to interact with the lipids and insert into biological membranes [136]. Moiety A and B are cleaved at an early stage of the translocation process by acidic pH naturalizing the disulfide bond between them allow moiety A to cross the membrane. In the case of DT, the toxin fragment that exists in the cytosol is the 20kDa moiety A, and both PE and DT eventually kill cells by transferring ADP moiety to diphthamide, a modified histidine residue, present in EF-2 [137,138]. For ricin-based immunotoxins, the internalization process is similar to that of PE. Depurination of rRNA occurred rapidly after the

toxin is released into the cytoplasm from ER, inducing cell apoptosis by protein synthesis inhibition.

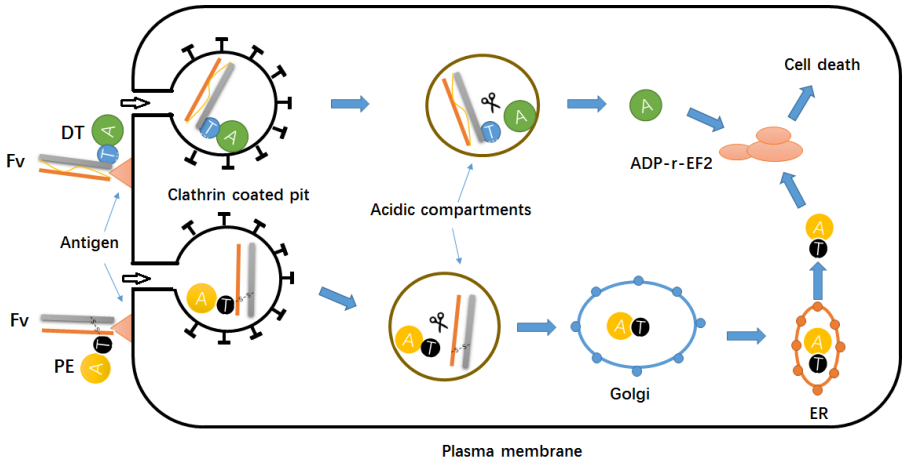

Figure 2.20. Toxic mechanism of immunotoxin in mammalian cells. Both DT and PE interacted with specific antigens on the cell surface and are internalized *via* clathrin-related endocytosis pathway, which is facilitated by low pH. Catalysis domains are released into cytoplasm under acidic environment and interact with ADP-r-EF2 to interfere protein synthesis, resulting in cell death.

2.2.4 Recent Clinical application of Immunotoxins for cancer treatment

2.2.4.1 Clinical application targeting hematologic malignancies

Many of immunotoxins have been designed and developed targeting a variety of hematologic malignancies, not only those connected through both circulatory system and immune system affecting the blood, bone marrow, lymph, and lymphatic system but multiple melanomas. Pastan and his colleagues have summarized lots of clinical studies in hematologic malignancies [7]. An update of those focused on new immunotoxin development and new clinical attempts are summarized in table 1.

Table 1. New immunotoxin development and new clinical trials against hematologic malignancies

	Immunotoxin	Toxin used	Target antigen	Tumor type	Clinical trial phase	No. of patients	Response	References
New Immunotoxins	PG001, PG002	PE38	CD7	ALL				65
	CD89-ETA',	ETA'	CD89	AML				66
	Gb-H22(scFv), GbR201K-H22(scFv)	granzyme B	CD64	AML				69
	DT390-scFv1567, DT390-biscFv1567	DT	CCR4	ALL ATLL PTCL CTCL				27
	HM1.24-ETA'	ETA'	CD317	Melanoma				72
Clinical trials	DT2219	DT	CD19 CD22	BCL	Phase I	25	13	12
	LMB-2	PE38	CD25	ALL	Phase I	17	8	73

2.2.4.2 New immunotoxin development for hematologic malignancies

CD7 is a transmembrane protein that belongs to the immunoglobulin superfamily, which is widely present on the surface of immune cells, such as thymocytes, peripheral blood T-cells, and natural killer cells [139-142]. It is believed that CD7 is overexpressed on T-cell lymphoma and leukemia cells [143,144]. Moreover, its rapid internalization after binding to its antigens makes it a perfect receptor for drug delivery in the following step [145]. To target CD7-

expressing lymphoma and leukemia cells, the monovalent and bivalent CD7 Nano-based immunotoxins PG001 and PG002 are constructed by Tang and his colleagues [146]. Both are conjugated with a derivative of PE as the activity domain. *In vivo* results showed that both immunotoxins can significantly prolong the survival of CEM cells implanted mice by approximately 50%, up to 53 days compared to 34 days of the control group. Moreover, it is worth noting that in the case of PG002 treatment, the body weight of mice was maintained even slightly increased at 25days after tumor implanted. In summary, both immunotoxins have been proved with remarkable ability to target and eliminating CD7 expressed lymphoma and leukemia cells. *In vivo* observation further proved that the efficacy of PG002 is 30 times greater than that of PG001. This is the first study for CD7 specific nanobody-based immunotoxins *in vivo*, which deserve further evaluation of their potential for anti-leukaemia in preclinical and clinical studies.

Fc fragment of IgA receptor (FCAR), as known as CD89, also belongs to the immunoglobulin superfamily, which is expressed by different myeloid leukemic cell populations. Mladenov and his team successfully created CD89-ETA', a reconstructed immunotoxin containing a single-chained anti-human CD89 fused with modified PE, to achieve specific targeting and killing [147]. After 72 h exposure to the recombinant protein, up to 90% of targeted cells were killed *in vitro* and the apoptosis-mediated cytotoxicity showed in a dose-dependent manner. *In vivo* experiment, leukemic primary cells derived from three previously untreated patients were also treated with CD89-ETA' immunotoxin. Compared with healthy primary cells, better binding shifts were observed on leukemic primary cells. Moreover, an average of 13% of leukemic primary cells

elimination efficiency was achieved. Even though the study only proved the efficacy of CD89-ETA' *in vitro*, the results showed the great potential of CD89-ETA' as a potent, novel immunotherapeutic agent.

CD64, which is more commonly known as Fc-gamma receptor 1, is a 72 KDa integral membrane glycoprotein that binds monomeric IgG-type antibody with high affinity and activates endocytosis, phagocytosis, antibody-dependent cellular cytotoxicity and the production of cytokines and superoxide [148,149]. Schiffer and his team constructed the novel immunotoxins Gb-H22(scFv) and its derivative GbR201K-H22(scFv) comprising a humanized single chain antibody H22 that specifically bind CD64 with high affinity and human granzyme B, a serine protease that expressed in cytotoxic T lymphocytes and natural killer cells. It has been proved that the Gb-H22(scFv) could significantly induce apoptosis in CD64+ U937 cells and primary Acute myeloid leukemia (AML) cells, whereas CD64- AML cells were unaffected [150]. Furthermore, they compared the effectiveness of both immunotoxins with H22(scFv)-ETA', which is also anti-CD64 based immunotoxin but have been evaluated extensively before [151]. Results showed that both new constructs reached the same level of cytotoxicity towards cells derived from patients [152]. Better performance was also observed. In the case of patients-derived serpin B9-negative AMML III, CMML II and serpin B9-positive CMML IV cells, the efficacy of both new constructs inducing cell apoptosis was significantly higher than the H22(scFv)-ETA', achieving an average of 25% and 30% cell death, whereas 10% for H22(scFV)-ETA'. These results suggest that CD64 is not only a promising diagnostic marker but also a novel target for specific CMML and AMML therapy, and the

new immunotoxins could offer an alternative to Pseudomonas Exotoxin A resistant AMML or CMML cells.

Because of the high expression of CC chemokine receptor 4 (CCR4) on some tumour cells such as T-cell acute lymphoblastic leukaemia (ALL), adult T-cell leukaemia/lymphoma (ATLL), adult peripheral T-cell Lymphoma (PTCL) and cutaneous T-cell lymphoma (CTCL), CCR4 seemed an excellent candidate for immunotoxin therapy [108]. Therefore, the diphtheria toxin based anti-human CCR4 immunotoxins were produced. The three isoforms DT390-scFv1567 (monovalent), DT390-biscFv1567 (bivalent) and single-chained Fold-back Diabody were examined both *in vitro* and *in vivo*. Given that the Diabody isoform could bound to its receptor with the highest affinity among the three versions, *in vitro* efficacy analysis confirmed that the single-chained fold-back diabody isoform was significantly more potent than its monovalent and bivalent isoforms (200-fold and 10-fold respectively) in inhibiting cellular proliferation and protein synthesis in human CCR4+ tumor cells. Moreover, the diabody isoform significantly prolonged the survival ability of the human CCR4+ tumour-bearing mouse model. The mice survived up to 34 days until they died, whereas others treated with bivalent, monovalent isoforms and C21 immunotoxin (control) lived only 31, 21 and 20 days. It was concluded that the novel anti-human CCR4 immunotoxin, more specifically the Diabody isoform, could be a promising drug candidate for cancer therapy [108].

To target the HM1.24 antigen (CD317) that overexpressed on multiple melanoma cells, a truncated variant PE (ETA') was fused with a CD317-specific svFv to make HM1.24-ETA' to induce apoptosis of target cells [153]. *In vitro*

results showed that the apoptosis induction occurred in a few hours after the treatment to cells, indicating that the drug could be rapidly internalized by cells and post-internalization processing executed efficiently. Compared with CD64-ETA', HM1.24-ETA' could significantly and specifically eliminate malignant plasma cells at low concentration. It was showed that the EC_{50} were only 28 ng/mL and 44 ng/mL on L363 and INA-6 cells after 72h treatment, whereas CD64-ETA' showed little or no effects on these cells.

2.2.4.3 New clinical trials of immunotoxins for hematologic malignancies

DT2219 is a reconstructed immunotoxin containing bispecific scFv of antibody targeting CD19 and CD22 and catalytic and translocation enhancing domain of DT. To evaluate its preliminary efficacy, side-effects and maximum tolerated dose (MTD), 25 patients with B-cell lymphoid malignancies were signed up for the Phase I clinical trial [93]. Patients were treated intravenously with different doses of DT2219 from 0.5 μg/kg/day to 80 μg/kg/day every two days for 7 days. Short term side-effects such as weight gain, low albumin, transaminitis, and fevers were observed in the 13 patients received a minimum dose of 40 μg/kg/day. Dose Limiting Toxicity (DLT) occurred in 2 patients with a dose of 40 and 60 μg/kg/day respectively. One experienced back pain and extreme strength loss and died of rapidly progressive disease, while the other developed grade 3 capillary leak but recovered in 10 days with supportive care. Regarding immunogenicity, neutralizing antibodies were detected in only 3 patients that treated with high dose of DT2219 after the first session and no consistent pattern was recognized in the whole process. The study also pointed out that the clinical activity and CD19/CD22 target expression were not related to each other at a lower dose. Only 9 patients received high dose treatment possessed

detectable drug level in blood. 2 of those responded to the treatment, 1 achieved complete remission after 2 cycles. Therefore, a safety and biologically active dose of 40~80 μg/kg/day for 4 cycles have been determined for phase II study of exploring DT2219 repetitive courses.

Phase I treatment with LMB-2, which is a single-chain immunotoxin contains the anti-CD25 mAb (anti-Tac) conjugated to PE38 was significantly limited by immunogenicity [154]. Therefore, the patients in Phase II trial were treated with LMB-2 after cyclophosphamide and fludarabine in order to reduce the antidrug antibody production and slow down the progression leukemia between cycles [155]. 15 out of 17 patients entered the second stage of 30-40 μg/kg/day LMB-2 treatment after receiving fludarabine and cyclophosphamide for the first cycle and were evaluated for response. Of those 15, 8 leukemia patients treated with 25+250 or 30+300 mg/m2 of fludarabine and cyclophosphamide responded to LMB-2 positively. 6 achieved complete remission (CR) including 5 with >25% leukemic cells and 2 partial remissions (PR). 5 with lymphomatous ATL showed no response to the LMB-2 due to the low dose fludarabine and cyclophosphamide pre-treatment. These studies showed that the less immunogenicity could result in a better performance of LMB-2 to leukemia ATL patients.

2.2.4.4 Clinical application of immunotoxin targeting solid tumors

To evaluate the functions of immunotoxins made with various of ricin and PE-conjugated to mAb or mAb fragments against solid tumors, new attempts have been performed in labs or in clinical trials [156-160], which are summarized in table 1. High expression molecules on the surface of the cancer cells have been

studied and some of them could potentially be a new target for the design of improved immunotoxins. Studies with significant improvement are listed in table 2.

Table 2. New immunotoxin development and new clinical trials against solid tumors

	Immunotoxin	**Toxin used**	**Target antigen**	**Tumor type**	**Clinical trial phase**	**No. of patients**	**Response**	**References**
New Immunotoxins	scPiPP-PE38	PE38	hCG	NSCLC				75
	NL1.1-PSA	cytolysin	ErbB2	Breast cancer				76
	BL-2	streptavidin-saporin complex	HuD	NSCLC NB				78
Clinical trials	SS1(dsFv)-PE38	PE38	mesothelin	Lung cancer	Phase II	55		79
	MOC31PE	PE38	EpCAM	EpCAM-positive cancer	Phase I	63	47	88

2.2.4.5 New immunotoxin development against solid tumor

Human chorionic gonadotropin (hCG) is a hormone that highly produced in pregnant females [161]. However, a significantly high expression level of hCG and its two subunits can also be detected in men and non-pregnant females harboring a variety of non-trophoblastic cancers [156]. cPiPP is a previously

developed antibody which has been proved with high affinity to hCG expressing tumor cell lines such as MOLT-4 (T-lymphoblastic leukemia) and U-937 (a histiocytic lymphoma) [162] and showed no harm to normal healthy donors [163]. However, the disadvantage of its instability caused by chemical conjugations remains, resulting in incomplete linkage or loss of linkage over time. In 2015, the binding site of cPiPP was engineered in single chain variable fragment format and genetically conjugated to PE38 in Nand's lab [156]. A new recombinant hCG-specific immunotoxin scPiPP-PE38 was created. *In vitro* results showed that over 90% of both U937 and Molt 4 cells were lysed when cells were incubated with 100 μg of scPiPP-PE38 after 24 hours, indicating that the new immunotoxin is capable of killing hCG-expressed cells with a high eliminating rate. Moreover, similar results were observed with A549, lung adenocarcinoma cells. It was also demonstrated that scPiPP-PE38 showed no or little harm on peripheral blood mononucleated cells (PBMCs) harvested from healthy donors at different doses. Future studies could further reveal the potential of the new immunotoxin as a therapeutic agent for hCG-overexpressed tumors.

As addressed in Weigle's article, one of the major issues of designing new immunotoxin by employing bacterial exotoxins is the requirement of the toxins to be internalized into targeted cells to exert their toxic effects, indicating that both the rate and route of internalization can directly impact the efficacy of the immunotoxin [157,164]. Therefore, the authors showed great interested in alternatives and designed a novel peptide-based immunotoxin NL1.1-PSA specifically targeting ErbB2, which is a receptor tyrosine-protein kinase that is expressed in over 30% of breast cancers [165]. The functioning site of the new

peptide-immunotoxin is a small peptide cytolysin acting at the cell membrane, which can lead to membrane disruption and cell death. The employment of the immunotoxin could significantly enhance the chance of overcoming chemoresistance and thereby more effectively eliminate ErbB2-positive breast cancer cells.

Another issue of immunotoxin is side effects, such as vascular leak syndrome. Attempt to address the issue has been made by Ehrlich and his team, a streptavidin-saporin complex was introduced into the new immunotoxin BL-2 as the functioning domain [159]. It is believed that the HuD, a paraneoplastic encephalomyelitis antigen containing RNA-binding domains [166], is expressed in small cells lung cancer (SCLC) cells and neuroblastoma (NB) cells at a significantly high level [167]. Therefore, the mouse anti-human-HuD monoclonal antibody was chosen and synthesized as the targeting domain of BL-2. *In vitro* results showed that BL-2 can specifically and aggressively eliminate SCLC and NB cells that express HuD antigens. *In vivo*, BL-2 was directly injected into tumors in nude mice bearing human SCLC or NB and the tumor progression was remarkably inhibited in both mouse models without causing toxicity in nude mice and the duration of tumor response was significantly prolonged. Future studies *in vivo* will be performed to further reveal the potential of the immunotoxin as a therapeutic option against HuD-positive tumors.

2.2.4.6 New clinical trials for solid tumors

A phase II clinical trial (NCT01362790) has been performed by National Cancer Institution (NCI). Participants recruitment has been finished and the study is currently ongoing (last updated on January 4, 2017). A promising immunotoxin

therapy of SS1P is employed to treat solid tumors. The SS1(dsFv)-PE38 is an immunotoxin that was reconstructed to target against mesothelin, a cell surface antigen highly expressed in lung adenocarcinoma [160]. The toxic site of the immunotoxin is a portion of PE. In the combination of two drugs: Pentostatin and Cyclophosphamide that can suppress the immune system, the team will examine the effectiveness of the immunotoxin to treat malignant mesothelioma. 55 individuals at least 18 years of age bearing malignant mesothelioma in the chest or abdomen will receive the first 30-day treatment cycle followed by three 21-day cycles of treatment. Overall survival, progression-free survival, and duration of response rates will be recorded and analyzed during the whole process. Estimated study completion date is September 4, 2017. Given that the proof that mesothelin is significantly overexpressed in Non-Small Cells Lung Cancer (NSCLC) [168], the study will provide clinical evidence for targeting mesothelin with immunotoxin therapy for NSCLC in the future.

Another team at Oslo University Hospital, Norway has carried out a Phase I clinical trial by using anti-EpCAM immunotoxin MOC31PE to treat patients with EpCAM-positive metastatic disease in combination with Sandimmune (cyclosporine, CsA), which is an immunosuppressant medication and natural product [169]. The primary aim of the study is to determine the MTD, safety, pharmacokinetics and immunogenicity of the immunotoxin in the patients. 63 individuals at the age of over 18 were divided into two groups and treated with MOC31PE along or with CsA in doses ranging from 0.5 to 8 μg/kg for 4 circles in 56 days. The MTD of the second group (treated with MOC31PE and CsA) was lower than that of the first group (treated with MOC31PE only), 6.5 μg/kg and 8 μg/kg respectively. The treatments were well tolerated and no co-

treatment-related toxicity was detected. 36% of patients had shown no improvement in the first group, whereas the proportion was only 15% in the second group and no dose dependency was observed in these “stable disease” patients in both groups. However, due to the low number of patients at each dose, the study simply implied that the combination of MOC31PE+CsA may have a promising potential of achieving repeated treatment of MOC31PE and further evaluation of the immunotoxin efficacy against EpCAM-positive metastatic disease in the clinic is required.

2.2.5 Summary and Discussion

Immunotoxins are recombinant proteins that normally possess a binding domain and an activation domain. By taking advantage of the specificity of antibodies as binding domain and the cytotoxicity of protein toxins as an activation domain, the hybrid immunotoxin can target the cancer cells, be accumulated on-site rapidly and induce apoptosis of the targeted cells efficiently.

Since the concept was initially instigated, the development of the immunotherapy has been advancing forward. New immunotoxins have been designed, reconstructed and launched; older generations of immunotoxins have been optimized to either cope with more scenarios or enhance their efficacy on specific targets of interests. Furthermore, clinical trials have also been carried out in hematologic malignancies as well as in solid tumors. However, only the Denileukin Diiftitx has been approved by the U.S. FDA for the treatment of CTCL. This indicates that the application of most immunotoxins in the clinic has been significantly limited.

Improving the accuracy of reaching targeted cells of interest and minimizing the side-effects such as VLS is one of the central challenges in treating hematologic malignancies with immunotoxin. The antigen selection is critical to addressing this issue. It is arguable that there is a single ideal antigen for targeting when treating antigenically diverse hematologic malignancies such as AML with immunotherapy. Rashidi and Walter proposed that these types of cancer can't be recognized as one disease for immunotoxin treatment [170]. In addition to that, not all the patients with same cancer could be compatible to immunotherapy with an antigen. Therefore, with the efforts like exploring new target antigens, improving existing immunotherapy modalities, and developing new classes of therapeutics, a personalized treatment strategy combining immunotherapy with other agents, or even muti-target bioengineering might be a new direction for hematologic malignancies.

In hematologic malignancies, the immunotoxins could be relatively easier to reach the cancer cells, whereas the tumor penetration is limited in solid tumors. As mentioned above, the efficiency of delivery and internalization to tumor cells can directly impact the efficacy of the immunotoxins. One possible method is to employ novel materials to facilitate the transportation of the immunotoxins to/in targeted cells, such as polymeric nanoparticles. Several engineered nanostructures like MOFs, Silica, *et al* have shown great potential for drug delivery in cancer therapies [171]. It was also reported that the co-internalization of endosome-disrupting polymer nanoparticles and immunotoxins can enhance the cytosol delivery and the efficacy of the immunotoxins [172]. The utilization of nanostructures in cancer therapy can raise the concern of extra cytotoxicity and immunogenicity, therefore current attempts have been focusing on the design

and synthesis of more biocompatible and less toxic nanostructures [173]. Moreover, nanostructures have also been modified to cope with more cases in different scenarios, expanding their potentials in cancer therapy [174,175].

Immunogenicity issue might be a less problem in patients with hematologic malignancies due to their suppressed immune system, but the application of the immunotoxins in those with solid tumors is significantly limited. The neutralizing antibodies could be formed after few cycles of immunotoxins treatment and significantly reduce their efficacy. Recent studies have been making efforts of identifying and remove the T- and B-cells epitopes to hide the from the immune system [158,176]. However, these modifications might compromise the cytotoxicity activity of the immunotoxins in some cases. Therefore, it is crucial to find a balancing point where the immunogenicity could be reduced and the integrity and potency could be reserved. Possible solutions could be designing new immunotoxins without B- or T- cells epitopes rather than removing them from the immunotoxins afterward. The epitopes-diminished immunotoxins combined with other medication that suppressed the immune systems will help the patients receive more treatment cycles and offering them a fighting chance against cancer.

Chapter 3 The Synthesis of Mg/Al Layered Double Hydroxide Nanoparticle *via* Co-precipitation Method

3.1 Introduction

Layered Double Hydroxides (LDHs), also known as hydrotalcite-like (HTI), hydrotalcite-type (HTt) or anionic clays belong to a big family of layered materials [177]. The first member of this natural mineral family was identified in Sweden in 1842, which is known as hydrotalcite with the formula $Mg_6Al_2(OH)_{16}CO_3{\cdot}4H_2O$ [66,178]. Most of the LDH materials can be described by a general formula $[M^{II}_{1-x}M^{III}_x(OH)_2^{x+}(A^{m-})_{x/m}{\cdot}nH_2O]$ (x=0.2−0.4; n=0.5−1), where M^{II} represents a divalent metal cation, M^{III} a trivalent metal cation and Am− an anion [6,179]. Structurally, like brucite $Mg(OH)_2$, each cation in LDH layers is surrounded with six OH^- ions forming an octahedral subunit, and every two subunits share edges and could expand the two-dimensional layer, theoretically, to infinity [180]. Anions Am− located between two layers balance the positive charge of cations *via* electrostatic interaction. With the contribution of hydrogen bonds between layers, the two layers are held together forming a three-dimensional structure.

Interestingly, not only can the layer cations of these materials be replaced among a wide range selection of cations, but also the anions located at the interlayer are believed to have possible substitutions among organic or

inorganic, simple or complex anions and simple anionic coordination compounds [181-183]. Furthermore, a unique property, which makes them diverse from other cationic-layered materials, is that they can recover the double-layered structure after thermal decomposition under mild conditions [8]. All these properties, such as high chemical versatility, anionic exchange capacity, and low cytotoxicity, are leading to a promising future in drug delivery and release, opening wide possibilities for researches and development for its clinical application. Compared with old-fashioned drug delivery methods which are suffering from problems such as drug degradation, poor bioavailability, and low circulation stability, the LDHs, as a new drug carrier, is much simpler to synthesize in the laboratory, have a high drug transportation efficiency, high drug loading density, low toxicity to target cells or organs and excellent protection to loaded molecules from undesired enzymatic degradation [6]. The earliest application of LDH materials in human therapy was as anti-acid and anti-peptic reagent [6,184-186]. However, recently LDHs have been employed for clinical disease diagnosis, chemical industry and as a drug carrier responsible for delivering therapeutic and bioactive molecules such as peptides, anti-inflammatory drugs, and even small nucleic acids to mammalian cells *in vitro* or *in vivo* with the purpose of crossing the cell membrane into the cytoplasm [187-189].

3.2 Material and Methods

3.2.1 Materials and instruments

Aluminum Chloride Hexahydrate AR ($AlCl_3 \cdot 6H_2O$, 500g), Magnesium Chloride Hexahydrate AR ($MgCl_2 \cdot 6H_2O$, 500g) and Sodium Hydroxide Pellet AR (NaOH,

500g) are purchased from Chem-supply Co. (Port Adelaide, South Australia, Australia). Falcon™ 50 mL Conical Centrifuge Tubes are purchased from Fisher Scientific Co. (by Thermo Fisher Scientific, Pittsburgh, Pennsylvania, USA). The model of centrifuge machine is Beckman Avanti J-26XPI equipped with JA-25.50 fixed angle rotor. Nano ZS from Malvern Instrument was utilized to examine the particle size distribution. Particles were imaged by JEOL JSM-2010 transmission electron microscope (TEM) (acceleration voltage of 200kV) and characterized by Fourier transform infrared spectroscopy (FTIR, model Nicolet 6700) and X-ray diffraction (XRD, model Rigaku Miniflex). The Synthesis of the Mg-Al LDH nanoparticles was achieved at Zhi Ping (Gordon) Xu's lab, Australian Institute for Bioengineering & Nanotechnology (AIBN) at the University of Queensland (UQ).

3.2.2 Co-precipitation

The pristine Mg/Al-Cl LDH (with the designed formula $Mg_2Al\text{-}(OH)_6Cl{\cdot}2H_2O$) is prepared by aqueous co-precipitation in the presence of excess Mg^{2+}. 3.0 mmol of $MgCl_2{\cdot}6H_2O$ and 1.0 mmol of $AlCl_3{\cdot}6H_2O$ were dissolved in 10 mL of fresh Milli Q water. 6.0 mmol of NaOH was dissolved in 40 mL of fresh Milli Q water as a basic solution. Then the salt solution was quickly added to a basic solution to precipitate under vigorous stirring at room temperature. The suspension was then stirred for 30 mins. During the preparation, precipitation and aging period, the suspension should be exposed to an N_2 environment to minimize the CO_2 contamination.

3.2.3 LDH purification

After 30 mins' continuous stirring, the mixture was transferred into a 50-mL Falcon centrifuge tube. The resulting white slurry was collected by centrifugation at 5000g for 10 mins. The supernatant was removed from the tube and 40 mL of fresh Milli Q was added into the tube. The precipitance was re-suspended through vortex until no solid was left at the bottom of or in the tube. Re-collect the white slurry by centrifugation at 4000g for 30 mins. Then the supernatant was discarded and excess salts were removed from the system. Repeat this routine to wash the mixture 2 or 3 times and eventually leave the pre-mature nanoparticles suspended in 40 mL fresh Milli Q water in the 50-mL centrifuge tube.

3.2.4 Autoclave

The suspension was transferred into a stainless-steel autoclave and hydrothermally treated at 100˚C for 16 hours. After the incubation, the autoclave was cooled down on the bench at room temperature and the suspension was carefully transferred into a new 50-mL centrifuge tube. The resultant transparent suspension contained 4.0 mg/mL of homogenously dispersed LDH nanoparticles.

3.2.5 Characterization

The particle size distribution of obtained mature LDH nanoparticles was determined by photon correlation spectroscopy on the Nanosizer instrument. The same instrument was also employed for zeta potential measurements. The nanoparticles were imaged by transmission electron microscopy (TEM) using a JEOL JSM-2010 transmission electron microscope (acceleration voltage of

200kV). Particles pellet was harvest after High-speed centrifugation (30 min, 16000 rpm/min) and dried at 100˚C to yield a white product with constant weight which will be analyzed by Fourier transform infrared spectroscopy (FTIR) using a Nicolet 6700 FTIR instrument in ATR mode and powder X-ray diffraction (XRD) using the X-ray diffractometer in order to verify chemical composition and crystal structure of the nanoparticles, respectively.

3.3 Results

3.3.1 X-ray diffraction pattern of LDH nanoparticles

The pristine LDH nanoparticles were collected by high-speed centrifugation and re-suspended in MilliQ water. The suspension looks transparent and homogeneous. A dry powder of the LDH materials was prepared for the XRD, and the pattern is shown in Figure 3.1.

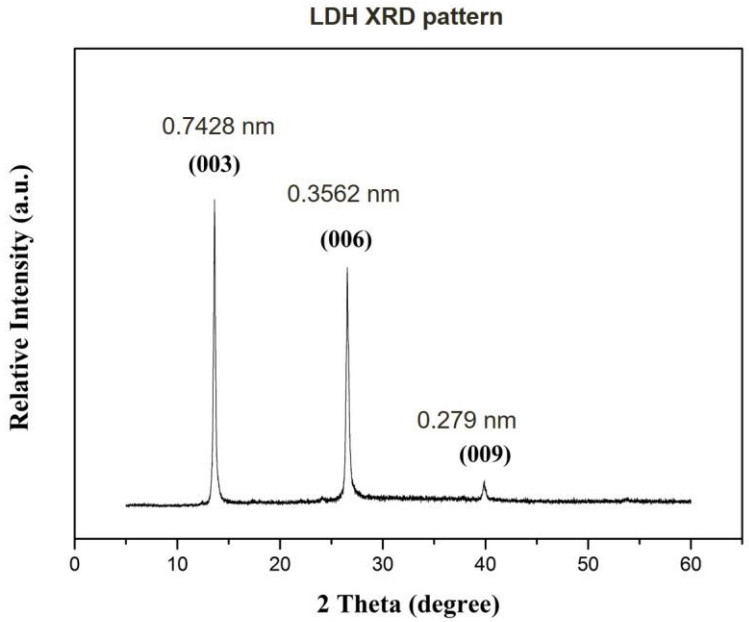

Figure 3.1. XRD pattern of pristine Mg_2Al-Cl LDH nanoparticles

The XRD pattern proved that the LDH presented the typical layered features. Strong and sharp peaks were detected from the planes (003) and (006), indicating the materials have an organized layer. The interlayer spacing is 0.7428 nm. LDH material units stacked with each other and the distance in between is 0.3562 nm. These parameters are similar to previous studies [190,191].

3.3.2 FTIR spectrum

The dry powder of pristine LDH nanoparticles was also examined by the FTIR spectrum and shown in Figure 3.2.

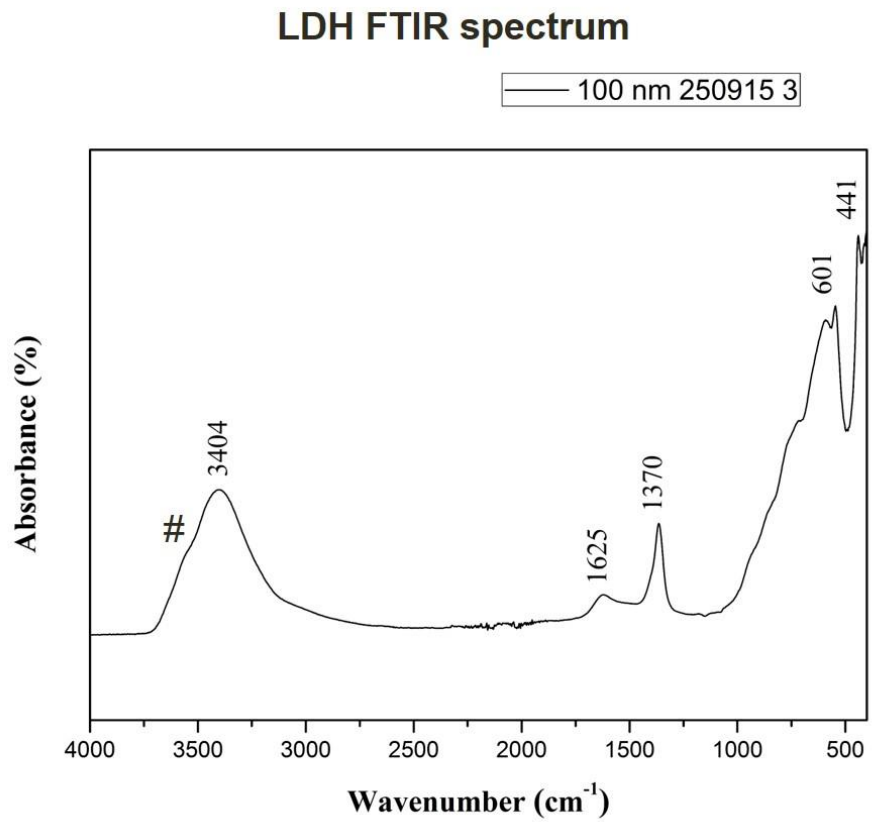

Figure 3.2. FTIR spectrum of pristine Mg_2Al-Cl LDH nanoparticles. "#" represents the shoulder peak.

Like previously reported, the FTIR spectrum in Figure 25 showed the typical of Mg_2Al-LDH materials. A broad band was detected at 3404 cm^{-1}, representing the OH^- group and a weak peak at 1625 cm^{-1}, representing the H_2O group. Due to the M-O vibrations and M-O-H bending, two weak peaks at 601 and 441cm^{-1} were also detected. Interestingly, a relatively strong peak was also observed at 1370 cm^{-1}, which is the CO_3^{2-} group that is converted from CO_2 captured from the air during the LDH materials preparation. If the whole synthesis process could be performed in an N_2 environment, the CO_3^{2-} group can be avoided. It can be also observed that there is a weak "shoulder" peak (labeled as "#") to the slight left of the 3404 cm^{-1}. Combined with the presence of the peak 411, these two peaks are considered as the direct evidence of the Mg_2Al-LDH [191,192].

3.3.3 LDH particle size distribution and zeta potential

Freshly made LDH materials were re-suspended in MilliQ water and the particle size and zeta potential were measured by zeta sizer (Figure 3.3 & 3.4).

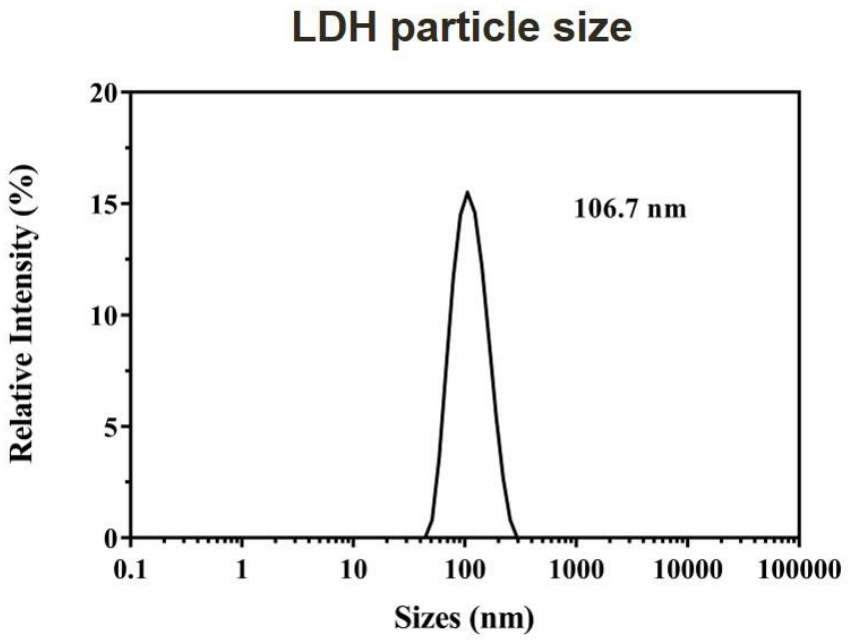

Figure 3.3. Particle size distribution of the Mg_2Al-Cl LDH nanoparticles

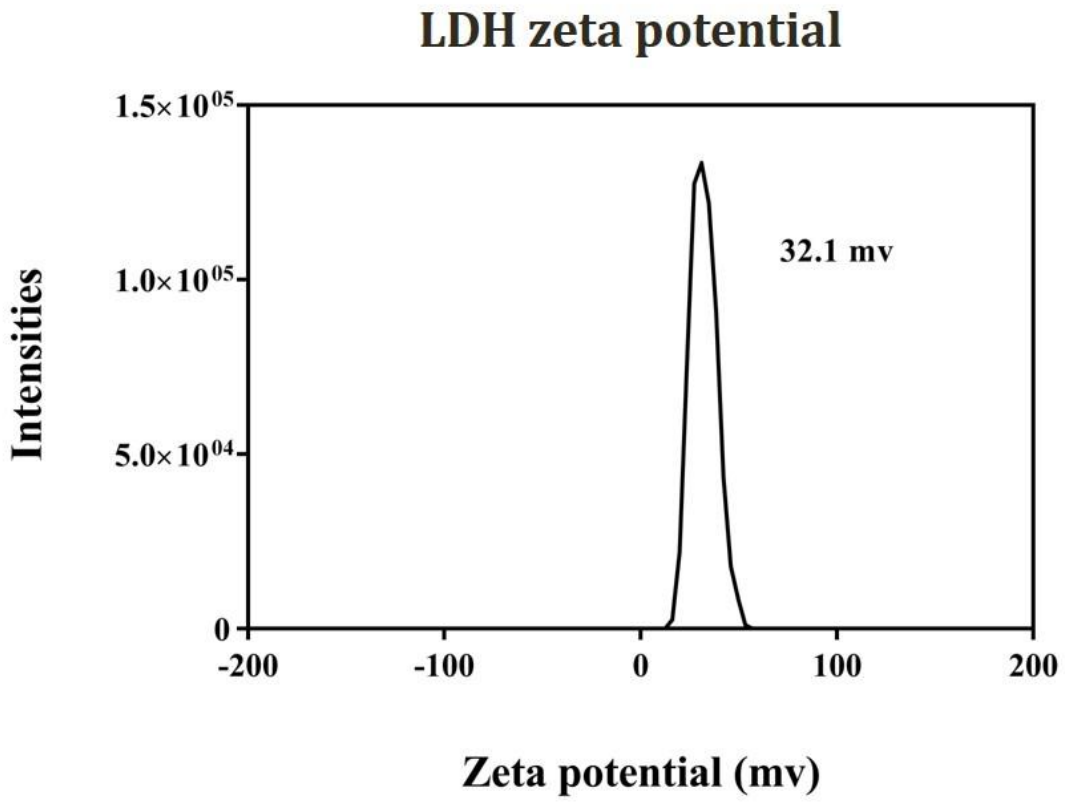

Figure 3.4. Zeta potential of the Mg_2Al-Cl LDH nanoparticles

The preparation of the LDH materials was performed with care to synthesize the stable and homogeneous Mg_2Al-Cl-LDH suspension. A narrow peak was observed centered at 106.7 nm with a narrow zeta potential distribution at 32.1 mV. The maximum size of the LDH materials for mammalian cellular uptake is 150~200 nm, therefore the new batch of the LDH materials was suitable for mammalian cells transfection.

3.3.4 TEM image of LDH nanoparticles

The LDH nanoparticles were also imaged by TEM. The image is shown in Figure 3.5. The pristine LDH nanoparticles were hexagonal in shape with the approximately 50~100 nm edges. Particle units were separated from each other

but with limited and casual stacking. No vertical orientated particles were captured in the image, so it was difficult to measure the thickness of the units. According to earlier reports [191], the thickness of the LDH nanoparticles was estimated 8~16 nm after taking into account of the XRD diffraction peaks and TEM images.

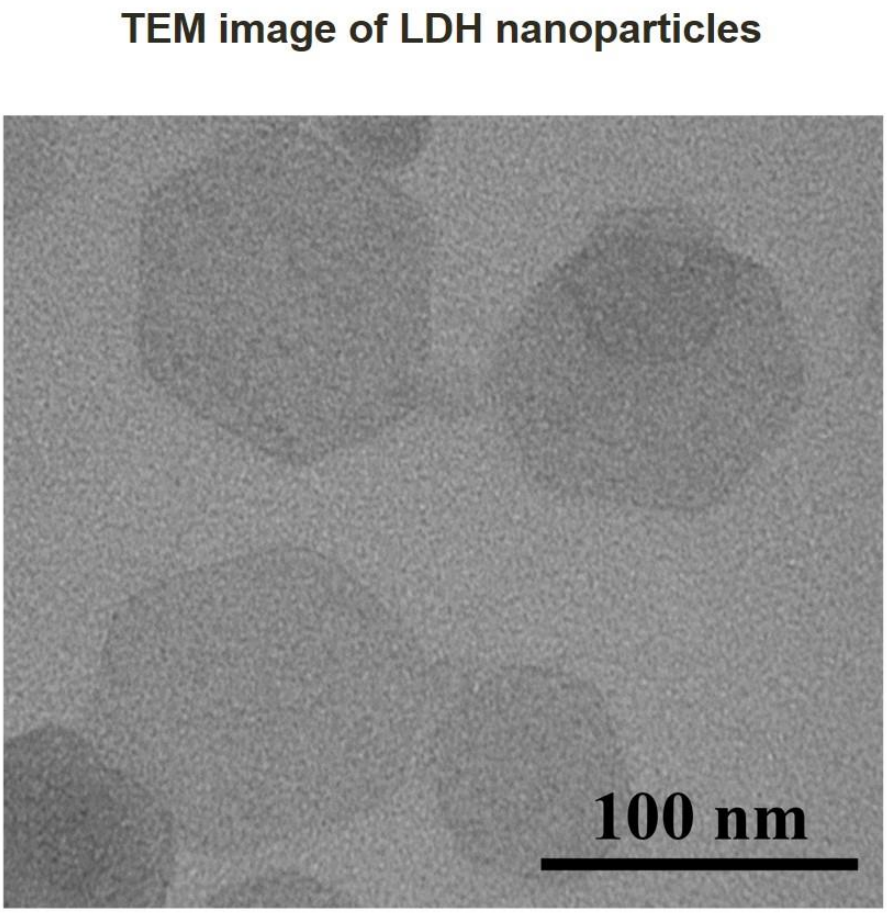

Figure 3.5. TEM image of the Mg_2Al-Cl LDH nanoparticles

3.4 Discussion

In this Chapter, the pristine LDH nanomaterials were synthesized and characterized. Freshly-made homogeneous LDH nanoparticles were

approximately 106 nm in size and 32.1 mV in zeta potential. XRD and FTIR proved the exist of the important molecular groups and the “shoulder” in FTIR image was the direct evidence of the presence of the Mg_2Al-Cl LDH nanoparticles.

Zeta potential is one of the crucial factors that affect the transfection efficiency of nanoparticles in mammalian cells. The LDH nanoparticle synthesized in this Chapter possessed 32.1 mV zeta potential. Due to the cell membrane is negatively charged, the LDH nanoparticles are more likely to adhere to the cell membrane and initiate the translocation process by endocytosis.

Another issue for transfection that needs to be considered is the particle size. It was believed that the particle sizes in the range of 40~150 nm were preferred by cells for the transfection *via* endocytosis pathway [193,194]. The LDH nanoparticles synthesized in the Chapter was 106 nm, which is suitable for the delivery. After intercalated with the CMV-EGF-ETA plasmids, the particle size could increase. It was believed that the LDH/plasmids hybrids were not suitable for mammalian cell transfection due to the increased particle size caused by expanded interlayer [191]. However, previous studies [3,4] and the preliminary transfection experiments on MCF-7 breast cancer cells in this project showed that mammalian cells can be transfected with LDH/plasmids hybrids and the transfection efficiency was almost equivalent to those of Lipo2000. The experiments results performed in Chapter 5 have confirmed the preliminary results. Therefore, the LDH nanoparticles can be used as a carrier to deliver plasmids into target cells and employed for the development of new cancer

therapy. In that case, patients with cancer could significantly benefit from the drug controlled release by LDH nanoparticles.

3.5 Conclusion

The LDH nanomaterials were successfully synthesized in a lab. The LDH composition analysis provided the direct evidence of the presence of Mg_2Al-LDH and confirmed by the TEM. The particle size and zeta potential are the key factors affecting the mammalian cell transfection efficiency. In our case, the synthesized pristine LDH nanoparticles with 106 nm in size and 32.1 mV in zeta potential are suitable for the cell transfection.

Chapter 4 Design and Construct the New Immunotoxin CMV-EGF-ETA

4.1 Introduction

4.1.1 Role of Epidermal Growth Factor Receptor (EGFR) binding in cancer progression

In targeting of cancer cells, it needs to be considered that the significant differences between somatic and cancer cells. One of the major differences is the activity of certain receptors that are present on the cell surface, as these receptors could activate intracellular signaling pathways, which enhance the cancers ability to survive. EGFR is a transmembrane tyrosine kinase receptor that plays a central role in cancer progression, angiogenesis, metastatic spread and the inhibition of apoptosis [195]. It is commonly seen in particular types of cancer such as small cell lung cancer, head and neck, prostate and breast cancer [196]. It consists of three basic components, the extracellular ligand binding domain, the transmembrane segment and the intracellular protein tyrosine kinase [197]. Among its multiple ligands, EGF and TGF-α are the most important ligands that could bind and stimulate EGFR [198]. Furthermore, it has been reported that the EGFR intracellular signaling pathways could be triggered not only by the increased concentration of EGFR specific ligands such as EGF and TGF-α but also by decreased receptor turnover or the presence of aberrant receptors due to EGFR gene mutations [199]

.

EGFR, when stimulated *via* binding of its specific ligand, undergoes a transition from an inactive monomeric structure to an active homodimer. The activated

homodimer will attract another pair of the ErbB family forming a ligand-EGFR-ErbB complex which will be endocytosed into the cell [200]. After phosphorylation in cells, the complex could activate multiple intracellular pathways, such as the JAK STAT pathway or Signal Transducers and Activators of Transcription, resulting in phosphorylation of STAT1/STAT3 and the activation of their target gene Nuclear Factor Kappa B (NFkB) transcription [201,202]. NFkB is recognized as a positive regulator of cancer survival and increase proliferation due to the ability to activate pro-survival and antiapoptotic signals transcriptionally. In cases of cancer, due to the overexpression of NFkB, this will activate oncogenes such as HER2, which plays a role in pathogenesis and progression of types of breast cancer. NFkB also stimulates AKT, a serine/Threonine specific protein kinase that promotes growth factor-mediated cell survival *via* the activation of NFkB, cell cycle *via* overcoming cell cycle arrest in G1 and G2 and simulates angiogenesis [203].

4.1.2 Pseudomonas Aeruginosa Exotoxin A (ETA)

Pseudomonas Aeroginosa is a Gram-negative bacillus which could be identified throughout a variety of different environments [204]. One of the most toxic factors secreted by P. Aeruginosa is ETA, a 613-amino acid protein with AB toxin structure-function properties, meaning that both the A and B domains are encoded on a single protein. B domain could facilitate the translocation of A domain into the cytoplasm of the cells. Then the A domain binds to a coenzyme nicotinamide adenine dinucleotide (NAD) [205]. NAD is recognized as a stimulator in many cellular oxidation-reduction reactions. The binding of exotoxin releases the nicotinamide from adenine dinucleotide (ADP-ribose). This ADP-ribose unit stays attached to the ETA. Subsequently, exotoxin A

transfers ADP-ribose to Elongation Factor-2, a protein involved in the translation and elongation of proteins, which in return, blocks protein synthesis in host cells, resulting in cell death [206]. Therefore, it is widely used in current cancer-targeting therapy researches.

4.2 Material and Methods

4.2.1 Materials and tools

The plasmid of the new immunotoxin was designed and synthesized based on two plasmids, 425(scfv)-EGF-ETA and pEGFP-C1. The function fragment (EGF-ETA) of 425(scfv)-EGF-ETA and the backbone of pEGFP-C1 (without EGFP gene) were ligated with each other to form the reconstructed plasmid. The primers for EGF-ETA fragment was designed *via* online tools, such as Primer 3 plus (http://www.bioinformatics.nl/cgi-bin/primer3plus/primer3plus.cgi) and NBE Tm calculator (http://tmcalculator.neb.com/#!/). The primers were examined by the online tool DINAMelt to check issues like cross-pairing (http://unafold.rna.albany.edu/?q=DINAMelt/Two-state-melting). Then they were ordered from Sigma-Aldrich. Quick polymer chain reaction (PCR) kit, quick ligation kit and restriction enzymes (RE), Nhe I and Xho I were purchased from New England Biolabs. PCR tubes were purchased from Bio-Rad and autoclaved by Tomy SX-700E high-pressure steam sterilizer with other equipment, such as transfer pipettes, pipettes tips, agar plates, *et al* before use. Nuclease free water was purchased from Promega. Standard Agarose Gel (low electroendosmosis, aka EEO) was purchased from AppliChem. 50X TAE buffer containing Tris-base, acetic acids and ethylenediaminetetraacetic acid (EDTA) was purchased from Bio-Rad and was diluted into 1X for dissolving agarose gel

powder. 1kb GeneRuler DNA ladders and DNA gel stain, SYBR™ Safe, was purchased from Invitrogen. 5x DNA loading dye was bought from Bioline (Germany) The concentration of the samples was evaluated by Nanodrop ND 1000 Spectrophotometric from Bio-Rad. Gel extraction kit for PCR product purification and Miniprep kit for plasmid amplification were purchased from Qiagen. Competent *E. coli* cells were a kind gift from Professor Alfred Lam's lab, G40, Menzies Health Institute, Griffith University, Gold Coast, Australia. Kanamycin, Luria-Bertani (LB) broth powder and agar powder were purchased from Sigma-Aldrich.

4.2.2 Primer design for EGF-ETA fragments

The EGF-ETA fragment of the 425(scfv)-EGF-ETA was amplified using EE-F (5' GCA TGA GCT AGC ATG AAT AGT GAC TCT GAA TGT CCC CTG 3') and EE-R (5' GCA TGA CTC GAG TTA GAA AAC CTG ATG TAT GGC CAG3'). 6-base pair (bp) nucleotides over-hang containing the REs Nhe I and Xho I cutting sites were designed at each of the ends of the primers respectively. After REs treatment, sticky ends at the both sides of the primers were created and ready for the ligation reaction. Primers were shipped in the form of dry powder in concealed tubes with instruction (EE-F 95.6 µg; EE-R 93.1 µg). Both tubes were quickly spin down before the open. To prepare 100 µM primer stocks, 79 µL and 83 µL of DNase free water was added to EE-F and EE-R tubes respectively, then 10 µL of primer solution from each tube were transferred into two new Eppendorf tubes (1.5-mL) and diluted to a concentration of 10 µM, which were used in the following PCR. The rest of the 100 µM stocks were preserved at -20 °C.

4.2.3 Polymer Chain Reaction (PCR) of EGF-ETA gene fragments

Purified 425-EGF-ETA template plasmid was obtained from a colleague at Prof. Ming Wei's lab and further diluted to a concentration of 1 ng/μL as the working stock for PCR. A 50 μL of the reaction mixture was prepared in a 0.5-mL sterilized PCR tube on ice as followed recipe:

Component	Volume	Final concentration
Standard Taq Reaction buffer (10X)	5 μL	1X
dNTPs solution Mix (10 mM)	1 μL	200 μM
Forward Primer (EE-F, 10 μM)	1 μL	0.2 μM
Reverse Primer (EE-R, 10 μM)	1 μL	0.2 μM
425-EGF-ETA plasmid template (1 ng/μL)	1 μL	Total plasmid amount: 1 ng
Taq DNA polymerase	0.25 μL	1.25 unit/50μL
Nuclease free water	40.75 μL	N/A

One extra tube was prepared following the same steps. The reaction system was gently mixed and quickly spin down on a micro-centrifuge for 5 seconds and placed on ice.

The PCR thermal cycler was set up as the following conditions:

Activity		Temperature	Time
Initial Denaturation		95 °C	30 seconds
30 cycles	Melting	95 °C	20 seconds
	Annealing	60 °C	45 seconds
	Amplification	68 °C	90 seconds
Final Extension		68 °C	300 seconds
Hold		4 °C	1 hour

According to former experience, the amplification rate of Taq polymerase is normally 1000 bp/min. Given that the length of the sequence of interest is 1365 bp, the time for extension was set up at 300 seconds. The tubes were put back on the ice after the PCR process finished and the PCR products were examined on agarose gel by gel electrophoresis.

4.2.4 PCR product isolation by Agarose gel running.

1% (w/v) of agarose gel was made for gel electrophoresis. 1 g of agarose dry powder was dissolved in 100 mL of 1X TAE buffer and microwaved for 1 minute for melting. The temperature of the solution was cooled down to 50 °C and 2 µL of SYBR™ Safe DNA gel stain was added to the solution. The liquid was gently mixed and carefully poured into the gel electrophoresis tank with a comb to avoid any bubbles. The solution was air-cooled for 30-40 minutes to solid, and 20 µL PCR products mixed with sample loading dye were carefully loaded into each well. Gel running was set up at 70 Volt for 50 minutes. The gel was examined under Bio-Rad Gel Doc for imaging.

4.2.5 Gel extraction for the purification of PCR product.

The protocol provided within the QIAquick Gel Extraction Kit was followed to perform PCR products extraction from agarose gel. Nanodrop the concentration of the purified PCR product after the gel extraction.

4.2.6 REs treatment to purified PCR product and pEGFP-C1 plasmid.

50 µL of the reaction mixture for REs digestion was prepared following the recipe as below. The instruction of buffer performance for Xho I and Nhe I showed both enzymes can achieve 100% activity in CutSmart buffer (NEB). Therefore, CutSmart buffer was utilized in the digestion reaction.

Component		**Volume**
Restriction enzymes	Xho I	1 µL
	Nhe I	1 µL
DNA		1 µg
10X CutSmart buffer		5 µL (1X)

The treatment was applied to the purified PCR product and pEGFP-C1 plasmid. Follow the protocol described in Section 4.3.4 and 4.3.5, the digested PCR products and pEGFP-C1 backbone (3980bp) were isolated and extracted from agarose gel using sterilized tools and Personal protective equipment to avoid unexpected UV damage to the performer. The concentration of fragments was evaluated *via* Nanodrop after gel extraction.

4.2.7 Ligation reaction of REs treated PCR product and the backbone of the pEGFP-C1 plasmid.

The concentration of digested PCR products was 3.6 ng/μL (260/280: 1.89) and the concentration of pEGFP-C1 backbone is 15.3 ng/μL (260/280: 1.93). To perform a successful ligation reaction, the insert is normally 3-fold molar excess to the vectors. Therefore, 20 μL of ligation reaction mixture was prepared in a 0.5-mL sterilized PCR tube as follow:

Component	Volume	Final concentration
Backbones (15.3 ng/μL)	1 μL	0.006 pmol
PCR products (3.6 ng/μL)	4 μL	0.016 pmol
2X ligation buffer	10 μL	1X
20X T4 DNA ligase	1 μL	1x
DNase free water	4 μL	N/A

The tube was gently mixed and briefly centrifuged in a micro-centrifuge. The mixture was incubated at room temperature (25 °C) for 15 minutes and chill on the ice afterward. The mixture was ready for *E. coli* transformation.

4.2.8 Competent *E. coli* transformation to amplify the reconstructed plasmid through gene cloning.

4.2.8.1 LB medium and agar preparation for E. coli

8 g LB dry powder was dissolved in 320 mL distill water (DS water) in a 500-mL bottle for the preparation of LB medium. 2.5 g LB powder and 1.5 g LB agar powder were dissolved in 100 mL DS water in a 200-mL bottle to make LB agar plates. Two bottles then were autoclaved in SX-700E at 121 °C, 15 psi (~104kPa) for 30 minutes for sterilization. The two bottles were cooled down on the bench at room temperature. 0.25 g Kanamycin powder was dissolved in 10

mL Milli Q water to make a 500X stock solution (25 μg/mL). 1 mL of LB medium was transferred to a stand-by 1.5-mL Eppendorf Tube A (without antibiotics) when the temperature of the LB medium dropped to approximately 55 °C. Then 640 μL and 200 μL of 500X Kanamycin stock were added to LB medium and LB agar solution respectively to reach a working concentration of 50 μg/mL. 15 ml of LB medium was transferred to a stand-by 50-mL Falcon Tube B (with antibiotics). The LB agar solution was carefully poured into 10 petri dish in a cell culture hood and air dried to solid.

4.2.8.2 E. coli transformation with recombinant plasmid CMV-EGF-ETA and microorganism culture for plasmid amplification.

50 μL of competent cells were thawed on ice until no crystal left in the tube. 2 μL of ligation mixture from Section 4.3.7 was mixed with cells suspension and incubated on ice for 10 minutes. The plasmid-cells mixture was heat-shocked in a water bath at 42 °C for 45 seconds. The mixture was immediately transferred on ice and incubated for 5 minutes. 1 mL of LB medium without Kanamycin was added to the mixture and the tube was incubated at 37 °C for 1 hour with shaking at low speed. Then 100 μL of resulting culture was spread out on the LB agar plates (with Kanamycin) and incubated at 37 °C for overnight. A single colony of *E. coli* on the agar plate was transferred to the 15 mL LB medium (with Kanamycin) using a sterilized loop and incubated at 37 °C for 8 hours with constant shaking at low speed. After incubation, 5 mL bacteria culture was transferred to 300 mL LB medium (with Kanamycin) and incubated at 37 °C with constant shaking at low speed until the OD value of the culture reach 0.9.

4.2.8.3 E. coli cells collection for harvesting CMV-EGF-ETA' plasmids.

Two methods were applied to harvest the CMV-EGF-ETA plasmids. Miniprep kit was used to obtain more purified plasmids for following experiments such as mammalian cell transfection. The protocol provided with the kit was followed to collect plasmids.

Alkaline Lysis method was utilized to obtain a large amount of plasmid but less purified for storage. Alkaline lysis solution I, II and III was prepared following the recipe below:

Solution	Ingredient
Alkaline lysis buffer I	50mM Glucose 25mM Tris-Cl (pH 8.0) 10mM EDTA (pH 8.0)
Alkaline lysis buffer II	0.2N NaOH 1% (w/v) SDS
Alkaline lysis buffer III	5M Potassium acetate Glacial acetic acid (pure)

300 mL of *E. coli* culture was transferred to a high-speed centrifuge bottle and centrifuged at 2700g for 15 minutes. The supernatant was carefully removed from the bottle and the cell pellet was resuspended in 10 mL Alkaline lysis buffer I and incubated on ice for 10 minutes. 20 mL freshly made Alkaline lysis buffer II was added into the bottle to lysis the cells with 10 seconds' gentle shaking and incubated on ice for 10 minutes. 15 mL ice-cold Alkaline lysis buffer III was added into the tube and incubated on ice for 10 minutes. The bottle was then centrifuged at 12000g for 30 minutes. The supernatant was

gently transferred to another sterilized high-speed centrifuge bottle and a volume of Isopropanol equivalent to 60% of the supernatant volume was added to the bottle to recover the plasmids. The mixture was centrifuged at 12000g for 15 minutes and the supernatant was gently removed. The plasmids pellet at the bottom of the bottle was risen and washed with 70% ethanol 3 times and dissolved in 15 mL fresh-made TE buffer for storage at -20 °C or in 15 mL DNase free water for near use. Both solvents contain 2 μg/mL DNase-free RNase A (pancreatic RNase).

4.3 Results.

4.3.1 Primer design for the EGF-ETA gene fragment.

The p425-EGF-ETA plasmid (6597bp) was formally designed and re-constructed in Prof. Ming Wei's lab *via* Vector NT1, which contains two important functional genes: Epidermal Growth Factor encoding EGF protein for cancer cells targeting and Exotoxin An encoding toxin ETA for killing cancer cells (Figure 4.1). The backbone of Vector NT1 lacks the promotor for eukaryotic cells, therefore the plasmid cannot be expressed in mammalian cells. The function group of EGF-ETA need to be taken out and sewn into a vector backbone containing eukaryotic promotor.

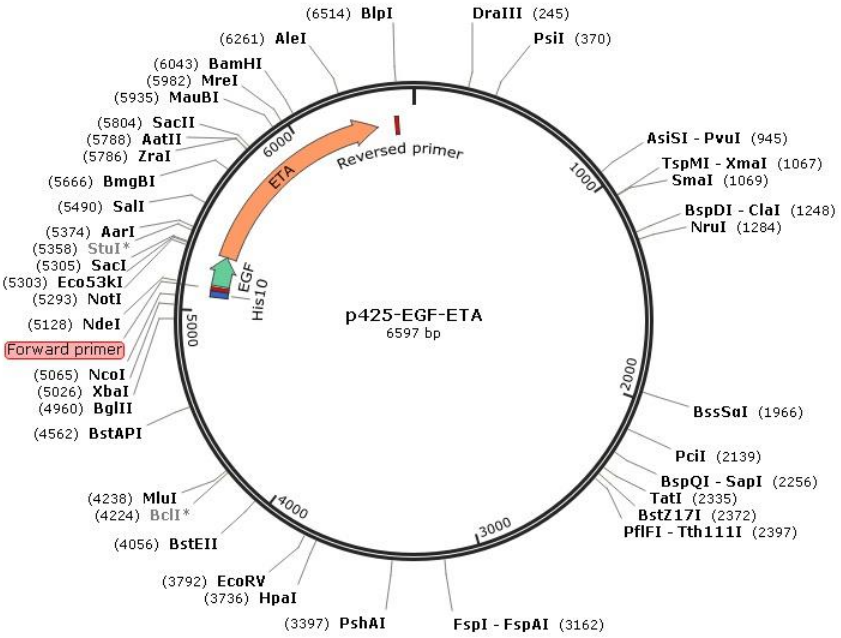

Figure 4.1. The plasmid map of p425-EGF-ETA.

The pEGFP-C1 is a 4731bp plasmid contains the eukaryotic promoter of CMV, which allow it to be expressed in mammalian cells (Figure 4.2). The function fragment of the plasmid is the gene of green fluorescent protein (GFP), which is a protein composed of 238 amino acid residues (26.9 kDa) that exhibit bright green fluorescence when exposed to light in the blue to ultraviolet range. It is widely used in gene transfection as a signal reporting gene [207-209]. Therefore, the EGF gene was removed from the of pEGFP-C1 plasmid and the backbone is a perfect candidate for carrying the target and toxin fragment of EGF-ETA into cancer cells and induce apoptosis of the targeted cells.

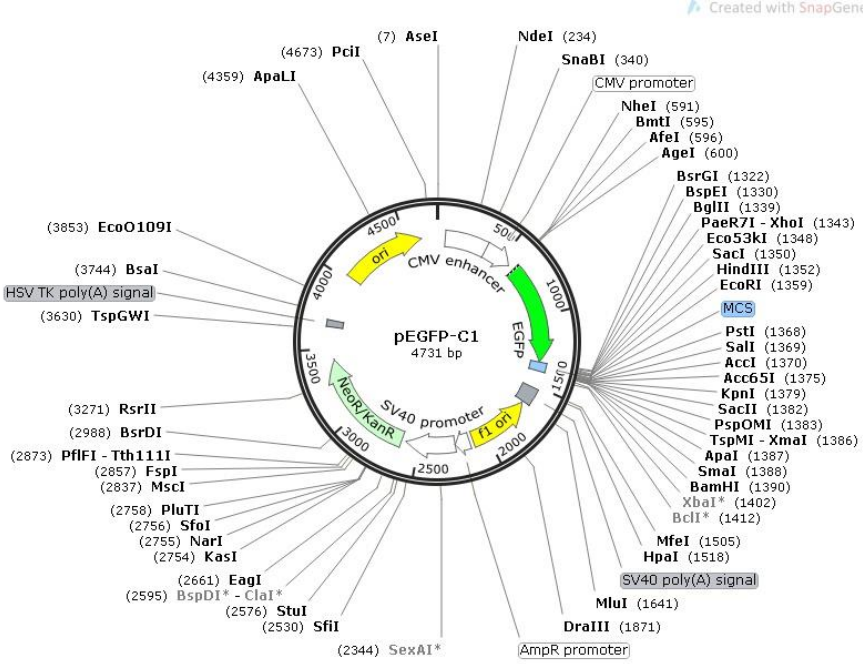

Figure 4.2. The plasmid map of pEGFP-C1.

Two REs Nhe I and Xho I was chosen to cut the pEGFP-C1 plasmid and the GFP fragment was removed. However, the p425-EGF-ETA plasmid lacks the same set of REs cutting sites near its function fragment, therefore 6bp nucleotides containing the cutting sites of chosen REs must be taken into account. The primers were designed *via* software primer 3 plus. The sequence containing 24bp of nucleotides from sequence number 5132 to 5156 were selected and its complementary sequence 5’ AAT AGT GAC TCT GAA TGT CCC CTG 3’ was created (Figure 4.3 A). A starting codon ATG and a 6bp sequence containing the Nhe I cutting site GCT AGC were added at the 5’ end of the complementary sequence, as well as an extension of 6bp GCA TGA to provide extra binding space for the Nhe I restriction enzyme. Therefore, the forward primer EE-F for the EGF-ETA fragment was determined: 5’ GCA TGA GCT AGC ATG AAT AGT GAC TCT GAA TGT CCC CTG 3’. For the creation of reversed primer, a sequence with 18bp of nucleotides from 6459 to 6479 was

selected and its complementary sequence 5' GAA AAC CTG ATG TAT GGC CAG 3' was created (Figure 4.3 B). A stopping codon TTA and a 6bp sequence containing the Xho I cutting site CTC GAG was added at the 5' end. Likewise, an extension sequence for Xho I was also inserted. Therefore, the sequence, 5' GCA TGA CTC GAG TTA GAA AAC CTG ATG TAT GGC CAG 3', was determined as the reverse primer EE-R for the EGF-ETA fragment.

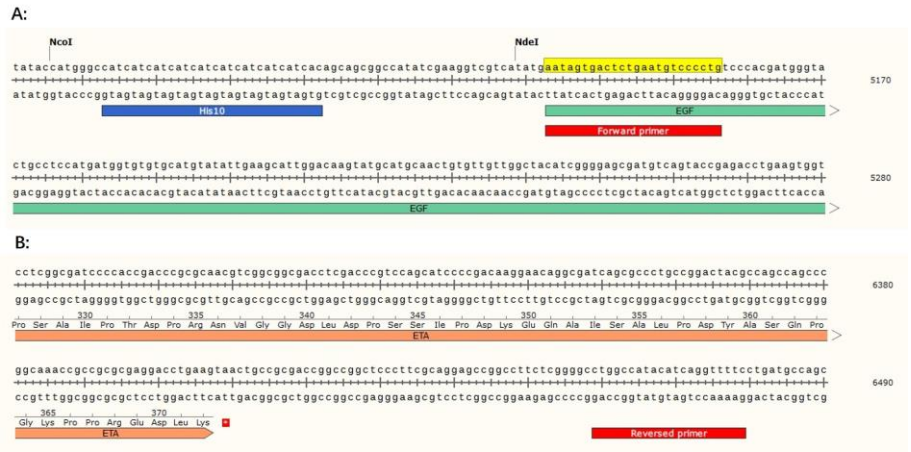

Figure 4.3. The sequence position of primers EE-F and EE-R in 425(scfv)-EGF-ETA plasmids. A: the EE-F is located from sequence number 5132 to 5156, which is in the Open Reading Frame (ORF) of the EGF gene; B: the EE-R is located from sequence number 6459 to 6479, which is outside the ORF of the ETA gene.

The forward primer EE-F was checked for Kozak consensus sequence. Kozak consensus sequence is a sequence which is normally present in eukaryotic mRNA and possesses the consensus RccAUGG sequence. It is believed that the Kozak sequence plays a major role in the initiation of the translation process [210]. In the EE-F primer, the sequence surrounding the starting codon is AGC ATG A or AGC AUG A after transcription. 5 out of 7 nucleotides matched the

Kozac sequence. Therefore, an “adequate” consensus to the Kozak sequence was achieved in the EE-F primer.

NEB T_m Calculator was used to estimate the T_m value for both primers. The GC content of the EE-F primer is 49% and the T_m value is 68 °C, whereas the GC content of the EE-R primer is 47% and the T_m value is 66 °C. The estimated annealing temperature to templates is 61 °C. The two primers were also examined for cross-pairing and self-pairing *via* online tool DINAMelt. Figure 32 showed the cross-pairing status between the two primers. An external loop containing 32 single stranded bases was detected and only one helix cross-pairing occurred. 4 base pairs were involved in the cross-pairing and the Tm of the dimer is 15.6 °C. Figure 33 showed the self-pairing status within the two primers. Two hairpin loops including 13 single stranded bases and 2 closing helices were revealed in the EE-F primer (Figure 4.4 A). Two dimers were formed including 4 and 3 base pairs respectively. The T_m of the dimers in EE-F primer is 49.5 °C. One external loop including 27 single stranded bases and 1 closing helix was detected in EE-R primer (Figure 4.4 B). The T_m of the dimer is 42.4 °C. Given that the annealing temperature was estimated at 61 °C, which is much higher than the T_m value of any dimers formed between or within two primers, suggesting that the secondary structures will be neutralized during the PCR progress.

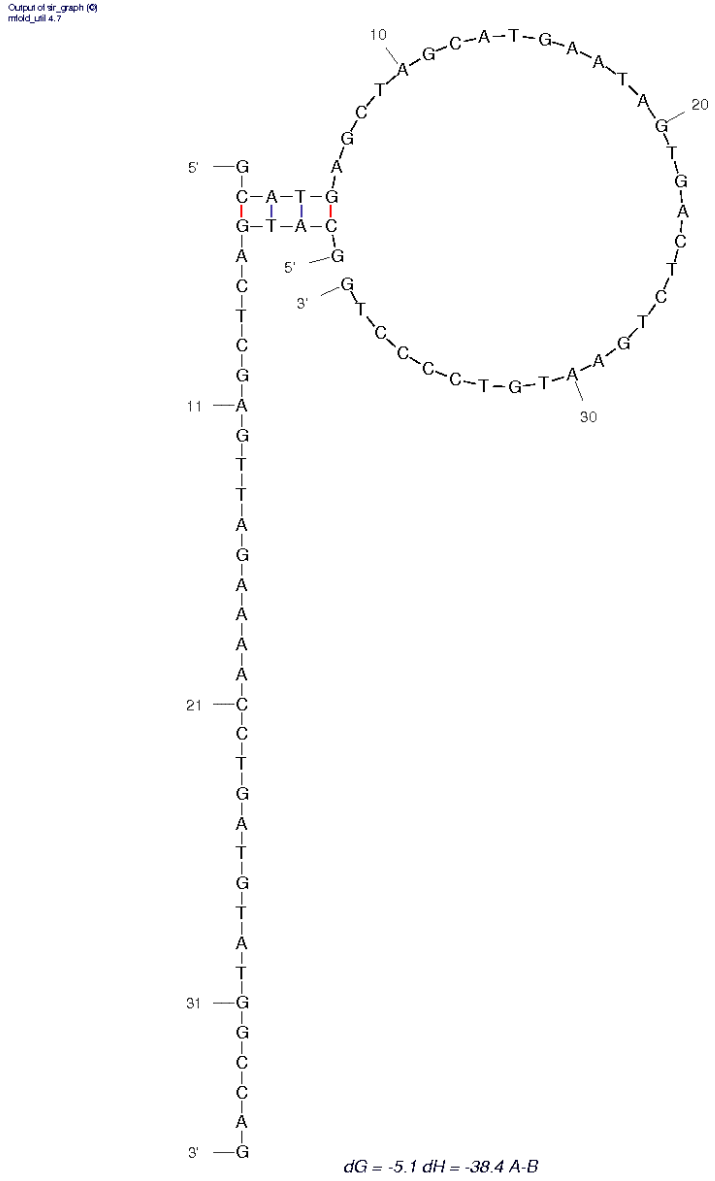

Figure 32. The thermodynamic status between two primers. An external loop containing 33 single stranded bases was detected and only one helix cross-pairing was formed. The Tm of the dimer is 15.6 °C

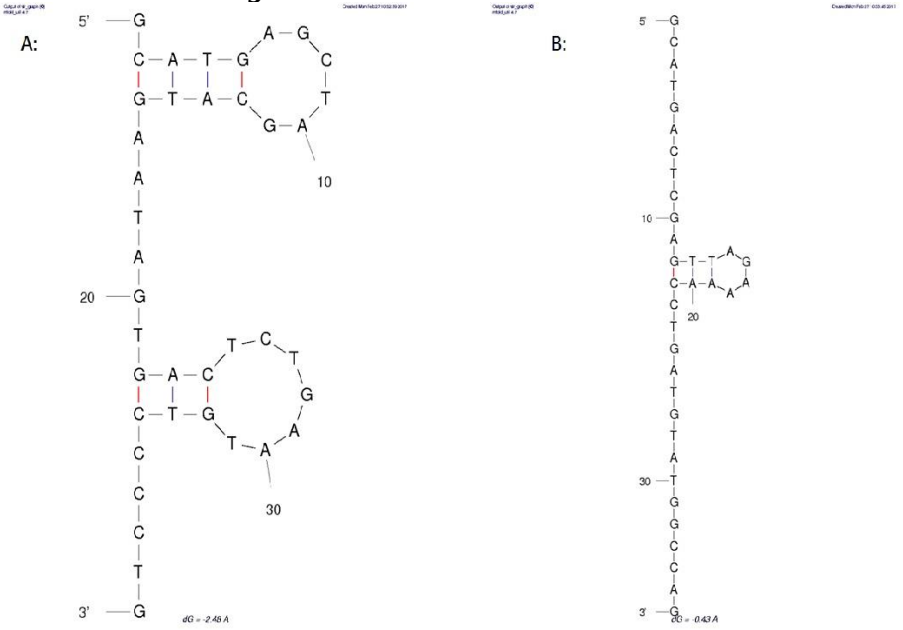

Figure 4.4. The thermodynamic status within A: the EE-F primer; B: the EE-R primer.

4.3.2 Amplification of EGF-ETA fragment *via* Polymer Chain Reaction (PCR) and purification of PCR product.

Two reaction systems were prepared and the PCR was run for 30 cycles. The PCR products were examined by Gel electrophoresis (Figure 4.5).

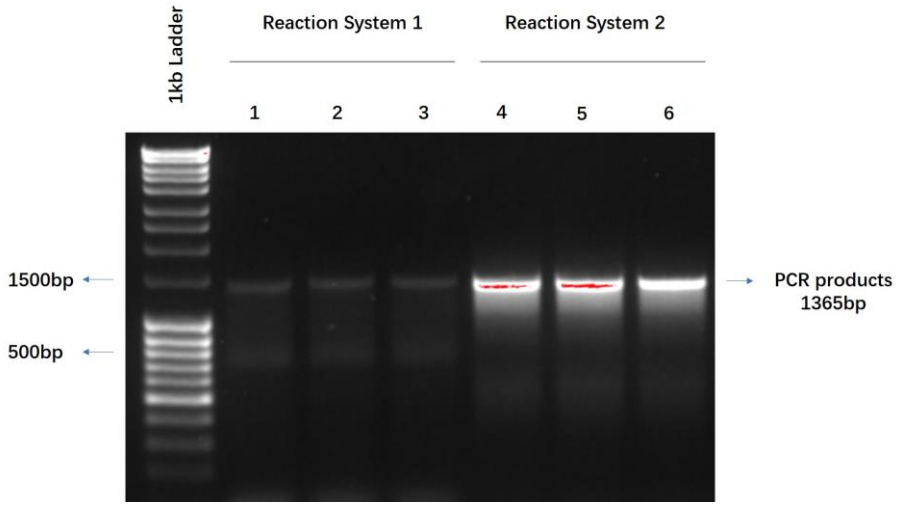

Figure 4.5. The PCR products examined and isolated by Gel electrophoresis.

Bright bands were observed in line 4, 5 and 6, which were slightly below the 1500bp band of the ladder in position. Given that the length of the sequence of interest is 1365bp, it was implied that the bright bands in these three lines are the EGF-ETA fragments. No clear bands of unspecific-binding were recognized in these three lines. Bands were also shown in line 1, 2 and 3 in the similar position, which was much weaker than those in the other 3 lines. Moreover, weak unspecific-binding bands were observed at the similar position of the 500bp band in the ladder. These could be caused by the uneven heat during the PCR process. The machine that performed PCR was relatively old and lack of maintenance. The heating or cooling process for the PCR tube socket for reaction system 1 could be compromised. The temperature in the tube couldn't be controlled precisely. The temperature for the annealing step might be lower than 60 °C, resulting in unexpected primer dimers or unspecific-bindings. Therefore, the PCR products from line 1, 2 and 3 were abandoned, the bright bands from line 4, 5 and 6 were chosen for gel extraction in the following step.

Small gel pieces containing the three bands were quickly cut and collect from the whole gel under UV light with sterilized tools to prevent damages to the DNA fragments from long-term UV light exposure. Gel extraction was performed using QIAquick Gel Extraction Kit. The concentration of the PCR products after gel extraction was evaluated by Nanodrop, which was 13.7 ng/μL (260/280: 1.91).

4.3.3 The creation of CMV-EGF-ETA plasmid through REs treatment, ligation, *E. coli* transformation and plasmid harvest.

4.3.3.1 CMV-EGF-ETA transformed E. coli colonies obtained by REs treatment, ligation, E. coli transformation.

The PCR products and pEGFP-C1 plasmids were firstly digested by two REs. The digested PCR products and the backbone of pEGFP-C1 were extracted from agarose gel and the concentration of both DNA fragments was evaluated by Nanodrop, which is 3.6 ng/μL (260/280: 1.89) and 15.3 ng/μL (260/280: 1.93) respectively, followed by the ligation performance (data not shown). E. coli was transformed by the ligation products and cultured selective LB agar at 37 °C for overnight. Colonies selected by Kanamycin were observed on the LB agars (Figure 4.6).

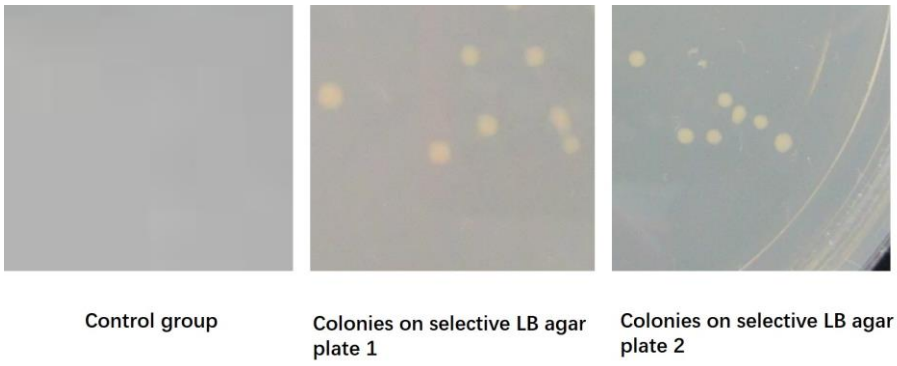

Figure 4.6. Transformed and un-transformed competent *E. coli* cells cultured on LB agar plate selected by Kanamycin.

In the control group, competent *E. coli* cells were not transformed by the ligation products. Due to the lack of anti-Kanamycin gene, the growth of all the bacteria was inhibited by the antibiotics. Therefore, there was no colonies growing on the control group plate. However, colonies were observed on selective LB agar plates 1 and 2, indicating that the DNA fragments yield from PCR process were successfully linked with the pEGFP-C1 backbone and the newly generated plasmids containing the anti-kanamycin gene on the pEGFP-C1 backbone can

be expressed within the *E. coli* cells, facilitating them to survive the environment with Kanamycin.

4.3.3.2 CMV-EGF-ETA plasmids amplification and confirmation by REs treatment.

A single colony from selective LB agar plate 1 was chosen for sub-culture to amplify the CMV-EGF-ETA plasmid. Two methods described in Section 4.3.8.3 were used to harvest the amplified plasmids. To examine the extracted plasmids from *E. coli* cells, PCR using the EE-F and EE-R primers and REs treatment was performed (Figure 4.7)

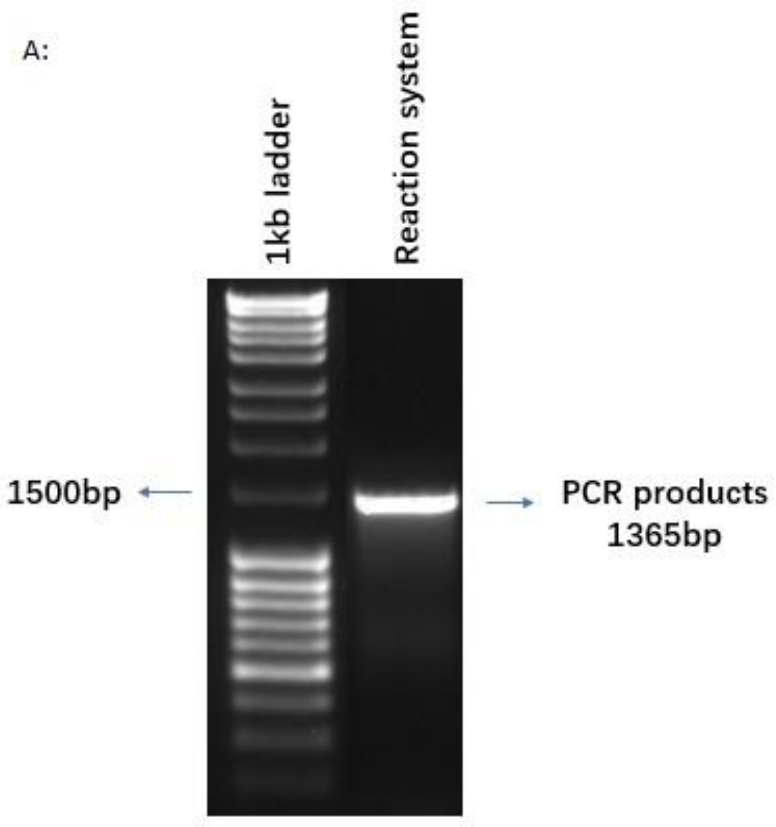

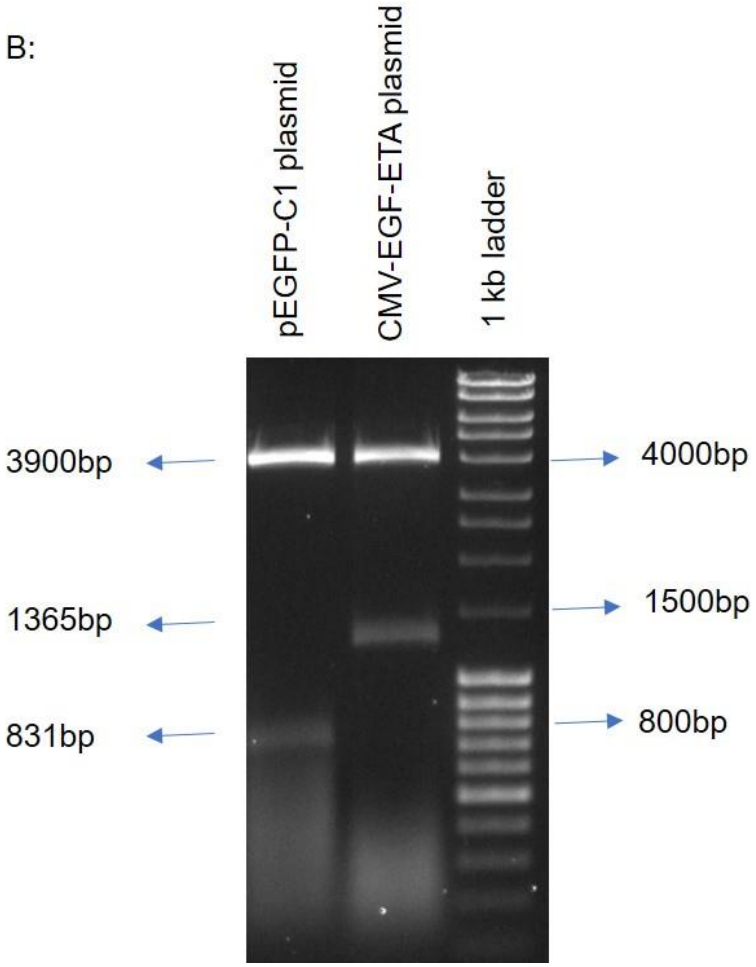

Figure 4.7. PCR (A) and REs (B) treatment using the plasmids harvested from *E. coli*.

As shown in the Figure 4.7 A, consistent PCR result in Section 4.4.2 was observed. A clear band was observed at the position slightly lower than the 1500bp band in the ladder indicating the newly created plasmid contains the EGF-ETA fragment, which is consistent with the PCR results in Section 4.4.2. No bands of unspecific-binding were shown in the gel image. The plasmids were also digested by the two REs (Figure 4.7 B), two clear bands near 4000bp and 1500bp were observed. Given that the length of the backbone of pEGFP-C1 and EGF-ETA fragments are 3900bp and 1365bp, it can be confirmed that the new plasmids contains both DNA fragments and can be functioned in Prokaryotic cells. The immunotoxin CMV-EGF-ETA was successfully designed

and synthesized through gene cloning and ready for examining the ability to induce apoptosis in cancer cells.

4.4 Discussion

In this Chapter, the aim is to design and synthesize the CMV-EGF-ETA plasmid for the following tests *in vitro*. Two DNA fragments of EGF-ETA and the backbone of pEGFP-C1 were removed from their original carrier and linked together. The EGF-ETA fragments were amplified and isolated through Polymer Chain Reaction and Gel extraction. The EE-F and EE-R primers for the EGF-ETA fragments were designed *via* online tool Primer3Plus and examined their thermodynamic status *via* DINAMelt and NEB T_m calculator. PCR was performed by using 425-EGF-ETA as a template. PCR products were examined, purified and extracted from agarose gel and digested by two restriction enzymes Xho I and Nhe I, so were the pEGFP-C1 plasmid. The EGF-ETA and the backbone of pEGFP-C1 fragments then were ligated and internalized into competent *E. coli* by heat shock. The transformed *E. coli* cells containing anti-biotics gene survived the Kanamycin selection and formed colonies on LB agar. A single colony was chosen and sub-cultured for the CMV-EGF-ETA plasmids amplification. The plasmids were harvested through two methods, more purified plasmids collected from QIGEN kit were used for following experiments and those yielded from Alkaline Lysis methods with relatively larger amount were reserved in - 20°C freezer.

When designing primers, the sequences surrounding the starting codon ATG should be consensus to the Kozac sequences, which is crucial for the plasmids expressed in mammalian cells. Kozac sequence is believed to be a

conservative sequence widely occurred in eukaryotic mRNAs. In DNA, the Kozak sequence is 5' RCC ATG G 3', where the ATG is the starting codon. R represents A, T, G or C and the A of the "ATG" is referred as number 1 position [211]. Mutagenesis studies and a survey of 699 vertebrate mRNAs claimed that, to achieve a "strong" consensus, the nucleotides at +4 position must be G and -3 position must be an or G. In the EE-F primer, the 7bp sequence containing ATG is AGC ATG A, where the nucleotides at positon of +4 is A and -3 is A and only one site matches. However, the nucleotide at the position of +4 with the second highest occurrence rate is A [212,213]. Therefore, an "adequate" consensus to the Kozak sequence was achieved insuring the expression of CMV-EGF-ETA proteins in cancer cells in the following experiments. Therefore, the examination of the consensus between the sequences near the starting codon and Kozac sequences for successful plasmid expression in mammalian cells is equally critical to that of the thermodynamic status of primers for successful PCR performance.

The annealing temperature in the PCR process should be determined by the gradient PCR experiment for several times, in which different annealing temperature points for primers and templates were set as follow: 58°C, 59.2°C, 60.4°C, 61.6°C, 62.8°C, 64°C, 65.2°C, 66.4°C, 68.6°C, 69.8°C, 71°C and 71.2°C. The temperature range could be narrowing down until the best annealing temperature for a specific set of primers and templates was revealed. In this chapter, the gradient PCR experiments for deciding the best annealing temperature of primer EE-F, EE-R and 425-EGF-ETA plasmid templates were not performed. This is because that when the PCR first test run was performed for examining the primers and the templates as well as the PCR machine, a

standard protocol of routine PCR was followed and the annealing temperature was set 60°C. Surprisingly, the PCR results showed in agarose gel turned out to be good. Even though the bands of interest from the first reaction system were weak and several unexpecting bands also showed in the gel image indicating unspecific-binding, the bands from the second reaction system were strong and clear enough for gel extraction. Given the aim of this experiment is to successfully obtain the EGF-ETA fragments through PCR process rather than achieving a perfect PCR performance, the bands from the second reaction system were decided to be extracted from the gel and ligated with pEGFP-C1 backbone. Results in Chapter 5 also proved the integrity and function of the EGF-ETA fragments in the CMV-EGF-ETA immunotoxins.

Initially, the ligation and *E. coli* transformation were not successful, given no colonies were observed on the LB selective agar. Trouble shooting for the experiments was carried out for months. Eventually, the problem revealed. Due to the large volume of the ligation mixture added to the competent *E. coli* cells for heat-shock, the transformation was inhibited. In the ligation system, polyethylene glycol (PEG) with a concentration of 5%-15% was existed for enhancing the ligation efficiency. However, the transformation efficiency could be significantly reduced when the PEG concentration is over 5% in the transformation system. After reducing the volume of ligation mixture added to the competent cells tube to 2 μL, colonies were observed on the LB selective agar indicating the ligation and *E. coli* transformation was successful.

4.5 Conclusion

To summaries, the new immunotoxin CMV-EGF-ETA was firstly designed and synthesized through gene cloning in the lab. The results during the procedure clearly showed that the DNA fragments of interest from two different origins were isolated and purified and eventually linked with each other to create the plasmid. The newly generated immunotoxin was ready to evaluate the ability to target cancer cells that overexpress EGFR and inducing their apoptosis.

Chapter 5 LDH nanoparticles

Encapsulating the immunotoxin CMV-EGF-ETA targets to A549 and MCF-7 cancer cells and induces cell death

5.1 Abstract

Previous studies have shown the capability of Layered Double Hydroxides (LDHs) in gene/drug delivery, which could be potentially developed into gene therapies for cancer treatment. In this chater, we present an attempt of employing Layered Double Hydroxide nanoparticles as gene carrier to deliver immunotoxin into tumor cells that overexpress epidermal growth factor receptor (EGFR) in order to control/suppress tumor growth. The reconstructed toxic plasmid contains epidermal growth factor (EGF) gene and Exotoxin A (ETA) gene. EGF is a known natural ligand of EGFR, which will function as a targeting molecule leading the Plasmid/LDH complex to cancer cells. Exotoxin A is a toxin produced by Pseudomonas aeruginosa that can cause damage to the host by destroying cells or disrupting normal cellular metabolism. Cellular uptake efficiency of Plasmid/LDH complex by Homo Sapiens Lung Carcinoma cell line (A549) and Homo Sapiens Breast Adenocarcinoma cell line (MCF-7) was evaluated *in vitro*. The cytotoxicity of the complexes to two tumor cells in culture was examined as well. The result showed that the transfection efficiency using LDH as drug carrier can achieve a similar level to that facilitated by Lipo2000.

Fluorescence microscope data also proved that the LDH nanoparticles helped the accumulation of the immunotoxin in both cell lines. Moreover, the cytotoxicity of the EGF conjugated immunotoxin to tumor cells was correlated with EGFR expression as well. In conclusion, active targeting immunotoxin into EGFR-overexpressed tumors can further enhance their anti-tumor activity. LDH nanoparticle, representing the inorganic material, can achieve high gene delivery efficiency *in vitro* as gene carrier and great potential for clinical application.

5.2 Introduction

In recent years, significant progress has been made in the development of gene therapy for cancer. Classic and new therapy, such as suicide, DNA vaccination, gene suppression/silencing *et al* aimed for more efficient and accurate strike to known or novel targets with improved gene delivery and efficacy [214-217]. However, the metastasis of cancer, especially in its stage III or IV, is still one of the major obstacles to achieving systemic gene delivery. Most of the current gene therapies are still suffering from poor selectivity and transfer efficiency, loss of drug efficacy in clinical application. As a consequence, the majority of current gene therapy trials for cancer treatment are at stage I and only a few managed to enter stage II/III or even stage IV. Therefore, efforts need to be made urgently to enhance the accuracy of tumor cell targeting, the safety of gene transportation in the bloodstream and the accumulation of transgene inside of targeted cells [218].

In this regard, nanotechnology has been employed for sustained, efficient gene delivery to tumor cells. Layered Double Hydroxides (LDHs) is one of the members of anionic clay materials family. Most of the LDH materials can be described by a general formula $[M^{II}_{1-x}M^{III}_{x}(OH)_2^{x+}(A^{m-})_{x/m}\cdot nH_2O]$ (x = 0.2-0.4; n = 0.5-1), where M^{II} represents a divalent metal cation, M^{III} a trivalent metal cation and A^{m-} an anion [6,8,66]. Compared with old-fashioned drug delivery methods which are suffering from problems such as drug degradation, poor bioavailability, and low circulation stability, the promising inorganic matrices, are much simpler to synthesize in the laboratory and offer a high drug transportation efficiency and drug loading density, low toxicity to cells or organs and excellent protection to loaded molecules from undesired enzymatic degradation [6]. A plethora of bio-molecules has been reported to loaded to LDHs through co-precipitation or anion-exchange reaction, including amino acid and peptides, ATPs, vitamins, and even polysaccharides [9]. Particularly, as a drug carrier, LDHs has performed remarkably in delivering nucleotides, including oligonucleotides (20bp~200bp) and plasmids (1kb~5kb). Recent studies have demonstrated that LDHs are efficient carriers to deliver siRNA into cortical neurons for gene silencing [10] and pEGFP-N_2 plasmid into Vero 3 (African Monkey Kidney) cells for expression of the gene of interest [4]. The studies demonstrated that the LDHs can deliver nucleotides into target cells safely and efficiently without comprising their biological function.

Although employing LDH nanoparticles for the development of potential gene therapy for cancer treatment has shown great promise, an ideal delivery system that can not only achieve safe drug transportation and fast drug accumulation in

cancer cells but also perform an accurate attack to targets would further enhance cancer treatment efficacy. Due to the simplicity of the LDH nanoparticles' composition and structure, it is difficult to modify the LDHs with a targeting molecule. Therefore, the epidermal growth factor (EGF) gene has been introduced into a reconstructed plasmid in our work. The epidermal growth factor receptor (EGFR) is a transmembrane glycoprotein that consists of one of four members of the erbB family of tyrosine kinase receptor [198] and plays a crucial role in regulating cellular proliferation, differentiation and survival [195]. It is believed that the epidermal growth factor receptor (EGFR) is overexpressed in a variety of tumor cell lines and EGF is the natural ligand of EGFR [198]. Therefore, the EGF could serve as a targeting molecule specifically aiming to EGFR overexpressed tumor cells to avoid or minimize many of nonspecific toxicities associated with gene therapies [196].

In this study, we present an attempt of employing Layered Double Hydroxide nanoparticles as gene carrier to deliver reconstructed toxic plasmid containing epidermal growth factor (EGF) gene into tumor cells that over-express epidermal growth factor receptor (EGFR) to control/suppress tumor growth. It was hypothesized that EGFR-targeted plasmid-Layered double hydroxide complexes could show enhanced anti-tumor activity. The pEGFP-C1 plasmid was firstly reconstructed by replacing the EGFP gene with EGF and Exotoxin A (ETA) genes and the newly reconstructed plasmid is named CMV-EGF-ETA. Then it was safely and efficiently delivered into EGFR-overexpressed tumor cells and the EGF-ETA protein is expressed. One cell is dead and lysed, the

EGF-ETA protein will be released into the extracellular environment and led to the EGFR-overexpressed tumor cells, inducing tumor cell apoptosis.

5.3 Materials and Methods

5.3.1 Materials and tools

Dulbecco's modified Eagle's Medium (DMEM, D5796), Fetal Bovine Serum (FBS, F2442-500ML), Dimethyl sulfoxide (DMSO) and Trypsin-EDTA solution (0.25%, T4049-100ML) were purchased from Sigma-Aldrich (Australia). SYBR™ Safe DNA gel stain (No.1621159), 100X Penicillin-Streptomycin solution, Opti-medium, Phosphate Buffer Saline tablets (FBS, 003002) and MTT assay powder were bought from Invitrogen, life technology. DNase I (2 U/μL) was bought from Thermo-fisher scientific. Standard Agarose gel powder (low Electro-endosmosis) was purchased from PanReac-AppliChem (USA). T25 and T75 cell culture flasks (vented cap, TC treated) were purchased from Corning Inc. (USA). Human lung carcinoma cell line A549 (CCL-185) and Human breast adenocarcinoma cell line MCF-7 (HTB-22) were purchased from the American Type Culture Collection (ATCC). 6-well and 96-well plates were purchased from Corning, Sigma-Aldrich.

5.3.2 Characterization of CMV-EGF-ETA and LDH Plasmid/LDH hybrids.

The CMV-EGF-ETA and LDH plasmid/LDH hybrids in total 10 ml were synthesized *via* an ion-exchange mechanism with a mass ratio LDN: plasmid= 1:1 and incubated at 37°C with gentle shacking for 15 minutes. Then the hybrids were centrifuged at 16000rpm for 30mins to remove free plasmids and freeze-dried to yield a product with a constant weight. The hybrids powder was

analyzed by Fourier transform infrared spectroscopy (FTIR) using a Nicolet 6700 FTIR instrument in ATR mode and powder X-ray diffraction (XRD) using the X-ray diffractometer in order to verify chemical composition and crystal structure of the nanoparticles, respectively

5.3.3 CMV-EGF-ETA and LDH interaction efficiency

5.3.3.1 Plasmid and LDH intercalation efficiency.

In order to determine the best mass ratio of LDH: plasmids, intercalation between LDH and plasmids with different mass ratio was performed as below. The mass of plasmids was fixed at 1 μg, whereas the mass of LDH varied in different systems.

Mass ratio	Component	Amount
5:1	LDH	5 μg
	Plasmid	1 μg
2:1	LDH	2 μg
	Plasmid	1 μg
1:1	LDH	1 μg
	Plasmid	1 μg
0.5:1	LDH	0.5 μg
	Plasmid	1 μg
0.2:1	LDH	0.2 μg
	Plasmid	1 μg
0.1:1	LDH	0.1 μg
	Plasmid	1 μg

1 μg of Plasmids were mixed with LDH with different mass in 6 Eppendorf tubes and incubated at 37°C for 15 minutes with gentle shacking. Then the LDH and plasmid intercalation efficiency were examined through Gel electrophoresis. The LDH/Plasmids complexes were mixed with DNA loading dye and loaded onto 1% agarose gel. Gel running was performed under 70 Volt for 50 minutes. Results were imaged by Gel Doc.

5.3.3.2 LDH protection efficiency

6 LDH/Plasmids intercalation systems from Section 5.3.3.1 were treated with DNase to examine the ability of LDH protecting plasmids from unexpected degradation. Reaction systems were prepared as follow:

Mass ratio	Component	Amount	DNase
5:1	LDH	5 μg	0.25 U/μL
	Plasmid	1 μg	
2:1	LDH	2 μg	0.25 U/μL
	Plasmid	1 μg	
1:1	LDH	1 μg	0.25 U/μL
	Plasmid	1 μg	
0.5:1	LDH	0.5 μg	0.25 U/μL
	Plasmid	1 μg	
0.2:1	LDH	0.2 μg	0.25 U/μL
	Plasmid	1 μg	
0.1:1	LDH	0.1 μg	0.25 U/μL
	Plasmid	1 μg	

The DNase I stock (2 U/μL) was diluted to 0.25 U/μL and added to each reaction system to treat the LDH/plasmid complex at 37°C for 30 minutes. The enzyme was inactivated at 75°C for 10 minutes and the LDH protection efficiency was examined through Gel electrophoresis. The DNase I treated LDH/Plasmids complexes were mixed with DNA loading dye and loaded onto 1% agarose gel. Gel running was performed under 70 Volt for 50 minutes. Results were imaged by Gel Doc.

5.3.3.3 Plasmid integrity examination after intercalation with LDH

LDH/plasmid complexes were synthesized at a mass ratio of 0.2:1 and incubated at 37°C for 15 minutes with gentle shacking. 1 volume of 1X PBS was added to the system to exchange the plasmids out of the LDH nanoparticles and incubated at 37°C for 15 minutes with gentle shacking. A duplicated system was also prepared and treated with DNase I at 37°C for 30 minutes after the second incubation. The enzyme was inactivated at 75°C for 10 minutes and the integrity of the plasmids after intercalation with LDH were examined through Gel electrophoresis. The mixtures were mixed with DNA loading dye and loaded onto 1% agarose gel. Gel running was performed under 70 Volt for 50 minutes. Results were imaged by Gel Doc.

5.3.4 Cell culture for A549 and MCF-7 cancer cell lines

5.3.4.1 Cell culture medium preparation

500 mL fresh frozen FBS was transferred from -20°C to 4°C to thaw for overnight. The liquid FBS was then heat-inactivated in a water bath at 56°C for

30 minutes. The FBS bottle was swirled every 10 minutes to ensure uniform heating of the serum. After 30 minutes, the bottle was immediately transferred to an ice bath to cool down the serum. Then the whole bottle of the serum was aliquoted into 10 sterilized falcon tubes (50 mL each) in a clean cell culture hood. 1 stand-by tube was placed in the hood for the preparation of the complete medium and the rest of the tubes were transferred to -20°C for storage.

Complete medium for A549 lung cancer cell line and MCF-7 breast cancer cell line was prepared as the following recipe:

DMEM medium (low glucose)	**FBS (heat-inactivated, aliquoted)**	**100X Penicillin-Streptomycin solution**
500 mL	50 mL	5 mL

The bottle was gently swirled to ensure the ingredients were mixed well. 100 mL of the complete medium was aliquoted to two sterilized falcon tubes (50 mL each) for the use in experiments, the rest of the medium were stored at 4°C as stocks.

5.3.4.2 A549 and MCF-7 cell line recovery from liquid nitrogen

Complete medium was warmed up at 37°C water bath for 30 minutes. The cell stocks containing 1 mL of frozen cell medium from liquid nitrogen were quickly transferred to the clean cell culture hood. 1 mL of the warm complete medium was added to each tube and the thawed in hand until no crystal ice left in the tubes. The melted cell suspension was quickly transferred to a sterilized 15 mL

centrifuge tube and spin down at 800rpm, 4°C for 5 minutes to remove DMSO. The supernatant was discarded and each of the cell pellets was re-suspended in the 1 mL warm complete medium. The cell suspension was gently pippeted up and down and transferred into the T25 cell culture flasks with the 5 mL complete medium. The T25 flasks were placed in the cell culture incubator at 37°C, 5% CO_2 environment. After the cell recovered, they were transferred to T75 flasks for sub-cultures.

5.3.4.3 Cell culture maintenance

Cells were split when the cell confluency reached 70-80%. Complete medium, 0.25% trypsin-EDTA and PBS were pre-warmed at 37°C water bath for 20 minutes. Cells were washed twice with PBS and detached from the flask bottom by 2 mL trypsin-EDTA. The enzyme digestion was terminated by adding the same volume of complete medium to the flask. The cell pellet was collected after 1500rpm, 4°C centrifuge in 15 mL sterilized tube and re-suspended with complete medium. The cell was seeded into new T75 flasks with 15 mL of complete medium with a splitting ratio of 1:10 or 1:20. The T75 flasks were placed in the cell culture incubator at 37°C, 5% CO_2 environment.

5.3.4.4 Cryopreservation for liquid nitrogen cell stocks

Complete medium was placed at 4°C until use. Freezing medium was prepared as complete growth medium supplemented with 5% DMSO (v/v) to a final volume of 10 mL. Cells were collected following the protocol described in Section 5.3.4.3 and cell counting was performed. 2×10^6 cells for A549 and 2.5×10^6 cells for MCF-7 were re-suspended in 1 mL freezing medium and

transferred into cryovials. Cells were frozen slowly by reducing the temperature at approximately 1°C per minute using a controlled rate cryo-freezer in -20°C for 2 hours and -80°C for overnight. Cell stocks were transferred and stored in liquid nitrogen on the second day.

5.3.5 A549 and MCF-7 cell line transfection with pEGFP-C1 plasmid using LDH and Lipofectamine 2000

Cells were collected following the protocol described in Section 5.3.4.3 and seeded at a density at 0.3×10^6 cells/well in a 6-well plate. Plates of A549 and MCF-7 cells were incubated at 37°C with 5% CO_2 for overnight.

pEGFP-C1 plasmids stock and fresh-made LDH were diluted to the concentration of 1 μg/μL for use. The transfection agents using LDH and Lipofectamine 2000 were prepared with the plasmids on ice as described below:

Transfection system	Plasmids	LDH	Lipo 2000	Opti-medium
LDH/Plasmids (mass ratio: 2:1)	2.5 μg/well	5 μg/well	N/A	100 μL
Lipo/Plasmids	2.5 μg/well	N/A	7 μL/well	100 μL

LDH was mixed with the pEGFP-C1 plasmids with a mass ratio of 2:1 and incubated at 37°C with gentle shacking. Then the mixture was added to 100 μL Opti-medium for pre-incubation and transfection. Plasmids and Lipofectamine 2000 were pre-incubated with 50 μL Opti-medium respectively for 10 minutes

and mixed with each other for 5 minutes on ice. Cells were washed with PBS twice and the medium was changed to 2 mL Opti-medium. Two transfection system were added to each well drop-wisely except the control groups. The cells were then cultured at 37°C, 5% CO_2 for 6 hours and topped up with the 2 mL complete medium. After another 18 hours' incubation, the cells were examined under Fluorescence microscope for imaging.

5.3.6 Cell Proliferation examination *via* MTT assay

5.3.6.1 Reagent prepared for MTT assay

12mM MTT reagent stock solution was prepared by dissolving 50 mg MTT powder in 10 mL sterilized fresh-made PBS. The solution was sterilized by filtration with 0.22 nm filter and stored at 4°C protected from light up to 4 weeks. 1 mL of the stock solution was diluted in 10 mL of complete medium to achieve working concentration (reagent A) before use. Reagent B was prepared by dissolving 1 mg SDS powder in 10 mL 0.01M HCl at 37°C with a gentle stir. 100 µL of reagent B was used for each well.

5.3.6.2 MTT assay for A549 and MCF-7 cells after transfection with CMV-EGF-ETA immunotoxin facilitated by LDH.

Cultured cells from T75 flasks were collected following the protocol from Section 5.3.4.3 and seeded in the 96-well plates with a cell density of 5000 cells/well. Then the cells were cultured overnight and transfected with CMV-EGF-ETA immunotoxin following the protocol described in Section 5.3.5. After 24 hours' transfection, the cells in the plates were gently centrifuged down and the medium was replaced by 100 µL pre-mixed MTT reagent A. The cells with

reagent A were incubated at 37°C for 4 hours and 100 µL reagent B was added to each well and mixed gently. Then the cells were incubated at 37°C for another 18 hours and the results were evaluated by POLARstar Omega plate reader.

5.4 Results

5.4.1 Characterization of LDH/plasmid hybrids

5.4.1.1 Chemical composition of LDH-Plasmid complex

The CMV-EGF-ETA and LDH plasmid/LDH hybrids in total 10 ml were synthesized *via* an ion-exchange mechanism with a mass ratio LDN: plasmid= 1:1 and incubated at 37°C with gentle shacking for 15 minutes. Then the hybrids were centrifuged at 16000rpm for 30mins to remove free plasmids and freeze-dried to yield a product with a constant weight. The pristine LDH nanoparticles, CMV-EFG-ETA plasmids and the hybrids were analyzed by FTIR (Figure 5.1)

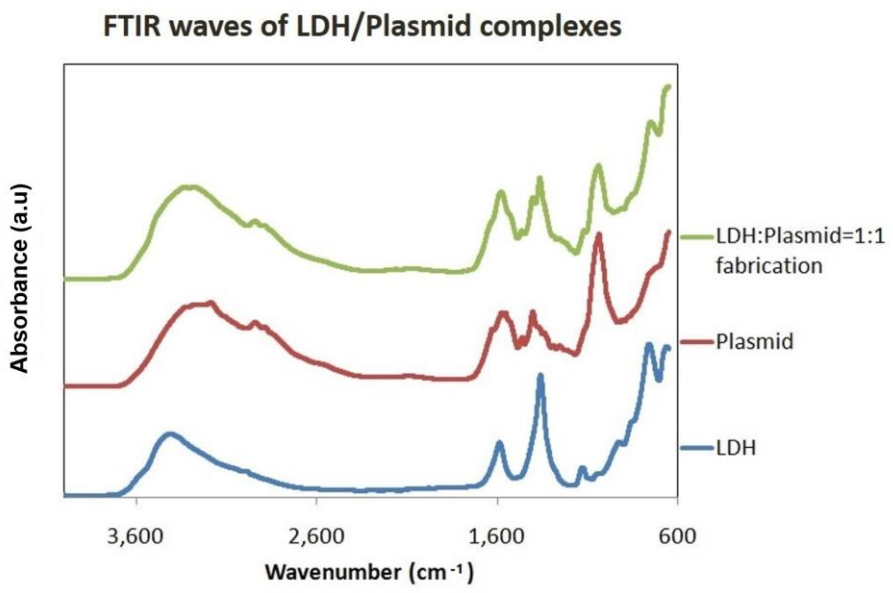

Figure 5.1. FTIR spectra for pristine LDH nanoparticles, CMV-EGF-ETA plasmids and LDH/Plasmids complexes. Samples were frozen to powder and placed on the FTIR plate.

The pristine LDH spectrum showed some peaks commonly appearing in Mg-Al LDH spectra: (a) the intense broadband around 3400-3500 cm^{-1} associated with stretching vibration of O-H in the brucite-like layer and water molecules; (b) the sharp band that appeared at 1352 cm^{-1} represents the CO_3 group which is an unavoidable contamination during the LDH synthesis; (c) according to GuZi *et al* [219], two peaks could be found at 500-600 cm^{-1} and 400-500 cm^{-1} which attributed to M-O stretching vibrations and particularly characteristic of Mg_2Al-LDH materials respectively, yet these two peaks are not shown in this image due to the narrow range of the" wavenumber" (abscissa). It could be observed that after the fabrication, peaks that separately possessed by both pristine LDH and plasmid all appeared in LDH-plasmid complex, indicating that all the important groups still existed and none of them was degraded during the complex synthesis.

5.4.1.2 Crystal structure analyses of LDH/Plasmids hybrids

The pristine LDH nanoparticles, CMV-EFG-ETA plasmids and the hybrids were also analyzed by XRD (Figure 5.2).

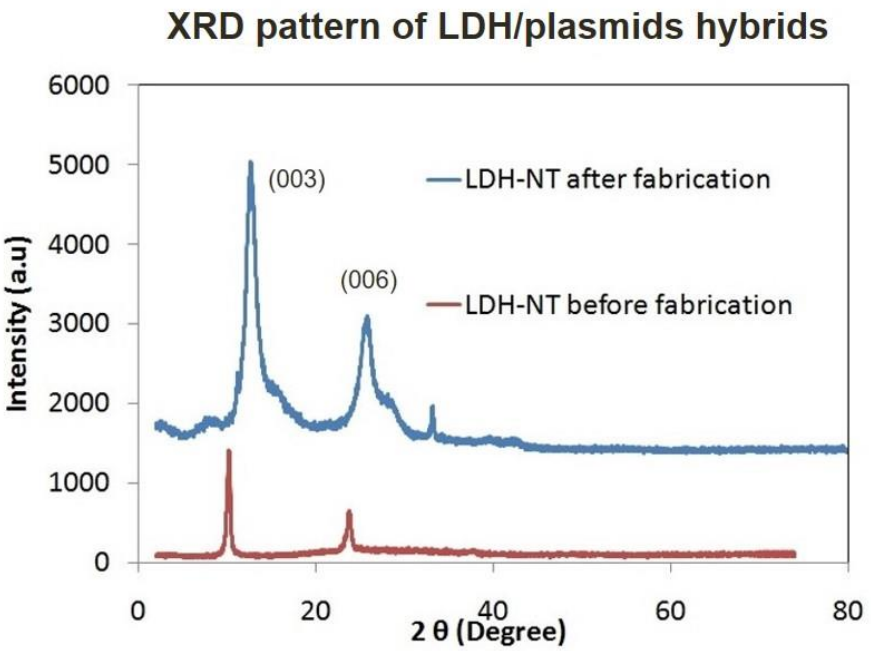

Figure 5.2. Powder XRD patterns for pristine LDHs and plasmid-LDHs. The pristine LDHs and plasmid-LDHs were freeze-dried to powder and then analyzed by XRD.

The patterns of the LDHs are typical of lamellar materials, characterized by basal reflections, associated harmonics at low 2θ angles and weaker non-basal reflections at higher angles [219]. The pristine LDH is well-crystallized as reflected by the sharp (003) and (006) basal reflections. The (003) spacing of LDH is 0.77nm. It could be clearly observed that after fabrication, the (003) remained sharp yet slightly broader; indicating that the inner layer spacing did not extend significantly. The result could suggest two possibilities: (a) there is absolutely no interaction between the LDH and plasmid, the image just showed that two compounds are simply mixed together; (b) the plasmids were more attached to the LDH surface rather than intercalated into the layers, therefore no significant spacing change was observed. To further prove that the plasmids actually interacted with the LDHs, gel electrophoresis was performed.

5.4.2 The interaction between CMV-EGF-ETA plasmids and LDH examined by Gel electrophoresis.

5.4.2.1 CMV-EGF-ETA plasmids, LDH interaction efficiency.

LDH/plasmids hybrids at different mass ratios of 5:1, 2:1, 1:1, 0.5:1, 02:1, 0.1:1 were prepared following the protocol described in Section 5.3.3.1 with fresh made LDHs and newly extracted plasmids. After incubation, the interaction efficiency between plasmids and LDH nanoparticles were examined by Gel electrophoresis (Figure 5.3).

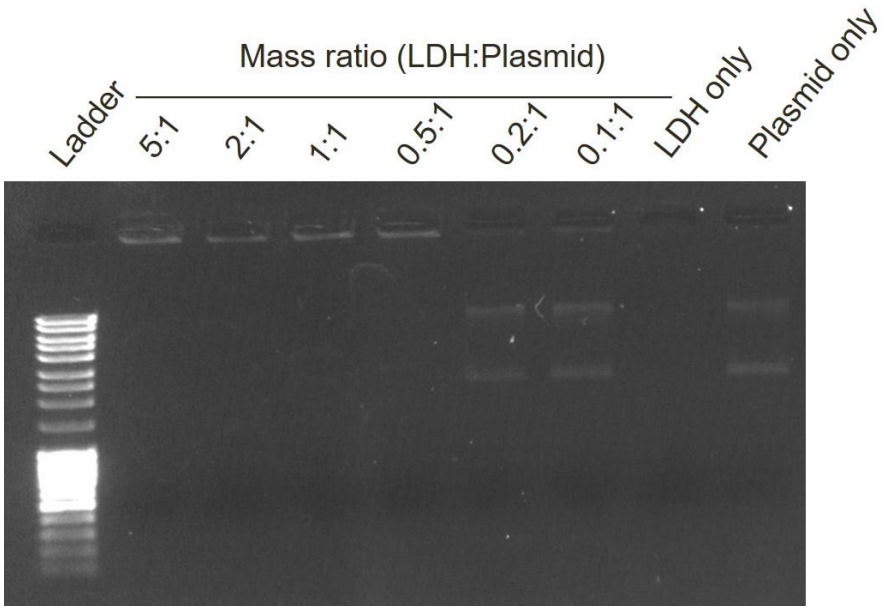

Figure 5.3. The agarose gel image of LDH-plasmid interaction under different mass ratio.

Under the LDH/plasmid mass ratio of 5:1-0.5:1, DNA bands were observed in the wells and no clear bands were detected on the gel, indicating that the all the plasmids were associated with LDHs and trapped in the well, no free plasmids were dragged into the gel by the current. On the other hand, at mass ratio 0.2:1 and 0.1:1, due to the amount of LDHs was significantly low, uncaptured

plasmids could mobile into the gel. Therefore, only weak bands were observed in the two wells and free plasmids were detected in the gel, indicating that only a small number of plasmids were combined with the LDH and the rest of the plasmids managed to move, showing relatively stronger bands on the gel. Plasmid DNA can exist in three conformations: supercoiled, open-circular (OC), and linear. Supercoiled plasmids DNA is also referred to as covalently closed circular DNA (CCC) [220]. In figure 39, the plasmids were not treated with a single RE and linear plasmids cannot be formed. Therefore, the uncut plasmids produced two bands on a gel, representing the OC and CCC conformations. The small, compact supercoiled knot of CCC-DNA sustains less friction against the agarose matrix than a large, floppy open circle of OC-DNA does. Therefore, for the same over-all size, supercoiled DNA runs faster than open-circular DNA (OC on the top, and CCC below). The ratio of the amounts of DNA in both bands depends on the age and quality of the plasmids preparation [221].

5.4.2.2 LDH protection efficiency.

A sandwich-like structure can be formed when the LDHs were associated with DNA, which is believed to provide a shelter for the DNA in the middle from unexpected degradation [6]. The LDH protection efficiency to the plasmids was examined and the result is shown below (Figure 5.4).

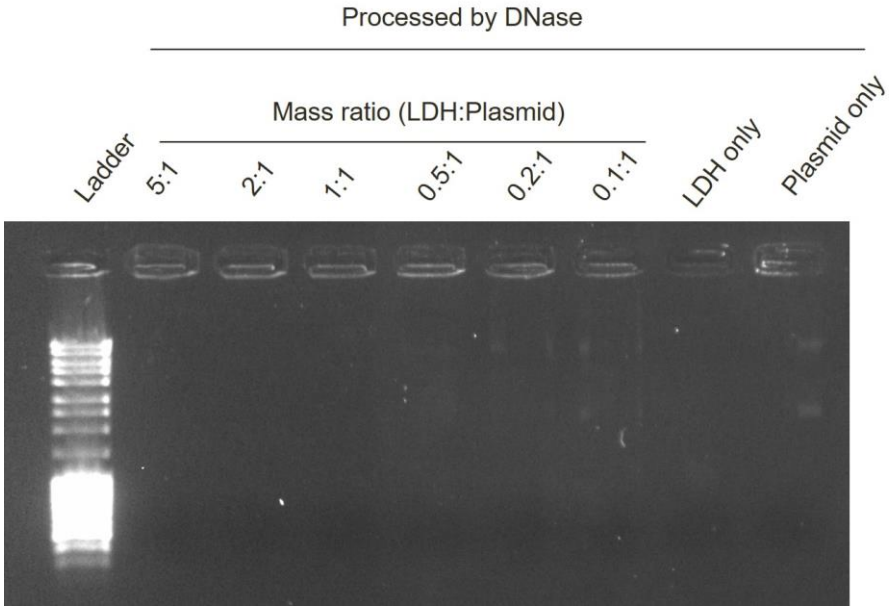

Figure 5.4. LDH protection efficiency under different LDH/plasmids mass ratio. All the samples were treated with DNase I after incubation.

Samples from Section 5.4.2.1 were treated with DNase I and examined by Gel electrophoresis. No bands were observed on the gel under any LDH/plasmids mass ratio, indicating that free plasmids were completely digested by the DNase. However, clear bands were detected in the LDH/plasmids hybrids wells. Due to the association between the LDH and the plasmids, the DNase binding sites on the plasmids were hidden by the layered structure of the LDH, therefore the enzyme cannot approach and cut the plasmids into small fragments, allowing the captured plasmids survived the critical environment. Interestingly, a small amount of DNA was also detected in the last well, suggesting that the plasmids or DNA fragments were somehow trapped in the well. After the DNase digestion to the naked plasmids, no DNA fragments should be detected in the well or on the gel. The issue will be discussed in the following Section.

5.4.2.3 Plasmids integrity examination

To ensure the loaded plasmids were not damaged during the ion-exchange process and can function normally in the following experiments, the integrity of the plasmids after the association was examined. Samples were prepared at LDH/plasmids mass ratio 1:5 following the protocol described in Section 5.3.3.1 and mixed with PBS to exchange the plasmids off the LDH after incubation. Due to the unexpected issue occurred in the last Section, DNase I was also used to examine the LDH protection efficiency (Figure 5.5)

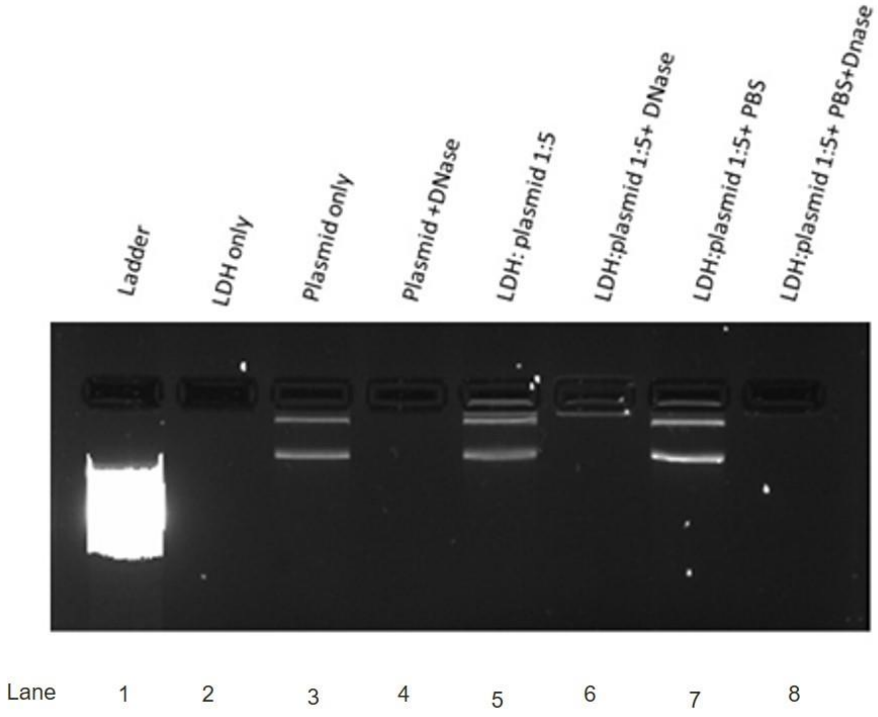

Figure 5.5. Plasmids integrity examination after associated with LDH. PBS was used to exchange the plasmids off the LDH and run it on the gel. LDH/plasmids hybrids were also treated with DNase to test the LDH protection efficiency.

As shown in the image, the two bands in the gel in line 7 were relatively brighter than those in line 5 and the band in the well in line 7 was weaker than that in line 5, indicating that the plasmids were successfully exchanged out of the LDH

structure because of the PBS. Moreover, the two bands in the gel (line 7) were detected at the similar position with those in line 3 and no DNA fragments were observed at other position in the gel in line 7, suggesting that no plasmids were damaged and the integrity were conserved during the two ion-exchange process. The results shown in line 4, 6 and 8 again demonstrated that the plasmids were protected by the LDH and survived the DNase treatment.

5.4.2.4 LDH facilitated mammalian cell transfection

Mammalian cell transfection using LDH as drug carrier was performed to prove that the LDH can facilitate the plasmids delivery into targeted cells. pEGFP-C1 plasmids were loaded to the LDH drug carrier and transported into cells cytoplasm to express the reporting Green Fluorescent Protein and live cells were stained with Hoechst (Figure 5.6).

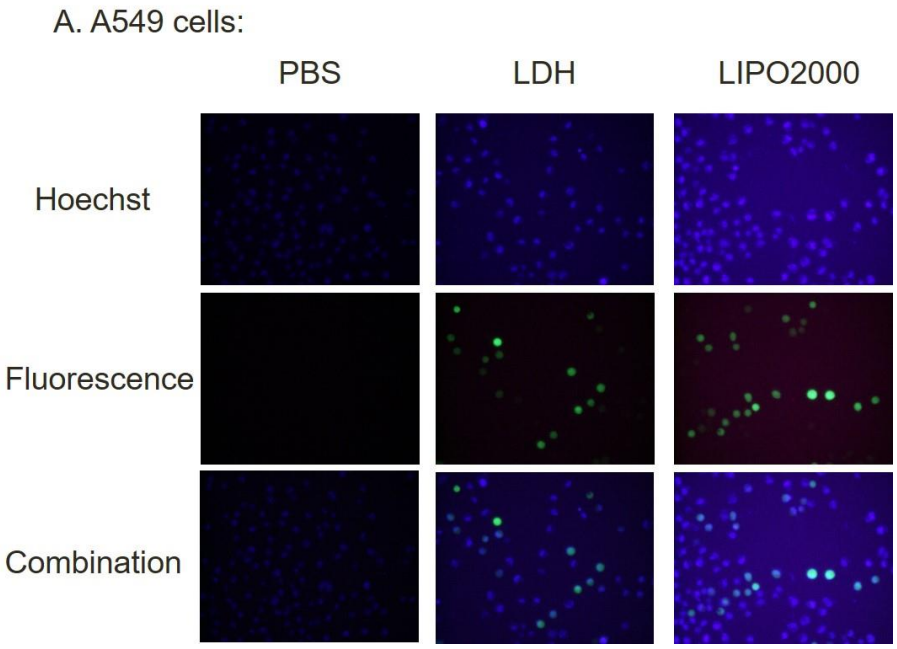

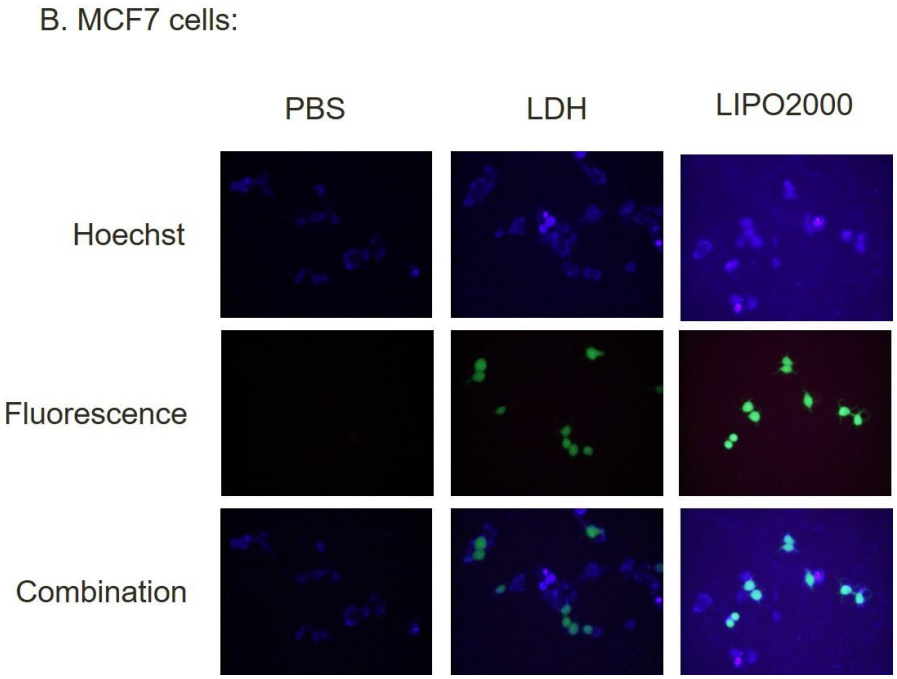

Figure 5.6. Mammalian cells cellular uptake efficiency facilitated by the LDH nanoparticles. A): A549 cells transfected with pEGFP-c1 plasmids facilitated by PBS, LDH and Lipo2000. B) MCF-7 cells transfected with pEGFP-c1 plasmids facilitated by PBS, LDH and Lipo2000. Cells were exposed to the complexes and incubated at 37 °C for 24 hours

Green fluorescence was detected in A549 and MCF-7 cells transfected by LDH and Lipo2000, indicating that the plasmids were delivered and released into both cells by the carrier LDH and the EGPs were successfully expressed. Moreover, the pEGFP-C1 and the CMV-EGF-ETA are structurally identical, only the functional gene is different. The GFP gene of the pEGFP-C1 was replaced by the EGF-ETA gene fragment to generate the CMV-EGF-ETA. Therefore, the successful transfection and the expression of the pEGFP-C1 plasmids in A549 and MCF-7 cells implied that the CMV-EGF-ETA plasmids can be transported and expressed in both cells, resulting in cell death.

5.2.4.5 In vitro cytotoxicity assay

A549 and MCF-7 cells were seeded in 96-well plates and were transfected with CMV-EGF-ETA plasmids facilitated by PBS, LDH and Lipo2000. MTT assay was performed to examine the cell viability. Results are shown in Figure 5.7.

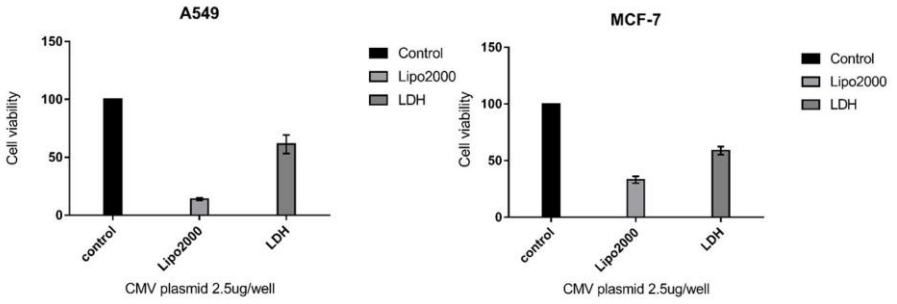

Figure 5.7. MTT assay of A549 and MCF-7 cells treated with reconstructed CMV-EGF-ETA plasmid (2.5 μg/well). Cellular uptake was facilitated by PBS, LDH and lipo2000. Cells were exposed to drugs for 12h. Left: A549 cells; right, MCF-& cells

After 12h exposure to the drugs, approximately more than 80% of A549 cells were killed by the CMV-EGF-ETA/lipo2000 complexes, whereas around 40% of A549 cells lysis occurred when treated with the CMV-EGF-ETA/LDH hybrids. On the other hand, the CMV-EGF-ETA/lipo2000 complexes induced the apoptosis of approximately 60% MCF-7 cells, whereas about 60% of MCF-7 cells survived the CMV-EGF-ETA/LDH hybrids exposure. The MTT assay clearly proved that the new designed CMV-EGF-ETA plasmids can be delivered into cells by employing LDH as a drug carrier and the toxic protein EGF-ETA was expressed in the mammalian cells, resulting in cell death. Moreover, it was also shown that more cells death occurred in A549 than in MCF-7 when the transfection was facilitated by Lipo2000. This could be simply explained by that, A549 is an EGFR-positive cell line, whereas the MCF-7 is an EGFR-negative

cell line [222,223]. The toxic protein EGF-ETA contains the EGF fragment, which is the antigen of EGFR that highly expressed on A549 cells. Therefore, the EGF protein was functioning as a targeting molecule allowing a "faster association" with EGFR-positive cells, resulting in more cell death in A549. However, the "faster association" seemed failed to happen when the cells were transfected by CMV-EGF-ETA/LDH hybrids. This might because of the sustained release of the immunotoxin managed by the LDH nanoparticle. To test the hypothesis, exposure time was extended from 12 hours to 24 hours. The result is shown in Figure 5.8.

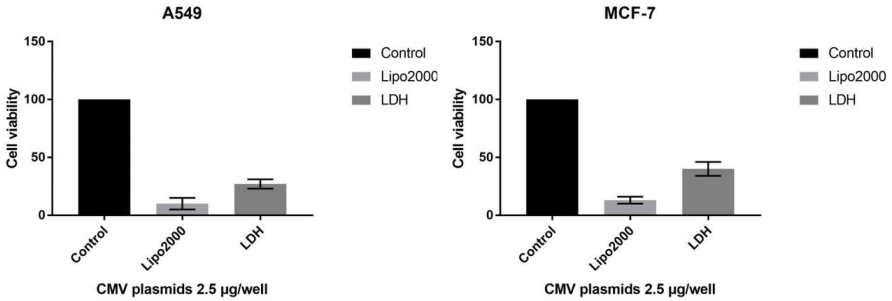

Figure 5.8. MTT assay of A549 and MCF-7 cells treated with reconstructed CMV-EGF-ETA plasmid (2.5 μg/well). Cellular uptake was facilitated by PBS, LDH and lipo2000. Cells were exposed to drugs for 24h. Left: A549 cells; right, MCF-& cells

As shown in the image, the longer incubation time led to the occurrence of the "faster association" in the EGFR-positive cells transfected with CMV-EGF-ETA/LDH hybrids. Approximately 15% more A549 cells were dead compared with MCF-7 cells. Interestingly, the proportion of cell death reached a similar level (about 90%) after the 24 hours' incubation with CMV-EGF-ETA/Lipo2000 complexes, indicating that once the amount of the plasmids was fixed, the EGF targeting molecule can only enhance the number of cell deaths per unit time but cannot affect the total number of the cell death. In another word, between the

EGF-positive and negative cells, how fast the cells were killed can be affected by the presence of the EGF targeting proteins; how many cells were killed in total can only be determined by the amount of toxic ETA proteins. Therefore, when the cells were incubated with a fixed number of CMV-EGF-ETA plasmids for long enough time, a similar amount of total cell death number will be achieved in EGF-positive and negative cells regardless of the presence of the EGF targeting proteins.

5.5 Discussion

In this chapter, the association efficiency between the CMV-EGF-ETA plasmids and the LDH nanoparticles was evaluated and the antitumor efficacy of the immunotoxin was examined *in vitro.* The plasmids were mixed with fresh-made pristine LDH in different mass ratios, given 1:5, 1:2, 1:1, 1:0.5, 1:0.2, 1:0.1, and gel electrophoresis was performed to test the LDH maximum loading capacity. Plasmids can be trapped in the wells due to the presence of the LDH and no free plasmids can be moved into the gel at the LDH/plasmids mass ratio 5:1~0.5:1. Uncaptured plasmids were detected in the gel at the LDH/plasmids mass ratio 0.2:1 and 0.1:1. Therefore, the LDH maximum loading capacity was achieved when the LDH/plasmids mass ratio was 0.5:1. The LDH/plasmids hybrids were also treated with DNase I after incubation. The plasmids combined with the LDH survived the critical environment but free plasmids were digested by the enzyme, which proved that the LDH can provide a shelter for the plasmids, protect them from unexpected degradation and potentially enhance the survival ability of the plasmids in the complicated environment in the future *in vivo* experiments. Moreover, the plasmids were not damaged during the ion-

exchange process and the integrity of the plasmids was conserved when exchanged off the LDH carrier by PBS, which ensured that the toxic protein can be expressed in the mammalian cells and induce cell death.

Due to the structural similarity of the pEGFP-C1 and CMV-EGF-ETA, pEGFP-C1 containing the reporting GFP gene was utilized to transfect the A549 lung cancer cells and the MCF-7 breast cancer cells to. After 24 hours' exposure to the LDH/plasmids hybrids, strong and clear green fluorescence was detected in cells under the fluorescence microscope, which proved the cell transfection can be facilitated by LDH. The anti-tumor efficacy of the immunotoxin was evaluated by MTT assay *in vitro.* It was proved that the immunotoxin could induce the apoptosis of up to 90% of the cell death. When the transfection was facilitated by the LDH, the sustained release of the plasmids in cells was achieved. Moreover, the EGF protein acted as a targeting molecule and increased the rate of the cell death, but the total number of the cell death was not affected by the EGF protein in EGFR-positive and negative cells.

In Figure 5.4, the naked plasmids should be completely degraded and no DNA can be detected in the well or gel after the DNase I digestion. However, DNA fragments were detected in the last well. Possible reasons that cause the issue are 1) unequal heating during the incubation resulting in incomplete digestion. The mixture was incubated at 37°C for 30 minutes, which was the optimized temperature for the DNase I to function at the highest digestion efficiency. The tube contains the plasmids and DNase mixture was prepared at last and placed at the edge of the heating equipment for incubation. Therefore, there might be a

chance that the tube was not receiving an equal heating during the incubation and the optimized temperature of the DNase was not achieved, resulting in plasmids partial degradation; 2) LDH cross contamination. The tube only contains LDH was the second last to prepare, faulty performance might cause contamination to the preparation of the next tube which only contains the plasmids, such as failed to change the pipette tips. In the contaminated sample, LDH can interact with the plasmids and protect them from DNase digestion and left the detectable trace in the last gel well; 3) the DNase digestion efficiency was compromised by the unclean equipment. All the equipment was autoclaved before using, but there is still a slight chance that the equipment could be contaminated after the sterilization. Therefore, the integrity of the DNase might be affected and some of the enzymes might be even degraded during the incubation, resulting in the incomplete digestion. To confirm the LDH protection efficiency, all the equipment was freshly sterilized and samples were prepared again with care. In line 4 in Figure 5.5, no DNA trace was detected either in the well or gel, which proved that the possible contamination was avoided and complete digestion to the plasmids by the DNase was achieved. Consistent results were observed in line 6 and 8.

Compared with the CMV-EGF-ETA/lipo2000 complexes, a relatively slower cell response to the CMV-EGF-ETA/LDH hybrids was observed. This is because of the complicated transfection process of the hybrids and the controlled drug release by the LDH host. As described in Chapter 2, Section 2.1.2.1, the LDH based drug carrier system enters the cells through the clathrin-mediated endocytosis, which is an active transport and consumes ATPs. Then the drug

loaded LDHs are gradually melted in the lysosome and the carried drugs are released into the cell cytoplasm. Unlike the drug release from the Lipofectamin2000, in which the drug directly enters the cytoplasm after the neutral co-lipid mediating fusion of the liposome with the cell membrane [224], the whole process of drugs carried by LDH entering cell cytoplasm is soft and sustained, leading to the drug long retention in cells and the controlled release into the cytoplasm.

The efficacy of the immunotoxins used in cancer therapy is violent, causing severe side-effects to the patients, such as VLS. The first aim of Phase I clinical trials is to find out the MTD of the newly developed immunotherapy to the patients and the dose used in the trial is limited. Moreover, the dose limitation might significantly compromise the efficacy of the immunotoxin resulting in clinical trial failure. Therefore, finding a balancing point where the drug dose could be decreased and drug efficacy could be reserved has always been the priority for Phase I clinical trials. However, patients could benefit from the mild LDH drug release mechanism. The LDH sustained drug release process acts like a buffer zone, which could potentially increase the patients MTD to the drugs without causing severe side-effects.

5.6 Conclusion

To summarize, the CMV-EGF-ETA plasmids can be associated with the LDH nanoparticles *via* ion-exchange mechanism and the LDH host can protect the loaded plasmids from unexpected degradation. Mammalian cells transfection can be achieved by employing the LDH as drug carriers. The new immunotoxin

CMV-EGF-ETA showed significant anti-tumor effects against A549 and MCF-7. The EGF protein functioning as a targeting molecule enhanced the rate of apoptosis in EGFR-positive cells. The LDH sustained drug release mechanism could potentially reduce side-effects and achieve long term treatment.

Chapter 6 Conclusion and Future Perspective

6.1 Conclusion

Lung cancer has been known as one of the major malignant neoplasms all around the world [225]. Recent studies have reported that the lung cancer incidence is increasing not only in the United States but also in China and other countries [226,227]. NSCLC accounts for 85% of all lung cancer cases in the United States, and most of the diagnosed patients with the NSCLC are not suitable for surgery treatment [228]. Therefore, improvements of new methods against the tumor in late stages are required. Triggering host immune response by antibody-based therapy against tumors is a promising approach with positive clinical documents [82,83]. It was proposed that the “magic Bullet” immunotoxin targeting cancer antigens could be developed, killing tumor cells within the human body without harming healthy cells [84]. Meanwhile, the inorganic nanoparticles LDH with layered structure was also introduced into clinical application as a potential drug carrier, which is easy to synthesize in lab, can achieve high drug loading and cell transfection efficiency, increase the survival ability of the loaded drugs, and most importantly, achieve long-term drug efficacy by the controlled drug release [9,229,230]. In the presenting study, newly designed immunotoxin CMV-EGF-ETA plasmids specifically targeting EGFR-positive cancer cells (including NSCLC) was assembled with the ~100 nm LDH nanoparticles. The hybrids were then delivered to A549 and MCF-7 cancer cells for inducing cell apoptosis.

The first aim was to establish the LDH drug delivery system in the lab and create the newly designed CMV-EGF-ETA immunotoxin plasmids. The LDH nanoparticles were synthesized by mixing $MgCl_2$ and $AlCl_3$ solution with NaOH solution and collected by high-speed centrifugation. After purification, the nano-materials were characterized. Chemistry analysis proved the successful synthesis of the homogeneous MgAl-Cl LDH with ~106 nm in size and 32.1 mV in zeta potential followed by the TEM confirmation. The small particle size and the positively charged surface of the LDH nanoparticles ensured the high cellular uptake by the mammalian cell *via* the clathrin-endocytosis pathway. On the other hand, the EGF-ETA fragments were amplified by PCR and fused with the backbone of pEGFP-C1 plasmids. After amplification through *E. coli* transformation, the products were examined by REs and proved the successful synthesis of the CMV-EGF-ETA plasmids.

Secondly, it was proposed that the CMV-EGF-ETA plasmids could be loaded into the LDH carrier with a high loading efficiency and an improvement of loaded drug survival ability. To test the hypothesis, freshly made LDH suspension was mixed with the fixed-amount plasmids at the different mass ratio and the hybrids were examined by gel electrophoresis. Maximum loading dose was achieved at LDH/plasmid mass ratio 0.5:1. In addition, the LDH nano-carrier protected the loaded plasmids from the DNase I digestion, meanwhile, the plasmids was not damaged during the process and the integrity was conserved, ensuring the protein expression in mammalian cells.

The third hypothesis of the study was that the LDH/plasmids hybrids could enhance the anti-tumor activity against EGFR-positive cancer cells. To test the

hypothesis, pEGFP-C1 with the GFP reporting gene was employed to prove the LDH can facilitate the mammalian cell transfection with high efficiency and CMV-EGD-ETA plasmids were delivered to A549 and MCF-7 cells to induce cell death. High toxicity efficiency was achieved given 90% of the cells in both cell line was killed. Cell death rate was higher in the EGFR-positive cells. Cells showed a relatively slower response to the LDH/plasmids hybrids but with long-term drug efficacy.

Limitations are acknowledged in this study. DNA sequencing should be utilized to confirm the successful synthesis of the CMV-EGF-ETA plasmids. However, due to limitation of the costs, the DNA sequencing test was replaced with REs treatment and gel electrophoresis. Even though the REs digestion is relatively less convincing, the *in vitro* experiments in Chapter 5 can also provide the indirect proof of the successful synthesis of the CMV-EGF-ETA plasmids with expected functions. Lack of *in vivo* experiments results could be the next limitation of this study due to the costs and time. Even though this is only a preliminary study of combining the recently emerged inorganic drug delivery system with newly designed immunotoxin, the output from the experiments on animal models could provide more significant evidence to support the *in vitro* results and lead to a stronger conclusion.

6.2 Future perspective

The results presented in this study are promising for the treatment of cancer with specific antigen receptors. The *in vitro* preliminary data in this study have shown the significant potential of using novel drug delivery system to facilitate immunotoxins to enhance the anti-tumor effects. However, the findings need to

be confirmed in animal models and clinical trials. Future studies could focus on several aspects. 1). experiments on animal models are required to further evaluate the efficacy of the new LDH/plasmids hybrids *in vivo.* 2) the size of the immunotoxin plasmids could also be reduced to achieve higher drug loading to the carriers. 3) study have reported that the environment in the blood stream could affect the integrity and the stability of the LDH nanoparticles [191]. Therefore, efforts need to be made to modify the drug carrier surface to adapt the extracellular environment. 4) inorganic drug carrier candidates could also be expanded. MOFs have drawn a lot of attention in delivering therapeutic drugs to cells and organs because of the high drug loading density, controlled drug release and biocompatibility [231-234]. 5) the co-drug delivery containing immunotoxin and anti-cancer pharmaceuticals might also be an alternative approach to achieve remarkable anti-cancer effects [81,235].

References

1. Wong, Y.; Cooper, H.M.; Zhang, K.; Chen, M.; Bartlett, P.; Xu, Z.P. Efficiency of layered double hydroxide nanoparticle-mediated delivery of sirna is determined by nucleotide sequence. *Journal of colloid and interface science* **2012**, *369*, 453-459.
2. Choy, J.-H.; Kwak, S.-Y.; Jeong, Y.-J.; Park, J.-S. Inorganic layered double hydroxides as nonviral vectors. *Angewandte Chemie* **2000**, *39*, 4041-4045.
3. Desigaux, L.; Belkacem, M.B.; Richard, P.; Cellier, J.; Léone, P.; Cario, L.; Leroux, F.; Taviot-Guého, C.; Pitard, B. Self-assembly and characterization of layered double hydroxide/DNA hybrids. *Nano letters* **2006**, *6*, 199-204.
4. Masarudin, M.J.; Yusoff, K.; Rahim, R.A.; Hussein, M.Z. Successful transfer of plasmid DNA into in vitro cells transfected with an inorganic plasmid–mg/al-ldh nanobiocomposite material as a vector for gene expression. *Nanotechnology* **2008**, *20*, 045602.
5. Tyner, K.M.; Roberson, M.S.; Berghorn, K.A.; Li, L.; Gilmour, R.F.; Batt, C.A.; Giannelis, E.P. Intercalation, delivery, and expression of the gene encoding green fluorescence protein utilizing nanobiohybrids. *Journal of controlled release* **2004**, *100*, 399-409.
6. Ladewig, K.; Xu, Z.P.; Lu, G.Q. Layered double hydroxide nanoparticles in gene and drug delivery. *Expert Opinion on Drug Delivery* **2009**, *6*, 907-922.

7. Ladewig, K. Nanoparticles with application in the delivery of nucleic acids to mammalian cells. **2009**.PhD thesis. 131.

8. Choi, S.-J.; Choy, J.-H. Layered double hydroxide nanoparticles as target-specific delivery carriers: Uptake mechanism and toxicity. *Nanomedicine* **2011**, *6*, 803-814.

9. Xu, Z.P.; Niebert, M.; Porazik, K.; Walker, T.L.; Cooper, H.M.; Middelberg, A.P.; Gray, P.P.; Bartlett, P.F.; Lu, G.Q.M. Subcellular compartment targeting of layered double hydroxide nanoparticles. *Journal of Controlled Release* **2008**, *130*, 86-94.

10. Wong, Y.; Markham, K.; Xu, Z.P.; Chen, M.; Lu, G.Q.M.; Bartlett, P.F.; Cooper, H.M. Efficient delivery of sirna to cortical neurons using layered double hydroxide nanoparticles. *Biomaterials* **2010**, *31*, 8770-8779.

11. Kwak, S.-Y.; Jeong, Y.-J.; Park, J.-S.; Choy, J.-H. Bio-ldh nanohybrid for gene therapy. *Solid State Ionics* **2002**, *151*, 229-234.

12. Ladewig, K.; Niebert, M.; Xu, Z.P.; Gray, P.P.; Lu, G.Q. Efficient sirna delivery to mammalian cells using layered double hydroxide nanoparticles. *Biomaterials* **2010**, *31*, 1821-1829.

13. Xu, Z.P.; Stevenson, G.S.; Lu, C.-Q.; Lu, G.Q.; Bartlett, P.F.; Gray, P.P. Stable suspension of layered double hydroxide nanoparticles in aqueous solution. *Journal of the American Chemical Society* **2006**, *128*, 36-37.

14. Ladewig, K.; Niebert, M.; Xu, Z.P.; Gray, P.P.; Lu, G.Q.M. Controlled preparation of layered double hydroxide nanoparticles and their application as gene delivery vehicles. *Applied Clay Science* **2010**, *48*, 280-289.

15. Xu, Z.P.; Braterman, P.S.; Yu, K.; Xu, H.; Wang, Y.; Brinker, C.J. Unusual hydrocarbon chain packing mode and modification of crystallite

growth habit in the self-assembled nanocomposites zinc− aluminum-hydroxide oleate and elaidate (cis-and trans-[zn2al (oh) 6 (ch3 (ch2) 7ch ch (ch2) 7coo-)] and magnesium analogues. *Chemistry of materials* **2004**, *16*, 2750-2756.

16. Choy, J.-H.; Jung, J.-S.; Oh, J.-M.; Park, M.; Jeong, J.; Kang, Y.-K.; Han, O.-J. Layered double hydroxide as an efficient drug reservoir for folate derivatives. *Biomaterials* **2004**, *25*, 3059-3064.
17. Del Hoyo, C. Layered double hydroxides and human health: An overview. *Applied Clay Science* **2007**, *36*, 103-121.
18. Gu, Z.; Thomas, A.C.; Xu, Z.P.; Campbell, J.H.; Lu, G.Q. In vitro sustained release of lmwh from mgal-layered double hydroxide nanohybrids. *Chemistry of Materials* **2008**, *20*, 3715-3722.
19. Rives, V.; Del Arco, M.; Martín, C. Layered double hydroxides as drug carriers and for controlled release of non-steroidal antiinflammatory drugs (nsaids): A review. *Journal of Controlled Release* **2013**, *169*, 28-39.
20. Chakraborty, J.; Chakraborty, M.; Ghosh, S.; Mitra, M.K. In *Drug delivery using nanosized layered double hydroxide, an anionic clay*, Key Engineering Materials, 2013; Trans Tech Publ: pp 133-167.
21. Javaid, A.; Bone, M.; Stanley, C. In *Effect of fenbufen on the quality of life of patients with pain from squamous-cell carcinoma of the bronchus*, Thorax, 1988; BRITISH MED JOURNAL PUBL GROUP BRITISH MED ASSOC HOUSE, TAVISTOCK SQUARE, LONDON, ENGLAND WC1H 9JR: pp P244-P244.
22. Carriazo, D.; Del Arco, M.; Fernández, A.; Martín, C.; Rives, V. Inclusion and release of fenbufen in mesoporous silica. *Journal of pharmaceutical sciences* **2010**, *99*, 3372-3380.

23. Li, B.; He, J.; Evans, D.G.; Duan, X. Inorganic layered double hydroxides as a drug delivery system—intercalation and in vitro release of fenbufen. *Applied clay science* **2004**, *27*, 199-207.

24. Whilton, N.T.; Vickers, P.J.; Mann, S. Bioinorganic clays: Synthesis and characterization of amino-andpolyamino acid intercalated layered double hydroxides. *Journal of Materials Chemistry* **1997**, *7*, 1623-1629.

25. Ambrogi, V.; Fardella, G.; Grandolini, G.; Perioli, L. Intercalation compounds of hydrotalcite-like anionic clays with antiinflammatory agents—i. Intercalation and in vitro release of ibuprofen. *International Journal of Pharmaceutics* **2001**, *220*, 23-32.

26. Del Arco, M.; Fernandez, A.; Martin, C.; Rives, V. Solubility and release of fenbufen intercalated in mg, al and mg, al, fe layered double hydroxides (ldh): The effect of eudragit® s 100 covering. *Journal of Solid State Chemistry* **2010**, *183*, 3002-3009.

27. Li, B.; He, J.; Evans, D.G.; Duan, X. Enteric-coated layered double hydroxides as a controlled release drug delivery system. *International journal of pharmaceutics* **2004**, *287*, 89-95.

28. Bombardier, C.; Laine, L.; Reicin, A.; Shapiro, D.; Burgos-Vargas, R.; Davis, B.; Day, R.; Ferraz, M.B.; Hawkey, C.J.; Hochberg, M.C. Comparison of upper gastrointestinal toxicity of rofecoxib and naproxen in patients with rheumatoid arthritis. *New England Journal of Medicine* **2000**, *343*, 1520-1528.

29. Jordan, K.; Arden, N.; Doherty, M.; Bannwarth, B.; Bijlsma, J.; Dieppe, P.; Gunther, K.; Hauselmann, H.; Herrero-Beaumont, G.; Kaklamanis, P. Eular recommendations 2003: An evidence based approach to the management of knee osteoarthritis: Report of a task force of the standing

committee for international clinical studies including therapeutic trials (escisit). *Annals of the rheumatic diseases* **2003**, *62*, 1145-1155.

30. Hasan, Z.; Jeon, J.; Jhung, S.H. Adsorptive removal of naproxen and clofibric acid from water using metal-organic frameworks. *Journal of hazardous materials* **2012**, *209*, 151-157.
31. Chowhan, Z.; Pritchard, R. Effect of surfactants on percutaneous absorption of naproxen i: Comparisons of rabbit, rat, and human excised skin. *Journal of pharmaceutical sciences* **1978**, *67*, 1272-1274.
32. Taha, A.S.; Hudson, N.; Hawkey, C.J.; Swannell, A.J.; Trye, P.N.; Cottrell, J.; Mann, S.G.; Simon, T.J.; Sturrock, R.D.; Russell, R.I. Famotidine for the prevention of gastric and duodenal ulcers caused by nonsteroidal antiinflammatory drugs. *New England Journal of Medicine* **1996**, *334*, 1435-1439.
33. Wei, M.; Shi, S.; Wang, J.; Li, Y.; Duan, X. Studies on the intercalation of naproxen into layered double hydroxide and its thermal decomposition by in situ ft-ir and in situ ht-xrd. *Journal of Solid State Chemistry* **2004**, *177*, 2534-2541.
34. Meyn, M.; Beneke, K.; Lagaly, G. Anion-exchange reactions of layered double hydroxides. *Inorganic Chemistry* **1990**, *29*, 5201-5207.
35. Hou, W.-G.; Jin, Z.-L. Synthesis and characterization of naproxen intercalated zn–al layered double hydroxides. *Colloid and Polymer Science* **2007**, *285*, 1449-1454.
36. Ay, A.N.; Zümreoglu-Karan, B.I.; Temel, A.; Rives, V. Bioinorganic magnetic core− shell nanocomposites carrying antiarthritic agents: Intercalation of ibuprofen and glucuronic acid into mg− al− layered

double hydroxides supported on magnesium ferrite. *Inorganic chemistry* **2009**, *48*, 8871-8877.

37. Perioli, L.; Posati, T.; Nocchetti, M.; Bellezza, F.; Costantino, U.; Cipiciani, A. Intercalation and release of antiinflammatory drug diclofenac into nanosized znal hydrotalcite-like compound. *Applied Clay Science* **2011**, *53*, 374-378.

38. Berber, M.R.; Minagawa, K.; Katoh, M.; Mori, T.; Tanaka, M. Nanocomposites of 2-arylpropionic acid drugs based on mg–al layered double hydroxide for dissolution enhancement. *european journal of pharmaceutical sciences* **2008**, *35*, 354-360.

39. Del Arco, M.; Cebadera, E.; Gutierrez, S.; Martin, C.; Montero, M.; Rives, V.; Rocha, J.; Sevilla, M. Mg, al layered double hydroxides with intercalated indomethacin: Synthesis, characterization, and pharmacological study. *Journal of pharmaceutical sciences* **2004**, *93*, 1649-1658.

40. Choi, S.-J.; Choi, G.E.; Oh, J.-M.; Oh, Y.-J.; Park, M.-C.; Choy, J.-H. Anticancer drug encapsulated in inorganic lattice can overcome drug resistance. *Journal of Materials Chemistry* **2010**, *20*, 9463-9469.

41. Lee, E.S.; Na, K.; Bae, Y.H. Doxorubicin loaded ph-sensitive polymeric micelles for reversal of resistant mcf-7 tumor. *Journal of Controlled Release* **2005**, *103*, 405-418.

42. Campbell, L.; Abulrob, A.-N.G.; Kandalaft, L.E.; Plummer, S.; Hollins, A.J.; Gibbs, A.; Gumbleton, M. Constitutive expression of p-glycoprotein in normal lung alveolar epithelium and functionality in primary alveolar epithelial cultures. *Journal of Pharmacology and Experimental Therapeutics* **2003**, *304*, 441-452.

43. Malam, Y.; Loizidou, M.; Seifalian, A.M. Liposomes and nanoparticles: Nanosized vehicles for drug delivery in cancer. *Trends in pharmacological sciences* **2009**, *30*, 592-599.

44. Knollman, B.; Chabner, B.; Brunton, L. Goodman & gilman's the pharmacological basis of therapeutics. New York: McGraw-Hill Medical: 2011.

45. Oh, J.-M.; Park, M.; Kim, S.-T.; Jung, J.-Y.; Kang, Y.-G.; Choy, J.-H. Efficient delivery of anticancer drug mtx through mtx-ldh nanohybrid system. *Journal of Physics and Chemistry of Solids* **2006**, *67*, 1024-1027.

46. Oh, J.-M.; Choi, S.-J.; Kim, S.-T.; Choy, J.-H. Cellular uptake mechanism of an inorganic nanovehicle and its drug conjugates: Enhanced efficacy due to clathrin-mediated endocytosis. *Bioconjugate chemistry* **2006**, *17*, 1411-1417.

47. Choi, S.-J.; Oh, J.-M.; Choy, J.-H. Anticancer drug-layered hydroxide nanohybrids as potent cancer chemotherapy agents. *Journal of Physics and Chemistry of Solids* **2008**, *69*, 1528-1532.

48. Weingart, J.D.; Thompson, R.C.; Tyler, B.; Colvin, O.M.; Brem, H. Local delivery of the topoisomerase i inhibitor camptothecin sodium prolongs survival in the rat intracranial 9l gliosarcoma model. *International journal of cancer* **1995**, *62*, 605-609.

49. Dey, J.; Warner, I.M. Spectroscopic and photophysical studies of the anticancer drug: Camptothecin. *Journal of luminescence* **1997**, *71*, 105-114.

50. O'Leary, J.; Muggia, F. Camptothecins: A review of their development and schedules of administration. *European Journal of Cancer* **1998**, *34*, 1500-1508.

51. Slevin, M.L. The clinical pharmacology of etoposide. *Cancer* **1991**, *67*, 319-329.

52. Imbert, T. Discovery of podophyllotoxins. *Biochimie* **1998**, *80*, 207-222.

53. Van Maanen, J.; Retel, J.; De Vries, J.; Pinedo, H.M. Mechanism of action of antitumor drug etoposide: A review. *Journal of the National Cancer Institute* **1988**, *80*, 1526-1533.

54. Tyner, K.M.; Schiffman, S.R.; Giannelis, E.P. Nanobiohybrids as delivery vehicles for camptothecin. *Journal of Controlled Release* **2004**, *95*, 501-514.

55. Dong, L.; Yan, L.; Hou, W.-G.; Liu, S.-J. Synthesis and release behavior of composites of camptothecin and layered double hydroxide. *Journal of Solid State Chemistry* **2010**, *183*, 1811-1816.

56. LIU, C.X.; HOU, W.G.; Li, Y.; LI, L.F. Synthesis and characterization of camptothecin intercalated into mg/al layered double hydroxide. *Chinese Journal of Chemistry* **2008**, *26*, 1806-1810.

57. Xue, Y.H.; Zhang, R.; Sun, X.Y.; Wang, S.L. The construction and characterization of layered double hydroxides as delivery vehicles for podophyllotoxins. *Journal of Materials Science: Materials in Medicine* **2008**, *19*, 1197-1202.

58. Qin, L.; Xue, M.; Wang, W.; Zhu, R.; Wang, S.; Sun, J.; Zhang, R.; Sun, X. The in vitro and in vivo anti-tumor effect of layered double hydroxides nanoparticles as delivery for podophyllotoxin. *International journal of pharmaceutics* **2010**, *388*, 223-230.

59. Canel, C.; Moraes, R.M.; Dayan, F.E.; Ferreira, D. Podophyllotoxin. *Phytochemistry* **2000**, *54*, 115-120.

60. Li, A.; Qin, L.; Wang, W.; Zhu, R.; Yu, Y.; Liu, H.; Wang, S. The use of layered double hydroxides as DNA vaccine delivery vector for enhancement of anti-melanoma immune response. *Biomaterials* **2011**, *32*, 469-477.

61. Hesse, D.; Badar, M.; Bleich, A.; Smoczek, A.; Glage, S.; Kieke, M.; Behrens, P.; Müller, P.P.; Esser, K.-H.; Stieve, M. Layered double hydroxides as efficient drug delivery system of ciprofloxacin in the middle ear: An animal study in rabbits. *Journal of Materials Science: Materials in Medicine* **2013**, *24*, 129-136.

62. Tammaro, L.; Vittoria, V.; Calarco, A.; Petillo, O.; Riccitiello, F.; Peluso, G. Effect of layered double hydroxide intercalated with fluoride ions on the physical, biological and release properties of a dental composite resin. *Journal of dentistry* **2014**, *42*, 60-67.

63. Murray, P.; About, I.; Lumley, P.; Franquin, J.-C.; Remusat, M.; Smith, A. Human odontoblast cell numbers after dental injury. *Journal of dentistry* **2000**, *28*, 277-285.

64. Hannigan, A.; Lynch, C.D. Statistical methodology in oral and dental research: Pitfalls and recommendations. *Journal of Dentistry* **2013**, *41*, 385-392.

65. Kwak, S.-Y.; Kriven, W.M.; Wallig, M.A.; Choy, J.-H. Inorganic delivery vector for intravenous injection. *Biomaterials* **2004**, *25*, 5995-6001.

66. Rives, V. *Layered double hydroxides: Present and future*. Nova Publishers: 2001.

67. Wang, Q.; O'Hare, D. Recent advances in the synthesis and application of layered double hydroxide (ldh) nanosheets. *Chemical reviews* **2012**, *112*, 4124-4155.

68. Alcantara, A.; Aranda, P.; Darder, M.; Ruiz-Hitzky, E. Bionanocomposites based on alginate–zein/layered double hydroxide materials as drug delivery systems. *Journal of materials chemistry* **2010**, *20*, 9495-9504.

69. Valarezo, E.; Tammaro, L.; González, S.; Malagón, O.; Vittoria, V. Fabrication and sustained release properties of poly (ε-caprolactone) electrospun fibers loaded with layered double hydroxide nanoparticles intercalated with amoxicillin. *Applied Clay Science* **2013**, *72*, 104-109.

70. Bao, H.; Yang, J.; Huang, Y.; Xu, Z.P.; Hao, N.; Wu, Z.; Lu, G.Q.M.; Zhao, D. Synthesis of well-dispersed layered double hydroxide core@ ordered mesoporous silica shell nanostructure (ldh@ m sio 2) and its application in drug delivery. *Nanoscale* **2011**, *3*, 4069-4073.

71. Alvarez-Lorenzo, C.; Blanco-Fernandez, B.; Puga, A.M.; Concheiro, A. Crosslinked ionic polysaccharides for stimuli-sensitive drug delivery. *Advanced drug delivery reviews* **2013**, *65*, 1148-1171.

72. Beneke, C.E.; Viljoen, A.M.; Hamman, J.H. Polymeric plant-derived excipients in drug delivery. *Molecules* **2009**, *14*, 2602-2620.

73. Wicklein, B.; Martín del Burgo, M.; Yuste, M.; Darder, M.; Llavata, C.E.; Aranda, P.; Ortin, J.; del Real, G.; Ruiz-Hitzky, E. Lipid-based bio-nanohybrids for functional stabilisation of influenza vaccines. *European Journal of Inorganic Chemistry* **2012**, *2012*, 5186-5191.

74. Huang, J.; Gou, G.; Xue, B.; Yan, Q.; Sun, Y.; Dong, L.-E. Preparation and characterization of “dextran-magnetic layered double hydroxide-fluorouracil” targeted liposomes. *International journal of pharmaceutics* **2013**, *450*, 323-330.

75. Ribeiro, L.N.; Alcântara, A.C.; Darder, M.; Aranda, P.; Araújo-Moreira, F.M.; Ruiz-Hitzky, E. Pectin-coated chitosan–ldh bionanocomposite

beads as potential systems for colon-targeted drug delivery. *International journal of pharmaceutics* **2014**, *463*, 1-9.

76. Chen, Y.; Chen, H.; Shi, J. Inorganic nanoparticle-based drug codelivery nanosystems to overcome the multidrug resistance of cancer cells. *Molecular pharmaceutics* **2013**, *11*, 2495-2510.

77. Jabr-Milane, L.S.; van Vlerken, L.E.; Yadav, S.; Amiji, M.M. Multi-functional nanocarriers to overcome tumor drug resistance. *Cancer treatment reviews* **2008**, *34*, 592-602.

78. Khan, M.; Ong, Z.Y.; Wiradharma, N.; Attia, A.B.E.; Yang, Y.Y. Advanced materials for co-delivery of drugs and genes in cancer therapy. *Advanced healthcare materials* **2012**, *1*, 373-392.

79. Creixell, M.; Peppas, N.A. Co-delivery of sirna and therapeutic agents using nanocarriers to overcome cancer resistance. *Nano Today* **2012**, *7*, 367-379.

80. Montesinos, R.N.; Béduneau, A.; Pellequer, Y.; Lamprecht, A. Delivery of p-glycoprotein substrates using chemosensitizers and nanotechnology for selective and efficient therapeutic outcomes. *Journal of controlled release* **2012**, *161*, 50-61.

81. Li, L.; Gu, W.; Chen, J.; Chen, W.; Xu, Z.P. Co-delivery of sirnas and anti-cancer drugs using layered double hydroxide nanoparticles. *Biomaterials* **2014**, *35*, 3331-3339.

82. Li, F.; Zhao, C.; Wang, L. Molecular-targeted agents combination therapy for cancer: Developments and potentials. *Int J Cancer* **2014**, *134*, 1257-1269.

83. Axelrod, M.; Gordon, V.L.; Conaway, M.; Tarcsafalvi, A.; Neitzke, D.J.; Gioeli, D.; Weber, M.J. Combinatorial drug screening identifies

compensatory pathway interactions and adaptive resistance mechanisms. *Oncotarget* **2013**, *4*, 622-635.

84. The nobel prize in physiology or medicine 1908, paul erlich - biography. *Nobel Lectures, Physiology or Medicine 1901-1921* **1967**.

85. Weidle, U.H.; Tiefenthaler, G.; Schiller, C.; Weiss, E.H.; Georges, G.; Brinkmann, U. Prospects of bacterial and plant protein-based immunotoxins for treatment of cancer. *Cancer Genomics Proteomics* **2014**, *11*, 25-38.

86. Kohler, G.; Milstein, C. Continuous cultures of fused cells secreting antibody of predefined specificity. *Nature* **1975**, *256*, 495-497.

87. Blythman, H.E.; Casellas, P.; Gros, O.; Gros, P.; Jansen, F.K.; Paolucci, F.; Pau, B.; Vidal, H. Immunotoxins: Hybrid molecules of monoclonal antibodies and a toxin subunit specifically kill tumour cells. *Nature* **1981**, *290*, 145-146.

88. Pastan, I.; Hassan, R.; FitzGerald, D.J.; Kreitman, R.J. Immunotoxin treatment of cancer. *Annu Rev Med* **2007**, *58*, 221-237.

89. Antignani, A.; Fitzgerald, D. Immunotoxins: The role of the toxin. *Toxins (Basel)* **2013**, *5*, 1486-1502.

90. Bachanova, V.; Frankel, A.; Cao, Q.; Lewis, D.; Verneris, M.; Lazaryan, A.; Burns, L.J.; Vallera, D. Remission induction in a phase 1 study of a bispecific single chain immunotoxin targeting cd22 and cd19 (dt2219) for refractory b-cell malignancies. *Blood* **2014**, *124*.

91. Hamlin, P.A.; Diefenbach, C.S.; Valacer, D.J.; Higgins, J.; Fanale, M.A. Phase i/ib study of the novel immunotoxin mt-3724 in relapsed/refractory non-hodgkin's b-cell lymphoma (nhl). *Blood* **2015**, *126*, 5112-5112.

92. Hassan, R.; Sharon, E.; Thomas, A.; Zhang, J.; Ling, A.; Miettinen, M.; Kreitman, R.J.; Steinberg, S.M.; Hollevoet, K.; Pastan, I. Phase 1 study of the antimesothelin immunotoxin ss1p in combination with pemetrexed and cisplatin for front-line therapy of pleural mesothelioma and correlation of tumor response with serum mesothelin, megakaryocyte potentiating factor, and cancer antigen 125. *Cancer* **2014**, *120*, 3311-3319.

93. Bachanova, V.; Frankel, A.E.; Cao, Q.; Lewis, D.; Grzywacz, B.; Verneris, M.R.; Ustun, C.; Lazaryan, A.; McClune, B.; Warlick, E.D. Phase i study of a bispecific ligand-directed toxin targeting cd22 and cd19 (dt2219) for refractory b-cell malignancies. *Clinical Cancer Research* **2015**, *21*, 1267-1272.

94. Liu-Chittenden, Y.; Jain, M.; Kumar, P.; Patel, D.; Aufforth, R.; Neychev, V.; Sadowski, S.; Gara, S.K.; Joshi, B.H.; Cottle-Delisle, C. Phase i trial of systemic intravenous infusion of interleukin-13-pseudomonas exotoxin in patients with metastatic adrenocortical carcinoma. *Cancer medicine* **2015**, *4*, 1060-1068.

95. Meany, H.J.; Seibel, N.L.; Krailo, M.; Villaluna, D.; Chen, Z.; Gaynon, P.; Neglia, J.P.; Park, J.R.; Hutchinson, R.; Sato, J.K. Feasibility study of a novel experimental induction protocol combining b43-pap (anti-cd19) immunotoxin with standard induction chemotherapy in children and adolescents with relapsed b-lineage all: A report from the children's oncology group. *Journal of Immunotherapy* **2015**, *38*, 299-305.

96. Garland, L.; Gitlitz, B.; Ebbinghaus, S.; Pan, H.; de Haan, H.; Puri, R.K.; Von Hoff, D.; Figlin, R. Phase i trial of intravenous il-4 pseudomonas

exotoxin protein (nbi-3001) in patients with advanced solid tumors that express the il-4 receptor. *Journal of Immunotherapy* **2005**, *28*, 376-381.

97. Robak, T.; Robak, E. Current phase ii antibody-drug conjugates for the treatment of lymphoid malignancies. *Expert opinion on investigational drugs* **2014**, *23*, 911-924.

98. Advani, A.S.; McDonough, S.; Coutre, S.; Wood, B.; Radich, J.; Mims, M.; O'Donnell, M.; Elkins, S.; Becker, M.; Othus, M. Swog s0910: A phase 2 trial of clofarabine/cytarabine/epratuzumab for relapsed/refractory acute lymphocytic leukaemia. *British journal of haematology* **2014**, *165*, 504-509.

99. Foss, F.M.; Saleh, M.N.; Krueger, J.G.; Nichols, J.C.; Murphy, J.R. Diphtheria toxin fusion proteins. *Curr Top Microbiol Immunol* **1998**, *234*, 63-81.

100. Olsen, E.; Duvic, M.; Frankel, A.; Kim, Y.; Martin, A.; Vonderheid, E.; Jegasothy, B.; Wood, G.; Gordon, M.; Heald, P.*, et al.* Pivotal phase iii trial of two dose levels of denileukin diftitox for the treatment of cutaneous t-cell lymphoma. *J Clin Oncol* **2001**, *19*, 376-388.

101. Prince, H.M.; Duvic, M.; Martin, A.; Sterry, W.; Assaf, C.; Sun, Y.; Straus, D.; Acosta, M.; Negro-Vilar, A. Phase iii placebo-controlled trial of denileukin diftitox for patients with cutaneous t-cell lymphoma. *Journal of Clinical Oncology* **2010**, *28*, 1870-1877.

102. Fuentes, A.C.; Szwed, E.; Spears, C.D.; Thaper, S.; Dang, L.H.; Dang, N.H. Denileukin diftitox (ontak) as maintenance therapy for peripheral t-cell lymphomas: Three cases with sustained remission. *Case reports in oncological medicine* **2015**, *2015*.

103. Niesen, J.; Stein, C.; Brehm, H.; Hehmann-Titt, G.; Fendel, R.; Melmer, G.; Fischer, R.; Barth, S. Novel egfr-specific immunotoxins based on panitumumab and cetuximab show in vitro and ex vivo activity against different tumor entities. *Journal of cancer research and clinical oncology* **2015**, *141*, 2079-2095.

104. Niesen, J.; Brehm, H.; Stein, C.; Berges, N.; Pardo, A.; Fischer, R.; ten Haaf, A.; Gattenlöhner, S.; Tur, M.K.; Barth, S. In vitro effects and ex vivo binding of an egfr-specific immunotoxin on rhabdomyosarcoma cells. *Journal of cancer research and clinical oncology* **2015**, *141*, 1049-1061.

105. Berstad, M.; Cheung, L.; Berg, K.; Peng, Q.; Fremstedal, A.; Patzke, S.; Rosenblum, M.; Weyergang, A. Design of an egfr-targeting toxin for photochemical delivery: In vitro and in vivo selectivity and efficacy. *Oncogene* **2015**, *34*, 5582-5592.

106. Mayor, M.; Yang, N.; Sterman, D.; Jones, D.R.; Adusumilli, P.S. Immunotherapy for non-small cell lung cancer: Current concepts and clinical trials. *European Journal of Cardio-Thoracic Surgery* **2015**, ezv371.

107. Weldon, J.E.; Skarzynski, M.; Therres, J.A.; Ostovitz, J.R.; Zhou, H.; Kreitman, R.J.; Pastan, I. Designing the furin-cleavable linker in recombinant immunotoxins based on pseudomonas exotoxin a. *Bioconjugate chemistry* **2015**, *26*, 1120-1128.

108. Wang, Z.; Wei, M.; Zhang, H.; Chen, H.; Germana, S.; Huang, C.A.; Madsen, J.C.; Sachs, D.H.; Wang, Z. Diphtheria-toxin based anti-human ccr4 immunotoxin for targeting human ccr4+ cells in vivo. *Molecular oncology* **2015**, *9*, 1458-1470.

109. Baluna, R.; Vitetta, E.S. Vascular leak syndrome: A side effect of immunotherapy. *Immunopharmacology* **1997**, *37*, 117-132.

110. Soler-Rodríguez, A.-M.a.; Ghetie, M.-A.; Oppenheimer-Marks, N.; Uhr, J.W.; Vitetta, E.S. Ricin a-chain and ricin a-chain immunotoxins rapidly damage human endothelial cells: Implications for vascular leak syndrome. *Experimental cell research* **1993**, *206*, 227-234.

111. Reiter, Y.; Brinkmann, U.; Jung, S.-H.; Lee, B.; Kasprzyk, P.G.; King, C.R.; Pastan, I. Improved binding and antitumor activity of a recombinant anti-erbb2 immunotoxin by disulfide stabilization of the fv fragment. *Journal of Biological Chemistry* **1994**, *269*, 18327-18331.

112. Brinkmann, U.; Reiter, Y.; Jung, S.-H.; Lee, B.; Pastan, I. A recombinant immunotoxin containing a disulfide-stabilized fv fragment. *Proceedings of the National Academy of Sciences* **1993**, *90*, 7538-7542.

113. Chaudhary, V.K.; Jinno, Y.; FitzGerald, D.; Pastan, I. Pseudomonas exotoxin contains a specific sequence at the carboxyl terminus that is required for cytotoxicity. *Proceedings of the National Academy of Sciences* **1990**, *87*, 308-312.

114. Hwang, J.; Fitzgerald, D.J.; Adhya, S.; Pastan, I. Functional domains of pseudomonas exotoxin identified by deletion analysis of the gene expressed in e. Coli. *Cell* **1987**, *48*, 129-136.

115. Siegall, C.B.; Chaudhary, V.K.; FitzGerald, D.J.; Pastan, I. Functional analysis of domains ii, ib, and iii of pseudomonas exotoxin. *Journal of Biological Chemistry* **1989**, *264*, 14256-14261.

116. Pappenheimer Jr, A. Diphtheria toxin. *Annual review of biochemistry* **1977**, *46*, 69-94.

117. Greenfield, L.; Bjorn, M.J.; Horn, G.; Fong, D.; Buck, G.A.; Collier, R.J.; Kaplan, D.A. Nucleotide sequence of the structural gene for diphtheria

toxin carried by corynebacteriophage beta. *Proceedings of the National Academy of Sciences* **1983**, *80*, 6853-6857.

118. Kaczorek, M.; Delpeyroux, F.; Chenciner, N.; Streeck, R.E.; Boquet, P.; Tiollais, P. Nucleotide sequence and expression of the diphtheria tox228 gene in escherichia coli. *Science* **1983**, *221*, 855-858.
119. Smith, W.; Tai, P.; Murphy, J.; Davis, B. Precursor in cotranslational secretion of diphtheria toxin. *Journal of bacteriology* **1980**, *141*, 184-189.
120. Gill, D.M.; Pappenheimer, A. Structure-activity relationships in diphtheria toxin. *Journal of Biological Chemistry* **1971**, *246*, 1492-1495.
121. Collier, R.; Kandel, J. Structure and activity of diphtheria toxin i. Thiol-dependent dissociation of a fraction of toxin into enzymically active and inactive fragments. *Journal of Biological Chemistry* **1971**, *246*, 1496-1503.
122. Murphy, J.R. Mechanism of diphtheria toxin catalytic domain delivery to the eukaryotic cell cytosol and the cellular factors that directly participate in the process. *Toxins* **2011**, *3*, 294-308.
123. Pastan, I.; FitzGerald, D. Pseudomonas exotoxin: Chimeric toxins. *Journal of Biological Chemistry* **1989**, *264*, 15157-15160.
124. Carroll, S.; Collier, R. Amino acid sequence homology between the enzymic domains of diphtheria toxin and pseudomonas aeruginosa exotoxin a. *Molecular microbiology* **1988**, *2*, 293-296.
125. Franz, D.R.; Jaax, N.K. Ricin toxin. *Medical aspects of chemical and biological warfare* **1997**, 631-642.
126. Chiou, J.C.; Li, X.P.; Remacha, M.; Ballesta, J.P.; Tumer, N.E. The ribosomal stalk is required for ribosome binding, depurination of the rrna

and cytotoxicity of ricin a chain in saccharomyces cerevisiae. *Molecular microbiology* **2008**, *70*, 1441-1452.

127. Falnes, P.Ø.; Sandvig, K. Penetration of protein toxins into cells. *Current opinion in cell biology* **2000**, *12*, 407-413.

128. Iglewski, B.H.; Kabat, D. Nad-dependent inhibition of protein synthesis by pseudomonas aeruginosa toxin. *Proceedings of the National Academy of Sciences* **1975**, *72*, 2284-2288.

129. Naglich, J.G.; Metherall, J.E.; Russell, D.W.; Eidels, L. Expression cloning of a diphtheria toxin receptor: Identity with a heparin-binding egf-like growth factor precursor. *Cell* **1992**, *69*, 1051-1061.

130. Kounnas, M.; Morris, R.E.; Thompson, M.; FitzGerald, D.; Strickland, D.; Saelinger, C. The alpha 2-macroglobulin receptor/low density lipoprotein receptor-related protein binds and internalizes pseudomonas exotoxin a. *Journal of Biological Chemistry* **1992**, *267*, 12420-12423.

131. Sandvig, K.; Olsnes, S. Diphtheria toxin entry into cells is facilitated by low ph. *The Journal of cell biology* **1980**, *87*, 828-832.

132. Lanzrein, M.; Sand, O.; Olsnes, S. Gpi-anchored diphtheria toxin receptor allows membrane translocation of the toxin without detectable ion channel activity. *The EMBO journal* **1996**, *15*, 725.

133. Almond, B.D.; Eidels, L. The cytoplasmic domain of the diphtheria toxin receptor (hb-egf precursor) is not required for receptor-mediated endocytosis. *Journal of Biological Chemistry* **1994**, *269*, 26635-26641.

134. Morris, R.; Manhart, M.; Saelinger, C. Receptor-mediated entry of pseudomonas toxin: Methylamine blocks clustering step. *Infection and immunity* **1983**, *40*, 806-811.

135. Simpson, J.C.; Smith, D.C.; Roberts, L.M.; Lord, J.M. Expression of mutant dynamin protects cells against diphtheria toxin but not against ricin. *Experimental cell research* **1998**, *239*, 293-300.

136. Montecucco, C.; Schiavo, G.; Tomasi, M. Ph-dependence of the phospholipid interaction of diphtheria-toxin fragments. *Biochemical Journal* **1985**, *231*, 123-128.

137. Moskaug, J.; Sandvig, K.; Olsnes, S. Low ph-induced release of diphtheria toxin a-fragment in vero cells. Biochemical evidence for transfer to the cytosol. *Journal of Biological Chemistry* **1988**, *263*, 2518-2525.

138. Iglewski, B.H.; Liu, P.V.; Kabat, D. Mechanism of action of pseudomonas aeruginosa exotoxin aiadenosine diphosphate-ribosylation of mammalian elongation factor 2 in vitro and in vivo. *Infection and immunity* **1977**, *15*, 138-144.

139. Aruffo, A.; Seed, B. Molecular cloning of two cd7 (t-cell leukemia antigen) cdnas by a cos cell expression system. *EMBO J* **1987**, *6*, 3313-3316.

140. Sempowski, G.D.; Lee, D.M.; Kaufman, R.E.; Haynes, B.F. Structure and function of the cd7 molecule. *Crit Rev Immunol* **1999**, *19*, 331-348.

141. Chabannon, C.; Wood, P.; Torok-Storb, B. Expression of cd7 on normal human myeloid progenitors. *J Immunol* **1992**, *149*, 2110-2113.

142. Rabinowich, H.; Pricop, L.; Herberman, R.B.; Whiteside, T.L. Expression and function of cd7 molecule on human natural killer cells. *J Immunol* **1994**, *152*, 517-526.

143. Vonderheid, E.C.; Bernengo, M.G.; Burg, G.; Duvic, M.; Heald, P.; Laroche, L.; Olsen, E.; Pittelkow, M.; Russell-Jones, R.; Takigawa, M. Update on erythrodermic cutaneous t-cell lymphoma: Report of the

international society for cutaneous lymphomas. *Journal of the American Academy of Dermatology* **2002**, *46*, 95-106.

144. Kita, K.; Miwa, H.; Nakase, K.; Kawakami, K.; Kobayashi, T.; Shirakawa, S.; Tanaka, I.; Ohta, C.; Tsutani, H.; Oguma, S. Clinical importance of cd7 expression in acute myelocytic leukemia. The japan cooperative group of leukemia/lymphoma [see comments]. *Blood* **1993**, *81*, 2399-2405.

145. Pauza, M.E.; Doumbia, S.O.; Pennell, C.A. Construction and characterization of human cd7-specific single-chain fv immunotoxins. *The Journal of Immunology* **1997**, *158*, 3259-3269.

146. Tang, J.; Li, J.; Zhu, X.; Yu, Y.; Chen, D.; Yuan, L.; Gu, Z.; Zhang, X.; Qi, L.; Gong, Z. Novel cd7-specific nanobody-based immunotoxins potently enhanced apoptosis of cd7-positive malignant cells. *Oncotarget* **2016**.

147. Mladenov, R.; Hristodorov, D.; Cremer, C.; Hein, L.; Kreutzer, F.; Stroisch, T.; Niesen, J.; Brehm, H.; Blume, T.; Brümmendorf, T.H. The fc-alpha receptor is a new target antigen for immunotherapy of myeloid leukemia. *International Journal of Cancer* **2015**, *137*, 2729-2738.

148. Hulett, M.D.; Hogarth, P.M. The second and third extracellular domains of fcγri (cd64) confer the unique high affinity binding of igg2a. *Molecular immunology* **1998**, *35*, 989-996.

149. Van de Winkel, J.; Anderson, C.L. Biology of human immunoglobulin g fc receptors. *J Leukoc Biol* **1991**, *49*, 511-524.

150. Stahnke, B.; Thepen, T.; Stöcker, M.; Rosinke, R.; Jost, E.; Fischer, R.; Tur, M.K.; Barth, S. Granzyme b-h22 (scfv), a human immunotoxin targeting cd64 in acute myeloid leukemia of monocytic subtypes. *Molecular cancer therapeutics* **2008**, *7*, 2924-2932.

151. Tur, M.K.; Huhn, M.; Thepen, T.; Stöcker, M.; Krohn, R.; Vogel, S.; Jost, E.; Osieka, R.; van de Winkel, J.G.; Fischer, R. Recombinant cd64-specific single chain immunotoxin exhibits specific cytotoxicity against acute myeloid leukemia cells. *Cancer research* **2003**, *63*, 8414-8419.

152. Schiffer, S.; Rosinke, R.; Jost, E.; Hehmann-Titt, G.; Huhn, M.; Melmer, G.; Barth, S.; Thepen, T. Targeted ex vivo reduction of cd64-positive monocytes in chronic myelomonocytic leukemia and acute myelomonocytic leukemia using human granzyme b-based cytolytic fusion proteins. *International Journal of Cancer* **2014**, *135*, 1497-1508.

153. Staudinger, M.; Glorius, P.; Burger, R.; Kellner, C.; Klausz, K.; Günther, A.; Repp, R.; Klapper, W.; Gramatzki, M.; Peipp, M. The novel immunotoxin hm1. 24-eta′ induces apoptosis in multiple myeloma cells. *Blood cancer journal* **2014**, *4*, e219.

154. Kreitman, R.J.; Wilson, W.H.; White, J.D.; Stetler-Stevenson, M.; Jaffe, E.S.; Giardina, S.; Waldmann, T.A.; Pastan, I. Phase i trial of recombinant immunotoxin anti-tac (fv)-pe38 (lmb-2) in patients with hematologic malignancies. *Journal of Clinical Oncology* **2000**, *18*, 1622-1636.

155. Kreitman, R.J.; Stetler-Stevenson, M.; Jaffe, E.S.; Conlon, K.C.; Steinberg, S.M.; Wilson, W.; Waldmann, T.A.; Pastan, I. Complete remissions of adult t-cell leukemia with anti-cd25 recombinant immunotoxin lmb-2 and chemotherapy to block immunogenicity. *Clinical Cancer Research* **2016**, *22*, 310-318.

156. Nand, K.N.; Gupta, J.C.; Panda, A.; Jain, S. Development of a recombinant hcg-specific single chain immunotoxin cytotoxic to hcg

expressing cancer cells. *Protein expression and purification* **2015**, *106*, 10-17.

157. Weigel, K.J.; Shen, L.; Thomas, C.L.; Alber, D.; Drapalik, L.; Schafer, Z.T.; Lee, S.W. Design and evaluation of a peptide-based immunotoxin for breast cancer therapeutics. *FEBS open bio* **2015**, *5*, 202-208.

158. Hassan, R.; Alewine, C.; Pastan, I. New life for immunotoxin cancer therapy. *Clinical Cancer Research* **2016**, *22*, 1055-1058.

159. Ehrlich, D.; Wang, B.; Lu, W.; Dowling, P.; Yuan, R. Intratumoral anti-hud immunotoxin therapy for small cell lung cancer and neuroblastoma. *Journal of hematology & oncology* **2014**, *7*, 1.

160. Mayor, M.; Yang, N.; Sterman, D.; Jones, D.R.; Adusumilli, P.S. Immunotherapy for non-small cell lung cancer: Current concepts and clinical trials. *European Journal of Cardio-Thoracic Surgery* **2016**, *49*, 1324-1333.

161. Cole, L.A. New discoveries on the biology and detection of human chorionic gonadotropin. *Reproductive Biology and Endocrinology* **2009**, *7*, 1.

162. Kathuria, S.; Sriraman, R.; Nath, R.; Sack, M.; Pal, R.; Artsaenko, O.; Talwar, G.; Fischer, R.; Finnern, R. Efficacy of plant-produced recombinant antibodies against hcg. *Human Reproduction* **2002**, *17*, 2054-2061.

163. Kabeer, R.S.; Pal, R.; Talwar, G. Human acute lymphoblastic leukaemia cells make human pregnancy hormone hcg and expose it on the membrane: A case for using recombinant antibody against hcg for selective delivery of drugs and/or radiations. *CURRENT SCIENCE-BANGALORE-* **2005**, *89*, 1571.

164. Weldon, J.E.; Pastan, I. A guide to taming a toxin–recombinant immunotoxins constructed from pseudomonas exotoxin a for the treatment of cancer. *The FEBS journal* **2011**, *278*, 4683-4700.

165. Slamon, D. Human breast cancer: Correlation of relapse and. *Science* **1987**, *3798106*, 235.

166. Szabo, A.; Dalmau, J.; Manley, G.; Rosenfeld, M.; Wong, E.; Henson, J.; Posner, J.B.; Furneaux, H.M. Hud, a paraneoplastic encephalomyelitis antigen, contains rna-binding domains and is homologous to elav and sex-lethal. *Cell* **1991**, *67*, 325-333.

167. Dalmau, J.; Furneaux, H.; Cordon-Cardo, C.; Posner, J. The expression of the hu (paraneoplastic encephalomyelitis/sensory neuronopathy) antigen in human normal and tumor tissues. *The American journal of pathology* **1992**, *141*, 881.

168. Kachala, S.S.; Bograd, A.J.; Villena-Vargas, J.; Suzuki, K.; Servais, E.L.; Kadota, K.; Chou, J.; Sima, C.S.; Vertes, E.; Rusch, V.W. Mesothelin overexpression is a marker of tumor aggressiveness and is associated with reduced recurrence-free and overall survival in early-stage lung adenocarcinoma. *Clinical Cancer Research* **2014**, *20*, 1020-1028.

169. Andersson, Y.; Engebraaten, O.; Juell, S.; Aamdal, S.; Brunsvig, P.; Fodstad, Ø.; Dueland, S. Phase i trial of epcam-targeting immunotoxin moc31pe, alone and in combination with cyclosporin. *British journal of cancer* **2015**.

170. Rashidi, A.; Walter, R.B. Antigen-specific immunotherapy for acute myeloid leukemia: Where are we now, and where do we go from here? *Expert review of hematology* **2016**, *9*, 335-350.

171. Sun, T.; Zhang, Y.S.; Pang, B.; Hyun, D.C.; Yang, M.; Xia, Y. Engineered nanoparticles for drug delivery in cancer therapy. *Angewandte Chemie International Edition* **2014**, *53*, 12320-12364.

172. Su, X.; Yang, N.; Wittrup, K.D.; Irvine, D.J. Synergistic antitumor activity from two-stage delivery of targeted toxins and endosome-disrupting nanoparticles. *Biomacromolecules* **2013**, *14*, 1093-1102.

173. Schneider, C.S.; Perez, J.G.; Cheng, E.; Zhang, C.; Mastorakos, P.; Hanes, J.; Winkles, J.A.; Woodworth, G.F.; Kim, A.J. Minimizing the non-specific binding of nanoparticles to the brain enables active targeting of fn14-positive glioblastoma cells. *Biomaterials* **2015**, *42*, 42-51.

174. Feng, X.; Yao, J.; Gao, X.; Jing, Y.; Kang, T.; Jiang, D.; Jiang, T.; Feng, J.; Zhu, Q.; Jiang, X. Multi-targeting peptide-functionalized nanoparticles recognized vasculogenic mimicry, tumor neovasculature, and glioma cells for enhanced anti-glioma therapy. *ACS applied materials & interfaces* **2015**, *7*, 27885-27899.

175. Wang, B.; Lv, L.; Wang, Z.; Jiang, Y.; Lv, W.; Liu, X.; Wang, Z.; Zhao, Y.; Xin, H.; Xu, Q. Improved anti-glioblastoma efficacy by il-13rα2 mediated copolymer nanoparticles loaded with paclitaxel. *Scientific reports* **2015**, *5*.

176. Mazor, R.; Onda, M.; Pastan, I. Immunogenicity of therapeutic recombinant immunotoxins. *Immunological reviews* **2016**, *270*, 152-164.

177. Cavani, F.; Trifirò, F.; Vaccari, A. Hydrotalcite-type anionic clays: Preparation, properties and applications. *Catalysis today* **1991**, *11*, 173-301.

178. Arulraj, J. Intercalation of organic anions and intracrystalline reactions in anionic clays. **2013**.

179. Park, D.-H.; Hwang, S.-J.; Oh, J.-M.; Yang, J.-H.; Choy, J.-H. Polymer–inorganic supramolecular nanohybrids for red, white, green, and blue applications. *Progress in Polymer Science* **2013**, *38*, 1442-1486.

180. Auerbach, S.M.; Carrado, K.A.; Dutta, P.K. *Handbook of layered materials*. CRC Press: 2004.

181. Miyata, S. Anion-exchange properties of hydrotalcite-like compounds. *Clays Clay Miner* **1983**, *31*, 305-311.

182. Wilson, O.; Olorunyolemi, T.; Jaworski, A.; Borum, L.; Young, D.; Siriwat, A.; Dickens, E.; Oriakhi, C.; Lerner, M. Surface and interfacial properties of polymer-intercalated layered double hydroxide nanocomposites. *Applied clay science* **1999**, *15*, 265-279.

183. Taviot-Guého, C.; Feng, Y.; Faour, A.; Leroux, F. Intercalation chemistry in a ldh system: Anion exchange process and staging phenomenon investigated by means of time-resolved, in situ x-ray diffraction. *Dalton Transactions* **2010**, *39*, 5994-6005.

184. Lin, M.; Sun, P.; Yu, H. Evaluation of buffering capacity and acid neutralizing-ph time profile of antacids. *Journal of the Formosan Medical Association= Taiwan yi zhi* **1998**, *97*, 704-710.

185. Simoneau, G. Absence of rebound effect with calcium carbonate. *European journal of drug metabolism and pharmacokinetics* **1996**, *21*, 351-357.

186. Tarnawski, A.; Pai, R.; Itani, R.; Wyle, F. The antacid talcid adsorbs and neutralizes all proteins secreted by h. Pylori including vaca cytotoxin: A new mechanism for its ulcer-healing action? *Digestion* **1999**, *60*, 449-455.

187. Chan, C.-H.; Chen, J.-K.; Chang, F.-C. Specific DNA extraction through fluid channels with immobilization of layered double hydroxides on

polycarbonate surface. *Sensors and Actuators B: Chemical* **2008**, *133*, 327-332.

188. Di Francia, G.; La Ferrara, V.; Manzo, S.; Chiavarini, S. Towards a label-free optical porous silicon DNA sensor. *Biosensors and Bioelectronics* **2005**, *21*, 661-665.

189. Liu, W.-T.; Zhu, L. Environmental microbiology-on-a-chip and its future impacts. *Trends in biotechnology* **2005**, *23*, 174-179.

190. Boclair, J.W.; Braterman, P.S. Layered double hydroxide stability. 1. Relative stabilities of layered double hydroxides and their simple counterparts. *Chemistry of Materials* **1999**, *11*, 298-302.

191. Xu, Z.P.; Walker, T.L.; Liu, K.-l.; Cooper, H.M.; Lu, G.M.; Bartlett, P.F. Layered double hydroxide nanoparticles as cellular delivery vectors of supercoiled plasmid DNA. *International journal of nanomedicine* **2007**, *2*, 163.

192. Xu, Z.; Zeng, H. Abrupt structural transformation in hydrotalcite-like compounds mg1-x al x (oh) 2 (no3) x⊙ n h2o as a continuous function of nitrate anions. *The Journal of Physical Chemistry B* **2001**, *105*, 1743-1749.

193. Prabha, S.; Zhou, W.-Z.; Panyam, J.; Labhasetwar, V. Size-dependency of nanoparticle-mediated gene transfection: Studies with fractionated nanoparticles. *International journal of pharmaceutics* **2002**, *244*, 105-115.

194. Leong, K.W. Polymeric controlled nucleic acid delivery. *MRS bulletin* **2005**, *30*, 640-646.

195. Andl, C.D.; Mizushima, T.; Nakagawa, H.; Oyama, K.; Harada, H.; Chruma, K.; Herlyn, M.; Rustgi, A.K. Epidermal growth factor receptor mediates increased cell proliferation, migration, and aggregation in

esophageal keratinocytes in vitro and in vivo. *Journal of Biological Chemistry* **2003**, *278*, 1824-1830.

196. Walker, F.; Abramowitz, L.; Benabderrahmane, D.; Duval, X.; Descatoire, V.; Hénin, D.; Lehy, T.; Aparicio, T. Growth factor receptor expression in anal squamous lesions: Modifications associated with oncogenic human papillomavirus and human immunodeficiency virus. *Human pathology* **2009**, *40*, 1517-1527.
197. Downward, J.; Parker, P.; Waterfield, M. Autophosphorylation sites on the epidermal growth factor receptor. *Nature* **1984**, *311*, 483-485.
198. Zhang, H.; Berezov, A.; Wang, Q.; Zhang, G.; Drebin, J.; Murali, R.; Greene, M.I. Erbb receptors: From oncogenes to targeted cancer therapies. *The Journal of clinical investigation* **2007**, *117*, 2051-2058.
199. Morelli, M.; Cascone, T.; Troiani, T.; De Vita, F.; Orditura, M.; Laus, G.; Eckhardt, S.; Pepe, S.; Tortora, G.; Ciardiello, F. Sequence-dependent antiproliferative effects of cytotoxic drugs and epidermal growth factor receptor inhibitors. *Annals of Oncology* **2005**, *16*, iv61-iv68.
200. Yarden, Y.; Schlessinger, J. Epidermal growth factor induces rapid, reversible aggregation of the purified epidermal growth factor receptor. *Biochemistry* **1987**, *26*, 1443-1451.
201. Alvarez, J.V.; Greulich, H.; Sellers, W.R.; Meyerson, M.; Frank, D.A. Signal transducer and activator of transcription 3 is required for the oncogenic effects of non–small-cell lung cancer–associated mutations of the epidermal growth factor receptor. *Cancer research* **2006**, *66*, 3162-3168.
202. Bharti, A.C.; Aggarwal, B.B. Nuclear factor-kappa b and cancer: Its role in prevention and therapy. *Biochemical pharmacology* **2002**, *64*, 883-888.

203. Hussain, A.R.; Ahmed, S.O.; Ahmed, M.; Khan, O.S.; Al AbdulMohsen, S.; Platanias, L.C.; Al-Kuraya, K.S.; Uddin, S. Cross-talk between nfkb and the pi3-kinase/akt pathway can be targeted in primary effusion lymphoma (pel) cell lines for efficient apoptosis. *PLoS One* **2012**, *7*, e39945.

204. Pollack, M. Pseudomonas aeruginosa exotoxin a. Mass Medical Soc: 1980.

205. Allured, V.S.; Collier, R.J.; Carroll, S.F.; McKay, D.B. Structure of exotoxin a of pseudomonas aeruginosa at 3.0-angstrom resolution. *Proceedings of the National Academy of Sciences* **1986**, *83*, 1320-1324.

206. Pier, G.B.; Lyczak, J.B.; Wetzler, L.M. *Immunology, infection, and immunity*. ASM press: 2004.

207. Voinnet, O.; Baulcombe, D.C. Systemic signalling in gene silencing. *Nature* **1997**, *389*, 553.

208. Long, Q.; Meng, A.; Wang, H.; Jessen, J.R.; Farrell, M.J.; Lin, S. Gata-1 expression pattern can be recapitulated in living transgenic zebrafish using gfp reporter gene. *Development* **1997**, *124*, 4105-4111.

209. Wu, J.; Sun, L.; Chen, X.; Du, F.; Shi, H.; Chen, C.; Chen, Z.J. Cyclic gmp-amp is an endogenous second messenger in innate immune signaling by cytosolic DNA. *Science* **2013**, *339*, 826-830.

210. De Angioletti, M.; Lacerra, G.; Sabato, V.; Carestia, C. B+ 45 g→ c: A novel silent β-thalassaemia mutation, the first in the kozak sequence. *British journal of haematology* **2004**, *124*, 224-231.

211. Kozak, M. Point mutations define a sequence flanking the aug initiator codon that modulates translation by eukaryotic ribosomes. *Cell* **1986**, *44*, 283-292.

212. Kozak, M. At least six nucleotides preceding the aug initiator codon enhance translation in mammalian cells. *Journal of molecular biology* **1987**, *196*, 947-950.

213. Kozak, M. An analysis of 5'-noncoding sequences from 699 vertebrate messenger rnas. *Nucleic acids research* **1987**, *15*, 8125-8148.

214. Uchibori, R.; Okada, T.; Ito, T.; Urabe, M.; Mizukami, H.; Kume, A.; Ozawa, K. Retroviral vector-producing mesenchymal stem cells for targeted suicide cancer gene therapy. *The journal of gene medicine* **2009**, *11*, 373-381.

215. Pavlenko, M.; Roos, A.; Lundqvist, A.; Palmborg, A.; Miller, A.; Ozenci, V.; Bergman, B.; Egevad, L.; Hellström, M.; Kiessling, R. A phase i trial of DNA vaccination with a plasmid expressing prostate-specific antigen in patients with hormone-refractory prostate cancer. *British journal of cancer* **2004**, *91*, 688-694.

216. Spooner, R.; Deonarain, M.; Epenetos, A. DNA vaccination for cancer treatment. *Gene therapy* **1995**, *2*, 173-180.

217. Yan, G.; Zou, R.; Chen, Z.; Fan, B.; Wang, Z.; Wang, Y.; Yin, X.; Zhang, D.; Tong, L.; Yang, F. Silencing rhoa inhibits migration and invasion through wnt/β-catenin pathway and growth through cell cycle regulation in human tongue cancer. *Acta biochimica et biophysica Sinica* **2014**, gmu051.

218. Ginn, S.L.; Alexander, I.E.; Edelstein, M.L.; Abedi, M.R.; Wixon, J. Gene therapy clinical trials worldwide to 2012–an update. *The journal of gene medicine* **2013**, *15*, 65-77.

219. Gu, Z.; Rolfe, B.E.; Thomas, A.C.; Campbell, J.H.; Lu, G.M.; Xu, Z.P. Cellular trafficking of low molecular weight heparin incorporated in

layered double hydroxide nanoparticles in rat vascular smooth muscle cells. *Biomaterials* **2011**, *32*, 7234-7240.

220. Casse, F.; Boucher, C.; Julliot, J.; Michel, M.; Denarie, J. Identification and characterization of large plasmids in rhizobium meliloti using agarose gel electrophoresis. *Microbiology* **1979**, *113*, 229-242.

221. Prazeres, D.M.F.; Schluep, T.; Cooney, C. Preparative purification of supercoiled plasmid DNA using anion-exchange chromatography. *Journal of Chromatography A* **1998**, *806*, 31-45.

222. Zhang, F.; Wang, S.; Yin, L.; Yang, Y.; Guan, Y.; Wang, W.; Xu, H.; Tao, N. Quantification of epidermal growth factor receptor expression level and binding kinetics on cell surfaces by surface plasmon resonance imaging. *Analytical Chemistry* **2015**, *87*, 9960-9965.

223. Subik, K.; Lee, J.-F.; Baxter, L.; Strzepek, T.; Costello, D.; Crowley, P.; Xing, L.; Hung, M.-C.; Bonfiglio, T.; Hicks, D.G. The expression patterns of er, pr, her2, ck5/6, egfr, ki-67 and ar by immunohistochemical analysis in breast cancer cell lines. *Breast cancer: basic and clinical research* **2010**, *4*, 35.

224. Dalby, B.; Cates, S.; Harris, A.; Ohki, E.C.; Tilkins, M.L.; Price, P.J.; Ciccarone, V.C. Advanced transfection with lipofectamine 2000 reagent: Primary neurons, sirna, and high-throughput applications. *Methods* **2004**, *33*, 95-103.

225. Graham, M.V.; Purdy, J.A.; Emami, B.; Harms, W.; Bosch, W.; Lockett, M.A.; Perez, C.A. Clinical dose–volume histogram analysis for pneumonitis after 3d treatment for non-small cell lung cancer (nsclc). *International Journal of Radiation Oncology* Biology* Physics* **1999**, *45*, 323-329.

226. Molina, J.R.; Yang, P.; Cassivi, S.D.; Schild, S.E.; Adjei, A.A. In *Non-small cell lung cancer: Epidemiology, risk factors, treatment, and survivorship*, Mayo Clinic Proceedings, 2008; Elsevier: pp 584-594.

227. Yu, Y.-H.; Liao, C.-C.; Hsu, W.-H.; Chen, H.-J.; Liao, W.-C.; Muo, C.-H.; Sung, F.-C.; Chen, C.-Y. Increased lung cancer risk among patients with pulmonary tuberculosis: A population cohort study. *Journal of Thoracic Oncology* **2011**, *6*, 32-37.

228. Birim, Ö.; Kappetein, A.P.; Waleboer, M.; Puvimanasinghe, J.P.; Eijkemans, M.J.; Steyerberg, E.W.; Versteegh, M.I.; Bogers, A.J. Long-term survival after non–small cell lung cancer surgery: Development and validation of a prognostic model with a preoperative and postoperative mode. *The Journal of thoracic and cardiovascular surgery* **2006**, *132*, 491-498.

229. Oh, J.M.; Choi, S.J.; Lee, G.E.; Kim, J.E.; Choy, J.H. Inorganic metal hydroxide nanoparticles for targeted cellular uptake through clathrin-mediated endocytosis. *Chemistry–An Asian Journal* **2009**, *4*, 67-73.

230. Choi, S.-J.; Oh, J.-M.; Choy, J.-H. Safety aspect of inorganic layered nanoparticles: Size-dependency in vitro and in vivo. *Journal of nanoscience and nanotechnology* **2008**, *8*, 5297-5301.

231. Horcajada, P.; Chalati, T.; Serre, C.; Gillet, B.; Sebrie, C.; Baati, T.; Eubank, J.F.; Heurtaux, D.; Clayette, P.; Kreuz, C. Porous metal-organic-framework nanoscale carriers as a potential platform for drug delivery and imaging. *Nature materials* **2010**, *9*, 172-178.

232. Taylor-Pashow, K.M.; Rocca, J.D.; Xie, Z.; Tran, S.; Lin, W. Postsynthetic modifications of iron-carboxylate nanoscale metal− organic frameworks

for imaging and drug delivery. *Journal of the American Chemical Society* **2009**, *131*, 14261-14263.

233. Della Rocca, J.; Liu, D.; Lin, W. Nanoscale metal–organic frameworks for biomedical imaging and drug delivery. *Accounts of chemical research* **2011**, *44*, 957-968.

234. Horcajada, P.; Serre, C.; Maurin, G.; Ramsahye, N.A.; Balas, F.; Vallet-Regi, M.; Sebban, M.; Taulelle, F.; Férey, G. Flexible porous metal-organic frameworks for a controlled drug delivery. *Journal of the American Chemical Society* **2008**, *130*, 6774-6780.

235. Lau, W.-M.; White, A.W.; Gallagher, S.; Donaldson, M.; McNaughton, G.; Heard, C.M. Scope and limitations of the co-drug approach to topical drug delivery. *Current pharmaceutical design* **2008**, *14*, 794-802.